

5-2010

## AMPA RECEPTOR ALLOSTERISM: MEASUREMENT OF THE CONFORMATIONAL CHANGES IN THE LIGAND BINDING DOMAIN OF A FUNCTIONAL RECEPTOR

Jennifer Gonzalez-McGehee

Follow this and additional works at: [https://digitalcommons.library.tmc.edu/utgsbs\\_dissertations](https://digitalcommons.library.tmc.edu/utgsbs_dissertations)



Part of the [Biochemistry, Biophysics, and Structural Biology Commons](#)

### Recommended Citation

Gonzalez-McGehee, Jennifer, "AMPA RECEPTOR ALLOSTERISM: MEASUREMENT OF THE CONFORMATIONAL CHANGES IN THE LIGAND BINDING DOMAIN OF A FUNCTIONAL RECEPTOR" (2010). *The University of Texas MD Anderson Cancer Center UTHealth Graduate School of Biomedical Sciences Dissertations and Theses (Open Access)*. 33.  
[https://digitalcommons.library.tmc.edu/utgsbs\\_dissertations/33](https://digitalcommons.library.tmc.edu/utgsbs_dissertations/33)

This Dissertation (PhD) is brought to you for free and open access by the The University of Texas MD Anderson Cancer Center UTHealth Graduate School of Biomedical Sciences at DigitalCommons@TMC. It has been accepted for inclusion in The University of Texas MD Anderson Cancer Center UTHealth Graduate School of Biomedical Sciences Dissertations and Theses (Open Access) by an authorized administrator of DigitalCommons@TMC. For more information, please contact [digitalcommons@library.tmc.edu](mailto:digitalcommons@library.tmc.edu).

AMPA RECEPTOR ALLOSTERISM: MEASUREMENT OF THE  
CONFORMATIONAL CHANGES IN THE LIGAND BINDING  
DOMAIN OF A FUNCTIONAL RECEPTOR

by

Jennifer Gonzalez-McGehee, B.S.

APPROVED:

---

[Advisor, Vasanthi Jayaraman, Ph.D.]

---

[Renhao Li, Ph.D.]

---

[Raymond Grill, Ph.D.]

---

[Lei Zheng, Ph.D.]

---

[John Spudich, Ph.D.]

---

APPROVED:

---

Dean, The University of Texas  
Graduate School of Biomedical Sciences at Houston

AMPA RECEPTOR ALLOSTERISM: MEASUREMENT OF THE  
CONFORMATIONAL CHANGES IN THE LIGAND BINDING  
DOMAIN OF A FUNCTIONAL RECEPTOR

A

DISSERTATION

Presented to the Faculty of  
The University of Texas  
Health Science Center at Houston  
and  
The University of Texas  
M. D. Anderson Cancer Center  
Graduate School of Biomedical Sciences  
in Partial Fulfillment

of the Requirements

for the Degree of

DOCTOR OF PHILOSOPHY

by

Jennifer Gonzalez-McGehee, B.S.  
Houston, Texas

May 2010

## **Dedication**

To my husband, Michael McGehee, M.D., for the love and support provided throughout our relationship while we both endured the rigors of higher education and establishing a new life together. Furthermore, I dedicate my dissertation to my parents, Eddie and Janie, and to my sisters, Christine and Erika, who have all provided me with the love and encouragement to pursue an education and never stood in the way of my dreams. To the rest of my family and friends, I express great appreciation for enhancing my life outside of the lab.

## **Acknowledgments**

Without the support and encouragement of several people, my efforts would not have resulted in this dissertation.

Dr. Michael Losiewicz and Dr. Jack Calentine gave me a wonderful start into my passion for biochemistry and chemistry. The late Dr. Jose Cimadevilla, director of the MARC program, was instrumental in my career choices. My first experience in a biochemistry lab was a joy with the help of Dr. Surinder K. Batra and Dr. Nicolas Moniaux. These two undoubtedly had a significant impact on my development as a scientist.

I would like to express my deepest gratitude to Dr. Vasanthi Jayaraman for this exciting project. She provided the ultimate personal and scientific mentorship, which has inspired me during my time here at UT-Houston GSBS and will continue to do so in my future career. I would also like to thank the members of my advisory and supervisory committees, Dr. Renhao Li, Dr. Henry Strobel, Dr. Andrew Morris, Dr. Kevin Ridge, Dr. Lei Zheng, Dr. John Spudich, and Dr. Raymond Grill for their dedication and invaluable feedback.

My special thanks to the members of the Jayaraman lab. Dr. Mei Du constantly shared her knowledge about molecular biology and life in general. My fellow graduate student, Anu Rambhadran, has provided camaraderie, support, and an enjoyable environment in the lab every day—it has been a pleasure to have her as a colleague and a friend.

I would also like to acknowledge my funding source, the NIH National Research Service Award (1F31 GM 82023-01).

AMPA RECEPTOR ALLOSTERISM: MEASUREMENT OF THE  
CONFORMATIONAL CHANGES IN THE LIGAND BINDING  
DOMAIN OF A FUNCTIONAL RECEPTOR

Publication No. \_\_\_\_\_

Jennifer Gonzalez-McGehee, Ph.D

Advisor: Vasanthi Jayaraman, Ph.D.

Ionotropic glutamate receptors are important excitatory neurotransmitter receptors in the mammalian central nervous system that have been implicated in a number of neuropathologies such as epilepsy, ischemia, and amyotrophic lateral sclerosis. Glutamate binding to an extracellular ligand binding domain initiates a series of structural changes that leads to the formation of a cation selective transmembrane channel, which consequently closes due to desensitization of the receptor. The crystal structures of the AMPA subtype of the glutamate receptor have been particularly useful in providing initial insight into the conformational changes in the ligand binding domain; however, these structures are limited by crystallographic constraint. To gain a clear picture of how agonist binding is coupled to channel activation and desensitization, it is essential to study changes in the ligand binding domain in a dynamic, physiological state. In this dissertation, a technique called Luminescence Resonance Energy Transfer was used to determine the conformational changes associated with activation and desensitization in a functional AMPA receptor ( $\Delta N^*$ -AMPA) that contains the ligand binding domain and transmembrane segments;  $\Delta N^*$ -AMPA has been modified such that fluorophores can be introduced at specific sites to serve as a readout of cleft closure or to establish intersubunit distances. Previous structural studies of cleft closure of the

isolated ligand binding domain in conjunction with functional studies of the full receptor suggest that extent of cleft closure correlates with extent of activation. Here, LRET has been used to show that a similar relationship between cleft closure and activation is observed in the “full length” receptor showing that the isolated ligand binding domain is a good model of the domain in the full length receptor for changes within a subunit. Similar LRET investigations were used to study intersubunit distances specifically to probe conformational changes between subunits within a dimer in the tetrameric receptor. These studies show that the dimer interface is coupled in the open state, and decoupled in the desensitized state, similar to the isolated ligand binding domain crystal structure studies. However, we show that the apo state dimer interface is not pre-formed as in the crystal structure, hence suggesting a mechanism for functional transitions within the receptor based on LRET distances obtained.

## Table of Contents

<b>Approval Sheet</b> .....	i
<b>Title page</b> .....	ii
<b>Dedication</b> .....	iii
<b>Acknowledgements</b> .....	iv
<b>Abstract</b> .....	v
<b>Table of Contents</b> .....	vii
<b>List of Illustrations</b> .....	xi
<b>List of Tables</b> .....	xiv
<b>Abbreviations</b> .....	xv
<b>Chapter 1—Introduction to the Allosteric Behavior of AMPA Receptors</b> .....	1
I. Ion channels.....	2
II. Ligand Gated Ion Channel Allostery.....	5
III. Structure and Function of the AMPA receptor.....	13
a. Glutamate Receptor Subtypes.....	13
b. Topology.....	14
c. Crystal Structures of the Isolated Ligand Binding Domain and Full Receptor.....	19
d. Cleft Closure and Activation.....	27
e. Dimer Interface Rearrangement and Desensitization.....	34
f. Significance.....	40
<b>Chapter 2—Electrophysiology of the AMPA Receptors</b> .....	42
I. The <i>Xenopus laevis</i> oocyte expression system.....	43



II. The Two-Electrode Voltage Clamp.....	49
<b>Chapter 3—Fluorescence Spectroscopy.....</b>	<b>53</b>
I. Introduction to Fluorescence.....	54
II. Fluorescence Resonance Energy Transfer.....	57
III. Lanthanide Resonance Energy Transfer.....	64
IV. Instrumentation.....	68
V. Anisotropy of the Fluorophores.....	69
<b>Chapter 4—LRET Part I: Cleft Closure Conformational Changes in the Ligand Binding Domain of a Functional AMPA Receptor.....</b>	<b>74</b>
I. Testing the Activation Hypothesis.....	75
II. Establishing LRET studies in a non-purified system.....	76
III. LRET Results and Discussion.....	88
a. Modified AMPA receptors.....	88
b. Receptor characterization by electrophysiology.....	91
c. LRET studies.....	94
IV. Future experiments.....	104
<b>Chapter 5—LRET Part II: Dimer Interface Rearrangement in a Functional AMPA Receptor.....</b>	<b>108</b>
I. Testing the Desensitization Hypothesis.....	109
II. Establishing LRET to study intersubunit distances.....	112
a. Labeling strategy.....	112
b. Receptor characterization by electrophysiology.....	118
III. LRET Results and Discussion.....	129

a. Intersubunit distance measurements for the states of the receptor.....	129
b. Mechanism for the resting, activated, and desensitized state.....	139
IV. Future experiments.....	142
<b>Chapter 6—LRET Part III: <math>\text{Ca}^{2+}</math> subdomain orientation of <math>\text{Na}^+/\text{Ca}^{2+}</math> exchangers.....</b>	<b>146</b>
I. $\text{Na}^+/\text{Ca}^{2+}$ exchanger Structure and Function.....	147
II. LRET Results and Discussion.....	148
<b>Chapter 7—Overall Conclusions.....</b>	<b>155</b>
<b>Appendix.....</b>	<b>164</b>
I. Molecular Biology.....	165
a. $\Delta\text{N}^+$ -AMPA receptors.....	165
b Primers for mutagenesis.....	165
c. mRNA synthesis.....	166
II. <i>Xenopus</i> Oocyte extraction and preparation.....	168
III. Pre-blocking and Expression.....	171
IV. Labeling oocytes (cells).....	172
V. Membrane Preparation.....	173
VI. Electrophysiology.....	174
VII. Radioactive Ligand Binding.....	175
VIII. Expression of the isolated LBD of GluR2.....	176
<b>Bibliography.....</b>	<b>177</b>

**Vitae.....196**

## List of Illustrations

<b>Figure 1</b> Various types of ion channels.....	3
<b>Figure 2</b> Two models of allostery shown, the MWC (concerted) model and the KNF (sequential) model.....	6
<b>Figure 3</b> Two mechanisms proposed for the conformational changes associated with ligand gated ion channels.....	11
<b>Figure 4</b> Subtypes of the eukaryotic ionotropic glutamate receptors.....	15
<b>Figure 5</b> Detailed schematic of AMPA receptor topology.....	17
<b>Figure 6</b> AMPA Receptor crystal structures.....	21
<b>Figure 7</b> Shown are the hypothesized states of the AMPA receptor in dimeric form.....	25
<b>Figure 8</b> Changes seen in the isolated LBD crystal structure and the functional response seen in the full receptor.....	28
<b>Figure 9</b> Receptor activation plotted as a function of cleft closure distance.....	32
<b>Figure 10</b> Shown are isolated LBD crystal structures or diagrams with mutations or allosteric modulators that can block desensitization.....	35
<b>Figure 11</b> Intersubunit distances of the different states of the receptor in the isolated LBD.....	38
<b>Figure 12</b> The <i>Xenopus laevis</i> expression system.....	44
<b>Figure 13</b> Western blots for optimizing the <i>Xenopus laevis</i> oocyte expression system.....	47
<b>Figure 14</b> The two-electrode voltage clamp.....	51
<b>Figure 15</b> The Jablonski Diagram.....	55

<b>Figure 16</b> Conditions for FRET.....	59
<b>Figure 17</b> FRET Efficiency versus Distance.....	62
<b>Figure 18</b> Terbium chelate excitation and emission spectrum.....	65
<b>Figure 19</b> A schematic representation of the anisotropy experiments.....	72
<b>Figure 20</b> A schematic representation of the experiments performed with the isolated LBD.....	78
<b>Figure 21</b> SDS-PAGE of GluR2 isolated LBD.....	81
<b>Figure 22</b> LRET lifetimes for the isolated LBD.....	84
<b>Figure 23</b> Diagram of the modified LRET experiments performed on modified AMPA receptors expressed in oocytes.....	89
<b>Figure 24</b> Functional studies of histag- $\Delta N^*$ -AMPA-S653C.....	92
<b>Figure 25</b> Membrane preparations of histag- $\Delta N^*$ -AMPA-S653C expressed in oocytes were collected before and after TAGZyme digestion.....	95
<b>Figure 26</b> LRET lifetimes for the Histag- $\Delta N^*$ -AMPA-S653C receptor.....	98
<b>Figure 27</b> Modified FRET/LRET as a molecular ruler.....	102
<b>Figure 28</b> Detailed schematic of stargazin topology.....	106
<b>Figure 29</b> AMPA receptor isolated LBD (GluR2-S1S2) crystal structure highlighting dimer interface conformational changes.....	110
<b>Figure 30</b> The modified GluR4 subunit of the AMPA receptor for LRET investigations.....	114
<b>Figure 31</b> Fluorophore control experiments.....	116
<b>Figure 32</b> Dose response curves for mutant and wild-type AMPA receptors.....	119

<b>Figure 33</b> Single channel recordings performed on membrane preparations of labeled, mutant receptors reconstituted in lipid bilayers.....	121
<b>Figure 34</b> Representative non-specific, background LRET for $\Delta N^*$ -GluR4-Th-S741-Th receptors expressed in HEK-293 cells.....	124
<b>Figure 35</b> Current traces from modified receptor subjected to LRET conditions to obtain various states of the receptor.....	127
<b>Figure 36</b> Sensitized emission measured at 510 nm for donor:acceptor tagged receptors expressed in oocytes.....	130
<b>Figure 37</b> Specific LRET signal obtained after background subtraction for donor:acceptor tagged receptors expressed in HEK-293 cells.....	132
<b>Figure 38</b> Sensitized emission measured at 488 nm for donor-only labeled $\Delta N^*$ -GluR4-S741 receptors expressed in oocytes.....	134
<b>Figure 39</b> Proposed mechanism for the resting, open, and desensitized state based on LRET investigations.....	144
<b>Figure 40</b> LRET measurements in the $Ca^{2+}$ regulatory domain of CALX1.1.....	151
<b>Figure 41</b> Proposed mechanism for activation, desensitization and inhibition by modulators.....	161

## List of Tables

<b>Table 1</b> Fluorescent Lifetimes and Distances for GluR2-LBD and Histag- $\Delta$ N*-AMPA-S653C Receptors.....	86
<b>Table 2</b> LRET lifetimes and calculated intersubunit distances.....	136
<b>Table 3</b> LRET lifetimes and distances between N-terminus His tag to different positions on CBD2.....	153

## Abbreviations

MWC model, Monod, Wyman and Changeux model

KNF model, Koshland, Nemethy, and Filmer model

AMPA receptors,  $\alpha$ -amino-5-methyl-3-hydroxy-4-isoxazolepropionate receptors,

NMDA receptors, *N*-methyl-D-aspartate receptors

LBD, ligand binding domain

D1, domain 1

D2, domain 2

GluA2<sub>cryst</sub>, Glutamate receptor, AMPA subtype 2, crystal structure

NMR, Nuclear Magnetic Resonance

FTIR, Fourier transform infrared spectroscopy

HEK-293 cells, human embryonic kidney-293 cells

HW, Unsubstituted willardiine

FW, Fluorowillardiine

IW, Iodowillardiine

FRET, Fluorescence Resonance Energy Transfer

LRET, Luminescence Resonance Energy Transfer

(Ni-NTA)<sub>2</sub>Cy3, Cy3 derivative of nitrilotriacetic acid chelate of nickel

GFP, green fluorescent protein

SDS-PAGE, sodium dodecyl sulfate polyacrylamide gel electrophoresis

CBD, Ca<sup>2+</sup> binding domain

NCX, Na<sup>+</sup>/Ca<sup>2+</sup> exchanger

CALX, *Drosophila* Na<sup>+</sup>/Ca<sup>2+</sup> exchanger

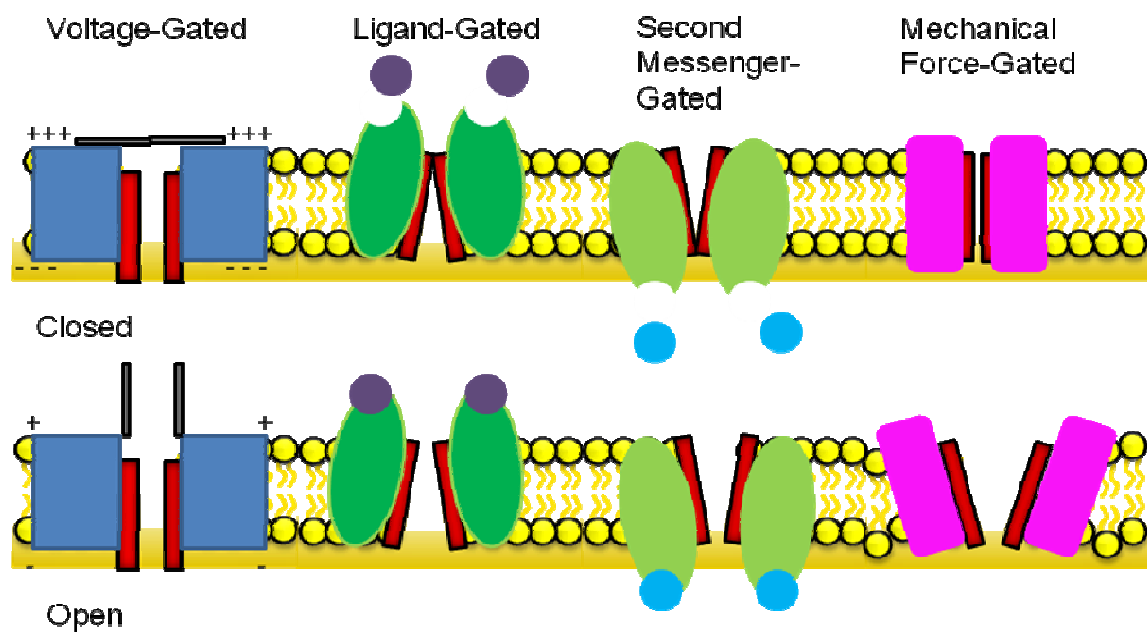


## **Chapter 1—Introduction to the Allosteric Behavior of AMPA Receptors**

## I. Ion channels

Ion channels are membrane proteins and function as a gateway for small, charged molecules called ions to pass across the cell membrane. Ion transport is essential for various physiological processes by controlling cell volume, allowing nutrients to enter the cell, and by generating electrical current. These proteins contain structural elements that are essential for their function. Ion channels are highly discriminatory for ions such as  $\text{Na}^+$ ,  $\text{K}^+$ ,  $\text{Ca}^{2+}$ , or  $\text{Cl}^-$  by way of a channel pore that serves as a selectivity filter. The ion channel gate opens and closes to control the flow of ions [1, 2]. As shown in Figure 1, ion channel gating can be regulated by an outside force such as membrane voltage, ligand binding, second-messenger binding, or mechanical force thus defining the different types of ion channels [1]. How an outside force causes a conformational change thus triggering a functional consequence is an essential question in ion channel studies. The detailed relationship between the structure and function of ion channels had remained unclear until 1998; Roderick Mackinnon solved the first structure for an ion channel [3]. The voltage-gated  $\text{K}^+$  channel structure revealed how the intricate pore confers its selectivity. Now with a multitude of ion channel structures available, insight into structure-function relationships has emerged. However, in spite of these detailed structures, questions still remain unanswered regarding membrane proteins in a physiologically relevant environment relating to protein dynamics, structural investigations of a functional ion channel, the role of ion channel regulatory proteins/modulators, and oligomerization, for example. In this dissertation, I used a molecular ruler (LRET, see Chapters 3-5) to determine structural changes due to

**Figure 1** Various types of ion channels. Voltage-gated ion channels respond to membrane voltage changes and open the gate (red). Ligand-gated ion channels respond to an extracellular ligand binding thus opening the gate. Second messenger-gated ion channels respond to intracellular second messengers such as  $\text{Ca}^{2+}$  to open the gate. Mechanical-force gated ion channels open when an outside force is applied [1].



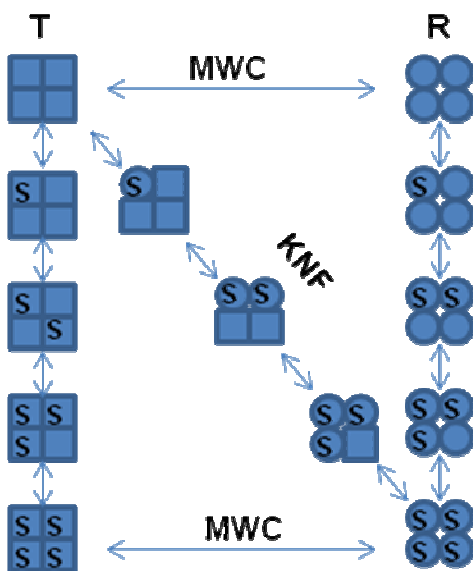
ligand binding in a functional ligand-gated receptor that ultimately lead to the gating of the ion channel.

## **II. Ligand Gated Ion Channel Allostery**

Two allosteric models, originally developed in the 1960s to describe enzyme regulation, have been proposed: the Monod, Wyman and Changeux model (MWC model) and the Koshland, Nemethy, and Filmer model (KNF model) [4, 5]. The two models were based on the idea of concerted as opposed to sequential events of allosteric proteins, respectively. These distinct models have been used to explain how conformational changes coupled to ligand binding and subunit interactions can lead to functional behavior of a protein [6], hence the molecular basis of allosterism.

In the MWC model as seen in Figure 2, allosteric proteins are oligomers of identical subunits and have at least one axis of rotational symmetry. For each subunit of the oligomer, there is only one binding site for the ligand (S). The idea of the equilibrium between two conformational states was introduced, where the discrete states are interconvertible ( $T \leftrightarrow R$ ) [4, 6, 7]. The states, named T for tense and R for relaxed, are in equilibrium at any homotropic ligated state due to a concerted transition of the protomers from one structure to the other, while still required to conserve their molecular symmetry; either squares or circles as in Figure 2. Here, the conformation of a single protomer is restricted by its association with the other protomers [4]. Ligand binding preferentially stabilizes the state in which the highest affinity for that ligand occurs. For example, the ligand binds to molecules in the T state with low affinity and R state with high affinity, so that the

**Figure 2** Two models of allostery shown, the MWC (concerted) model and the KNF (sequential) model. Each subunit has two tertiary conformations as shown by squares (low affinity) and circles (high affinity) caused by ligand (S) binding. Global conformation states are shown by T and R [6].



equilibrium is shifted toward the relaxed, high-affinity state. In the unligated state, the two states are thought to be in equilibrium. The modulation of the equilibrium by ligand binding is adequate in producing cooperative ligand binding [4, 6]. In the MWC model, several identical subunits are assembled into a cooperative and symmetrical quaternary structure. Conformational changes are thought to affect only the quaternary interactions between subunits as opposed to tertiary folding in each subunit [4, 6, 7]. There are no intermediate conformations in this model, and it cannot explain negative binding cooperativity, meaning that ligand binding does not promote subsequent binding [6].

In contrast, as seen in Figure 2 [6], the KNF model does not require equilibrium of quaternary structure; it describes how individual subunits (circles or squares) can switch states upon ligand binding. The transition from T state to R state occurs sequentially through intermediate states induced by ligand binding to individual subunits; this also influences neighboring subunits in the protein. It allows mixed tetramers in which some of the subunits are in their weak binding state (T) or strong binding state (R). Hence, each intermediate state has its mixed structure [5], as seen in the diagonal in Figure 2 [6]. The KNF model also suggests that in the absence of ligand, allosteric transitions do not occur [5]. In addition, this model can describe both negative and positive cooperativity. Negative cooperativity occurs when T-R interactions are stronger than T-T or R-R interactions. Positive cooperativity occurs when T-T and R-R interactions are stronger [8].

In the following years since the initial proposal of these allosteric models, it has become apparent that neither the KNF nor the MWC model can completely

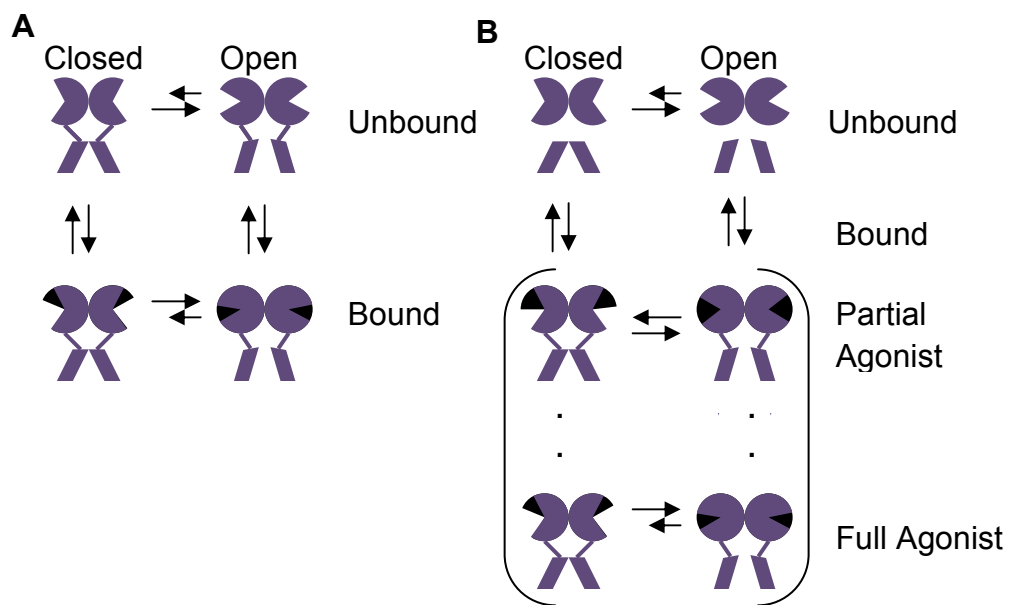


clarify the allosteric behavior of all proteins. Hence, more complex models have been developed and these models still retain some properties of the initial KNF and MWC models [9]. Due to the universal equilibrium concept and the simple formulation, the MWC model has allowed the behavior of many allosteric proteins using only a few parameters to be determined. On the other hand, the KNF model involves a more comprehensive understanding of the functional and structural properties of all the intermediates, as well as end states. Both models are simple representations that both propose an allosteric mechanism through the modification of equilibrium conformations of the protein induced by ligand binding. Additionally, these early models allow the basic parameters for allosteric proteins to be probed and tested and can lead to some initial insight into how subunit interactions and ligand binding are coupled to conformational changes in the context of regulatory behavior [10].

In terms of allosteric receptors, ligand-gated ion channels are allosteric membrane proteins with multiple subunits composed of a distinct ligand binding domain and functional ion channel domain. Agonist binding causes conformational changes that ultimately lead to the gating of the ion channel, or closed and open states [1]. The thought is that receptors can exist in a variety of discrete conformational states differing in the ability of that state to produce a response. More specifically, ligands can interact with the receptor in such a way as to control the conformational state. In the context of ligands, a full agonist can elicit a maximal response, and a partial agonist only elicits submaximal activation even at saturating concentrations.

In Figure 3, two mechanisms to depict allosteric protein behavior of ligand-gated ion channels are shown [11]. In Figure 3 A [11], the MWC model suggests that the receptor is in equilibrium between two conformations, closed (inactive) and open (active) [4, 7]. The MWC model assumes that conformational states exist independently of the ligand and that the ligand controls in which conformational state the receptor exists. Agonist binding stabilizes the receptor in the open conformation. The ligand can act as an agonist or partial agonist depending upon its affinity for open or closed state of the receptor and can stabilize the same conformation states. Full agonists stabilize the open state more effectively than the partial agonists, thus full agonists produce a greater activation as compared to partial agonists [12]. Competitive antagonists stabilize the closed state [4, 7]. In Figure 3 B [13], the KNF model, on the other hand, suggests that the ligand can induce new conformational states in the receptor [5]. A ligand acts as an agonist, partial agonist, or antagonist based on its ability to induce conformational states that are active or inactive. For instance, full agonists stabilize a conformation that fully activates the ion channel. In contrast, partial agonists elicit sub-maximal conformational changes that are not as effective in activating the channel, and hence partial agonists are not as effective in shifting the closed to the open equilibrium of the open state in the ion channel. Deactivation of the channel is the sequential reverse of activation [11]. These models help define the relationship between ligand binding and conformational changes of the receptor that trigger a response.

**Figure 3** Two mechanisms proposed for the conformational changes associated with ligand gated ion channels. (A) MWC, two-state model and (B) KNF, induced-fit model [11].



Ionotropic glutamate receptors are ligand gated ion channels that are suitable for studying allostery. These receptors couple agonist binding in the ligand binding domain to channel activation at the ion pore defined by the transmembrane domain [14]. The AMPA-subtype of the glutamate receptors are important excitatory neurotransmitter receptors in the mammalian central nervous system and have been the focus of many wide-ranging structural and pharmacological studies [14-16].

### **III. Structure and Function of AMPA Receptors**

Ionotropic glutamate receptors are the main excitatory neurotransmitter receptors in the mammalian central nervous system. When glutamate binds to the receptor, cations such as sodium, potassium, and sometimes calcium pass through the ion channel, facilitating the propagation of the synaptic signal [17-21]. These receptors have been implicated in learning and memory, the regulation of synaptic strength, as well as neuropathologies such as epilepsy, ischemia, and amyotrophic lateral sclerosis [22-30]. Additionally, glutamate receptors have been shown to engage in various functions outside the central nervous system [31-33]. The question that this dissertation will focus on is how does a small molecule like glutamate induce allosteric changes in glutamate receptors and in turn dictate function.

#### **a. Glutamate Receptor Subtypes**

Ionotropic glutamate receptors can be divided into three subtypes,  $\alpha$ -amino-5-methyl-3-hydroxy-4-isoxazolepropionate (AMPA) receptors, *N*-methyl-D-aspartate

(NMDA) receptors, and kainate receptors, based on their pharmacological properties in addition to sequence homology (Figure 4) [14]. Each subtype binds glutamate; however, NMDA is a full agonist for NMDA receptors, AMPA is a full agonist for AMPA receptors, and kainate is a full agonist for kainate receptors [16]. Although highly homologous, each subtype plays divergent roles in the mammalian central nervous system. NMDA receptors respond to changes in membrane potential as well as the required glutamate and co-agonist glycine in the synaptic cleft [34]. AMPA receptors are the primary mediators of fast excitatory synaptic transmission in response to glutamate, displaying fast kinetics [35]. Kainate receptors also play a role in neurotransmission, exhibiting modulatory functions in the pre- and post-synaptic cell [36].

#### b. Topology

Native channels formed by tetrameric AMPA receptors consist of four subunits, GluR1, -2, -3, and -4. Any of the subunits can form the AMPA receptor, and each subunit alone can form functional homomeric channels. The receptor's subunits assemble as back to back dimers [14, 15, 17, 37, 38]. In a single subunit, AMPA receptors have distinct domains including an extracellular N-terminal domain, an extracellular ligand binding domain, three transmembrane segments and a re-entrant loop that form the transmembrane domain, and an intracellular C-terminus, as shown in Figure 5 [17, 25, 39, 40].

The N-terminal domain (NTD) shows homology to the bacterial leucine-isoleucine-valine-binding protein (LIVBP), a periplasmic binding protein, and has

**Figure 4** Subtypes of the eukaryotic ionotropic glutamate receptors. The subunits that compose each subtype is shown [14].

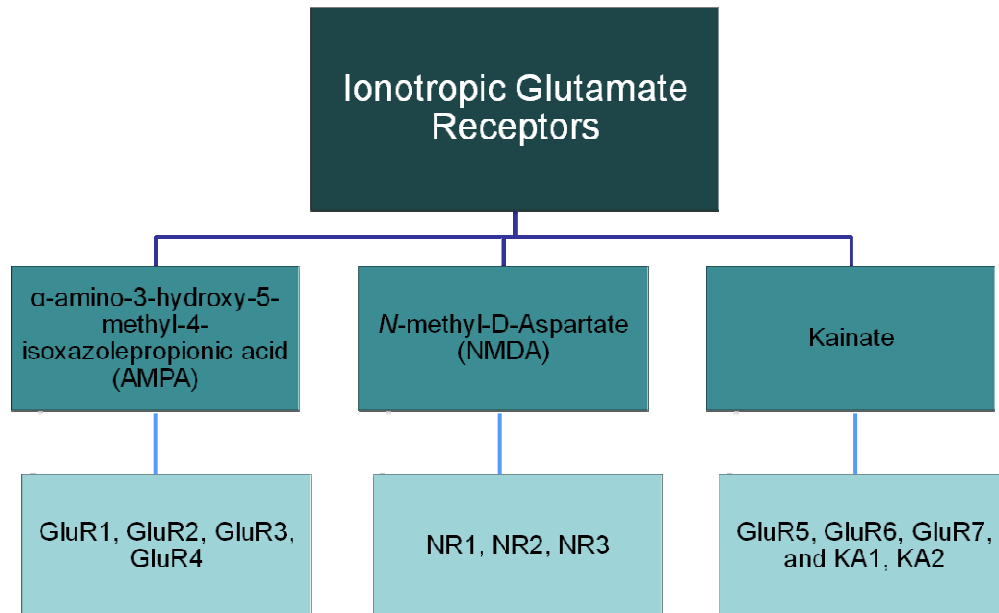
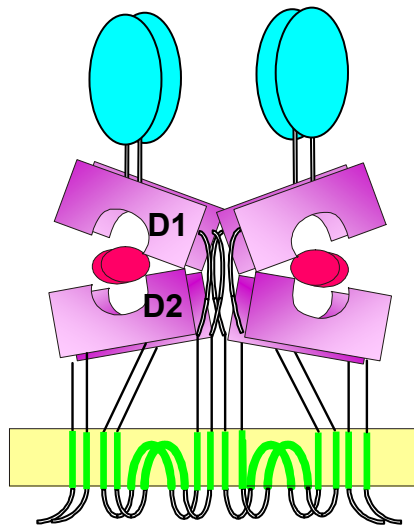


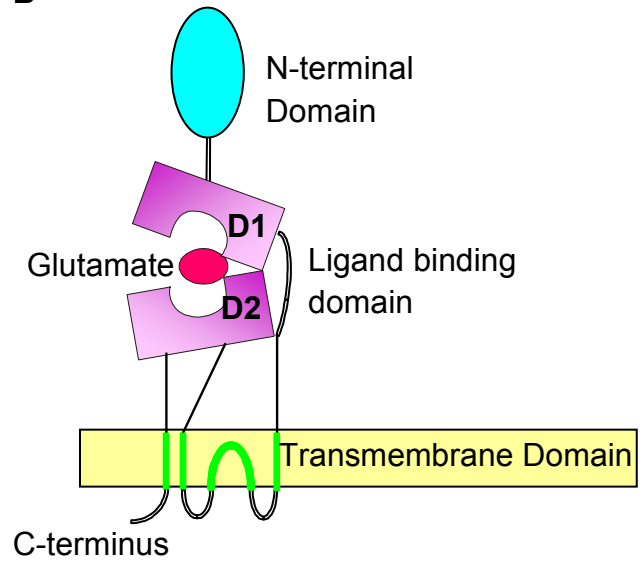


**Figure 5** Detailed schematic of AMPA receptor topology. (A) AMPA receptor tetramer. (B) A single subunit contains an extracellular N-terminal domain, an extracellular ligand binding domain, three transmembrane segments and a re-entrant loop that form the transmembrane domain, and a intracellular C-terminus.

**A**



**B**



structural similarity to the ligand binding domain of the metabotropic glutamate receptors. In NMDA receptors, the NTD binds to negative allosteric modulators, however, in AMPA receptors, no ligands or modulators for the NTD have been identified. The NTD functions in receptor assembly in AMPA receptors [41-50]. The ligand binding domain (LBD) of the AMPA receptors is formed by domain 1 (D1) and domain 2 (D2). The LBD domain has been excised and expressed as a soluble protein that has been crystallized in various ligated forms [42, 51]; the isolated ligand binding domain will be discussed in detail in the following section. The AMPA receptor transmembrane domain shares homology with other ion channel p-loop sequences and bears a resemblance to a flipped bacterial KcsA potassium channel pore, as seen in the Mackinnon's crystal structure. The pore sequence confers its selectivity properties [3, 52, 53]. The C-terminus varies in size and is an important site for modulation in targeting and localization of the receptor [54, 55].

### c. Crystal Structures of the Isolated Ligand Binding Domain and the Full Receptor

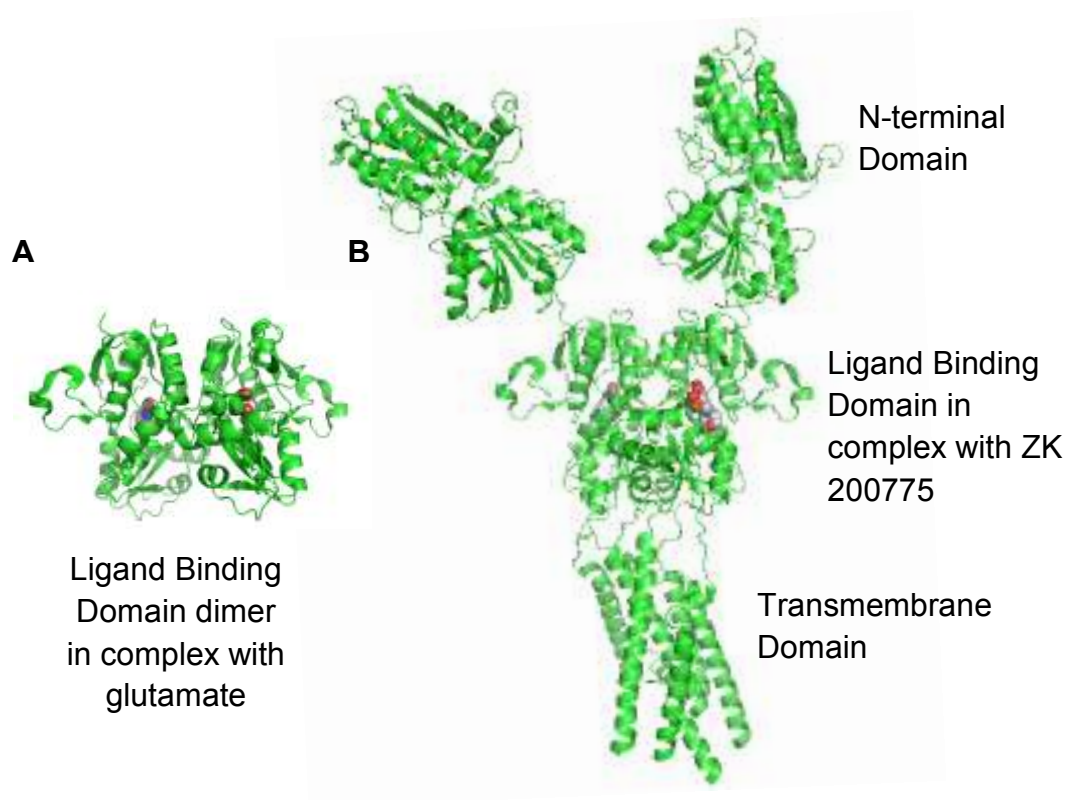
Until December 2009, the crystal structure of the full AMPA receptor had not been solved. Detailed structural investigations began by exploiting the modular characteristics of the AMPA receptor and producing a soluble construct of the GluR2 ligand binding domain formed by two polypeptide sequences, S1 and S2, that form domain 1 and 2 (D1 and D2) joined by a glycine-threonine linker. The isolated ligand binding domain protein was easily expressed in large quantities in a bacterial expression system and was shown to have a similar ligand binding affinity as the full receptor. Crystal structures of the isolated LBD have been obtained in the absence of ligand as well as in the agonist, antagonist, and allosteric modulator

bound states [17, 21, 56-61] . Figure 6 A shows the bi-lobed, cleft structure of the isolated ligand binding domain dimer in complex with glutamate [56]; the isolated LBD tends to crystallize as a dimer. The crystal structures of the isolated LBD of the AMPA receptor have been particularly useful in providing initial insight into the conformational changes in the ligand binding domain associated with functional transitions in the receptor; however, these structures are in the absence of the transmembrane segments, the primary functional portion of the protein.

Is the isolated LBD a good model for the full receptor? This question was partially answered by Sobolevsky et al.; a crystal structure of the full receptor was produced, GluA2<sub>cryst</sub> (Figure 6 B). The receptor was expressed in high quantities in infected Sf9 insect cells. In order to obtain GluA2<sub>cryst</sub>, many modifications were made on the full receptor to increase the resolution of the crystals, including point mutations, several amino acid deletions at the NTD and the C-terminus, and the removal of some of the predicted glycosylation sites. Optimization of the detergent as well as the addition of an antagonist further improved the resolution to 3.6 Å [62]. The determination of the structure revealed further insight into the mechanism of activation and desensitization of these receptors similar to what is observed in the isolated LBD.

As described previously, the full length glutamate receptor is modular, where each of the domains in a single subunit is stacked in layers with the NTD on top, followed by the LBD, and the transmembrane domain at the base. The NTD forms a clam-shell similar to the LBD, and they are connected by linker regions. Additionally, the LBD domain is connected to the transmembrane domain by linker

**Figure 6** AMPA Receptor crystal structures. (A) Isolated ligand binding domain dimer in complex with glutamate [56]. (B) Full length AMPA receptor dimer, GluA2<sub>crist</sub> in complex with ZK 00775 [62].



regions [62]. This arrangement revealed by the crystal structures suggests that conformational changes at the NTD would affect the conformation of the LBD and in turn the transmembrane domain, affecting the function of the channel. Although this has not been shown in the AMPA receptors, several structural implications from NMDA receptor electrophysiological studies have been revealed [41-50]. Drugs binding to the NTD cleft in NMDA receptors have been shown to affect the function of the channel; drugs binding to the AMPA receptor NTD have yet to be identified. These implications will be further discussed in the Chapter 7.

Moreover, the receptor has a distinctive symmetry and subunit arrangement. The extracellular domains have an overall two-fold axis of symmetry that relates one of the NTD dimer to the other dimer, one LBD dimer to the other dimer, and half of the transmembrane domain to the other dimer. However, the transmembrane domain has an approximate four-fold axis of rotational symmetry, resulting in a breakdown of symmetry. In addition to the dimer subunit interactions, there are extensive interactions across the dimer for both the NTD and the LBD. Interestingly, there is a subunit crossover between the NTD and LBD, where a LBD domain in a single subunit is associated with dimer 1, and the NTD of that same subunit is associated with dimer 2. The crossover could provide a reason as to why the NTD is important for receptor assembly and stability [62].

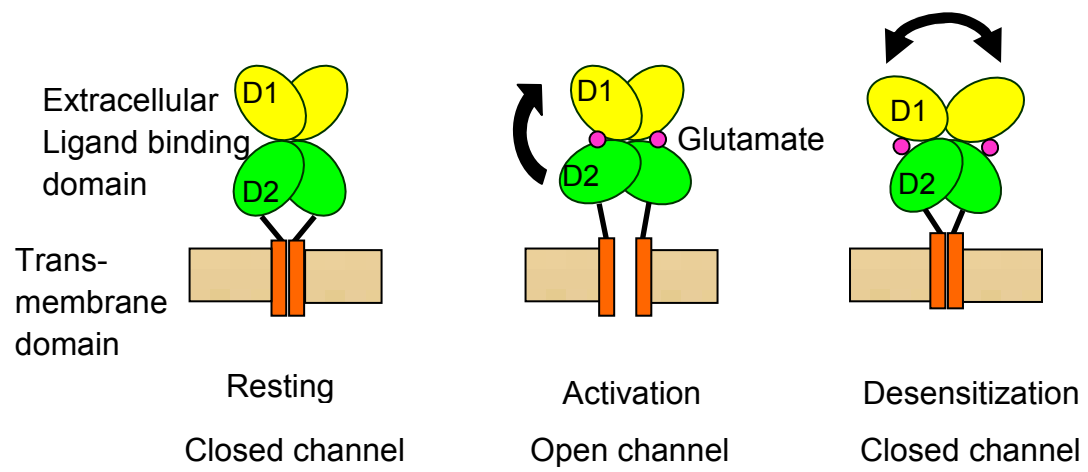
Next, the full-length crystal structure reveals that the transmembrane domain consists of three transmembrane segments (M1, M3, and M4) and a re-entrant loop (M2), as shown in Figure 6 B. M1 is the first transmembrane segment linked to S1 of the LBD on the outside of the transmembrane domain. M2 is found within the

pore, and M3 lines the pore and is connected to S2 of the LBD. M4 is on the outside of the transmembrane domain and is connected to S2 of the LBD. It is hypothesized that ligand binding results in a conformational change that leads to the separation of the regions that link the LBD to the transmembrane domain and pulls apart the M3 segment lining the pore resulting in channel opening, as discussed in the next section [62].

Based on the crystal structures and functional studies, the hypothesized mechanism for activation and desensitization is shown in Figure 7 [61]. As previously mentioned, the ligand binding domain crystallizes as a dimer, and the dimer interface is formed by contacts in D1. D2 is flexible in order to respond to ligand binding. In the resting state of the protein, the dimer interface is coupled, no ligand is bound, and the channel is closed. In addition to crystal structures, small-angle X-ray scattering, NMR (nuclear magnetic resonance), and time-resolved FTIR (Fourier transform infrared spectroscopy) have been performed on the isolated ligand binding domain to describe the movement of D1 and D2 upon ligand binding. These studies suggest that during activation, the agonist binds to D1, and then the flexible D2 responds to the ligand binding and moves up towards D1 [63-65]. This is the closed-cleft conformation stabilized by ligand binding as discussed in the next section. The movement of D2 towards D1 is thought to pull apart the linkers to the channel thus changing the orientation of the transmembrane domain leading to the opening of the ion channel. Upon prolonged presence of glutamate, these receptors desensitize. In the desensitized state, stress on the linker regions results in the decoupling of the dimer interface leading to channel closure [56, 66].



**Figure 7** Shown are the hypothesized states of the AMPA receptor in dimeric form. In the apo state, there is no ligand bound, and the ion channel is closed. For activation, a ligand such as glutamate binds to the extracellular ligand binding domain, and D2 moves up towards D1. This movement pulls the linker to the transmembrane segments apart thus opening the channel. In the desensitized state, stress on these linker regions results in the decoupling of the dimer interface leading to channel closure [61].

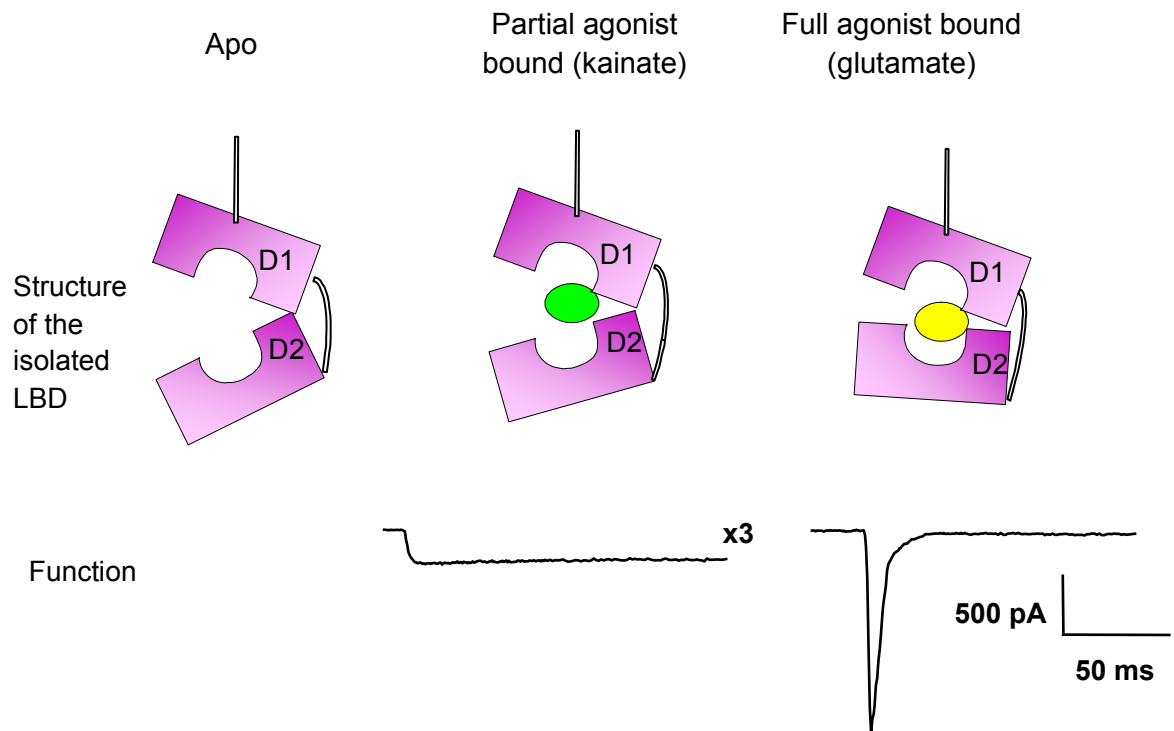


Despite the invaluable information obtained from detailed structures of the isolated ligand binding domain and the intact receptor, are the crystal structures true representations of the conformational changes seen in the ligand binding domain of a functional receptor? I will address this question in this dissertation by studying conformational changes in the ligand binding domain of a functional receptor in its dynamic state.

#### d. Cleft Closure and Activation

Ligand binding alters the conformational state of the AMPA receptor and produces a functional response, thus describing ligand-gated ion channel allostery. A comparison of structures of the isolated ligand binding domain of the AMPA receptor in complex with various ligands has revealed insight into the allosteric behavior of these receptors. These structural studies in conjunction with functional studies have provided insight into how ligand binding is coupled to receptor activation, as shown in Figure 8. In the apo state, the cleft is fully open, and no current is elicited. Partial agonists, such as kainate, lead to an intermediate cleft closure (~12 degrees more closed compared to the apo state) with less activation of the receptor, represented as the peak current elicited from HEK-293 cells. In Figure 8, glutamate, a full agonist of the receptor, results in a large degree of cleft closure (~20 degrees more closed compared to the apo state) and greater activation of the receptor when bound. Competitive antagonists stabilize the ligand binding domain in the open cleft conformation, similar to the apo state, due to steric hindrance, thus preventing channel opening [56, 59, 60, 67]. Together, this data suggests that there

**Figure 8** Changes seen in the isolated LBD crystal structure and the functional response seen in the full receptor. The extent of cleft closure correlates to the extent of receptor activation [56, 59, 68].



is a strong correlation between the extent of cleft closure and the extent of activation of the ion channel.

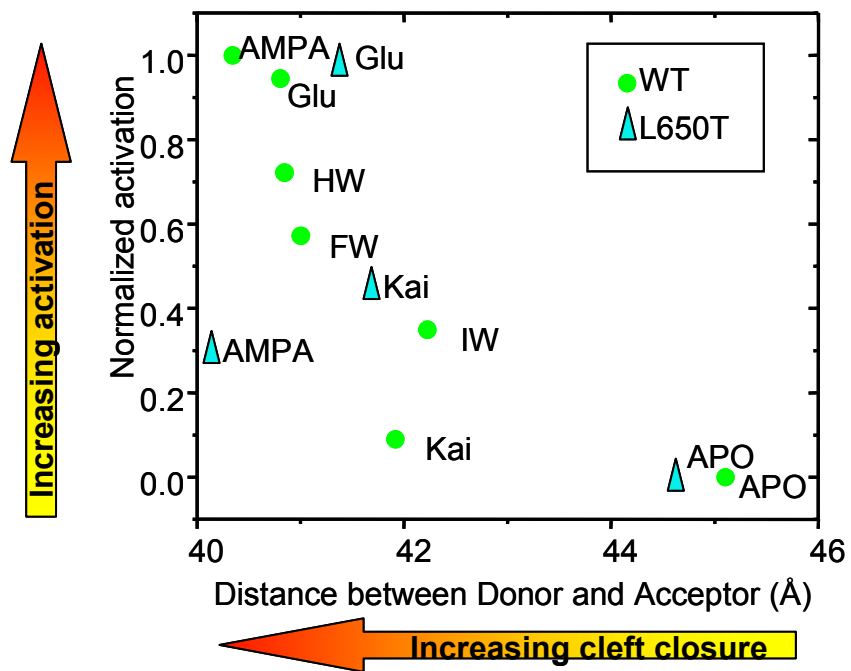
A study of partial agonism by Jin et al., has shed some light onto how agonists with varying efficacies induce different conformations, hence suggesting the KNF model, or a multistate induced fit model [5]. Jin and coworkers used a series of 5-substituted willardiines as a tool to investigate the molecular basis of partial agonism for AMPA receptors [59]. The willardiine study allowed subtle and graded conformational changes in the ligand binding domain due to their partial agonist characteristics to be correlated with the changes in the activity of the ion channel. Here, the increasing size of the substituent gave gradually smaller macroscopic currents ( $H > F > Br > I$ ) as measured by electrophysiology, so the size of the substituent is correlated to its ability to activate the channel. The induced fit model suggests that partial agonists elicit sub-maximal conformational changes that are not as effective in activating the channel, which was then investigated by structural studies. Compared to glutamate, the partial agonists exhibited less cleft closure. Thus, the increasing size of the 5-substituent yields an increasing degree of cleft closure [59]. Each partial agonist induces a distinct conformation, which also suggests the KNF induced fit model [5]. Using single channel recordings, subconductance states have been found to vary depending on the characteristics of the agonist. Thus, the degree of cleft closure determines an individual subunits response the ligand binding and ultimately ion channel opening. So, each subunit's opening can then contribute to the opening of higher

subconductance states as it becomes more favored as the coupling efficiency increases between ligand binding and activation of the channel [59].

Additionally, mutagenesis has also been used to investigate the allosteric mechanism of AMPA receptor activation, and one mutant has been found to be an exception to the current hypothesis for activation. Based on the crystal structures, it is thought that kainate acts as a partial agonist because it is sterically hindered between residues Y450 and L650 as it tries to enter the LBD [56, 57]. Mutations at these residues result in a wide range of activations by agonists and mutations to smaller, flexible amino acids are expected to increase the activation of kainate [11, 56, 69]. Previous studies of the L650T mutation in an AMPA receptor have been shown to have a higher activation in response to kainate and a decreased activation by AMPA relative to the wild-type receptor [70]. Studies using LRET as a molecular ruler in the Jayaraman laboratory have measured cleft closure distances of the isolated LBD protein in various ligated states as well as in the presence of mutations. Activation of the receptor is plotted as a function of cleft closure as measured by LRET, or distance between a donor and acceptor fluorophores, shown in Figure 9 [70, 71]. In the wild-type, a similar trend with the crystal structure data for cleft closure is followed. In the L650T mutant, kainate binding results in a greater amount of cleft closure than the wild-type displayed by the increased activation for kainate. However, AMPA in the L650T mutant results in decreased activation yet has cleft closure greater than that of glutamate, which induces much larger currents than AMPA [70]. The data with the L650T mutation contradicts the hypothesis that cleft closure alone determines the extent of activation. This study might suggest

**Figure 9** Receptor activation plotted as a function of cleft closure distance. Wild-type AMPA receptor (green circles) data shown in response to AMPA, glutamate, 5-substituted willardiines (HW, unsubstituted; FW, fluorowillardiine; and IW, iodowillardiine), kainate, and the apo state. L650T (cyan triangles) data shown in response to AMPA, glutamate, kainate, and in the apo state [70, 71].



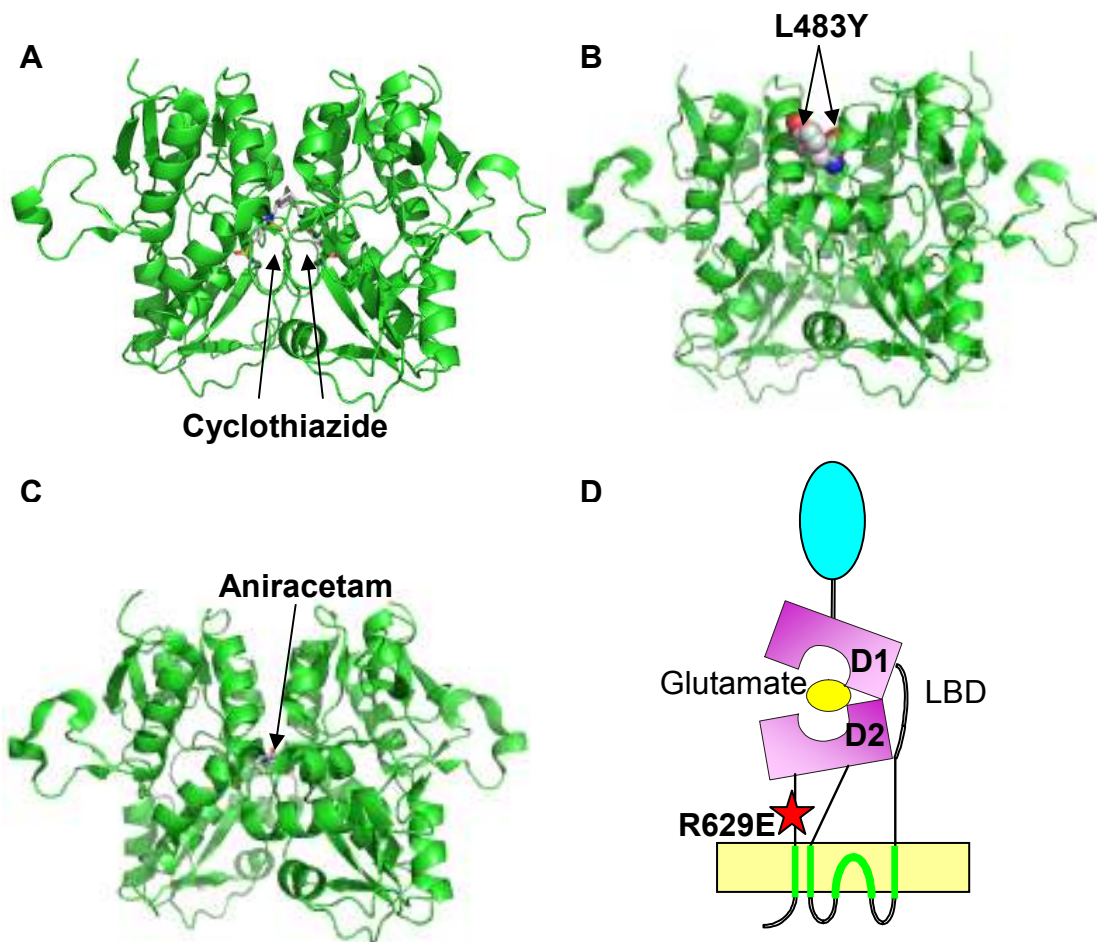


that there is another mechanism that controls receptor activation. However, it is not clear if the L650T mutation results in a change in the allosteric mechanism or if the contradictory results are due to the fact that the mutant was studied in the isolated LBD and would behave differently in the context of channel segments. This is yet another example as to why it is important to study conformational changes seen in the isolated ligand binding domain in a functional receptor in a dynamic state.

#### e. Dimer Interface Rearrangement and Desensitization

Glutamate binding to the LBD induces a closed cleft conformation and decreases the stability of the coupling of the dimer interface resulting in dimer interface rearrangement to relieve the stress placed on the linkers to the transmembrane domain. Once the dimer interface decouples, the transmembrane domain can then relax to a more stable conformation, a closed ion channel [61]. Additionally, the stability of the dimer interface can control the stability of the open channel. Several mutations and allosteric modulators have been found to block desensitization, as shown in Figure 10. Crystal structures of the isolated LBD have revealed that cyclothiazide, an allosteric modulator, and mutations in the dimer interface, such as L483Y, that stabilize the dimer interface block the entrance to the desensitized state [61, 72-74]. Other allosteric modulators such as aniracetam can act by stabilizing the open state, closed cleft conformation when a ligand binds [75]. In addition, a mutation outside the LBD was also found to affect desensitization. The R629E mutation is located in the segment connecting the ligand binding domain to the transmembrane segments [76]. No structural information exists for this mutant currently; hence, it is still not clear how this particular mutation, R629E, blocks

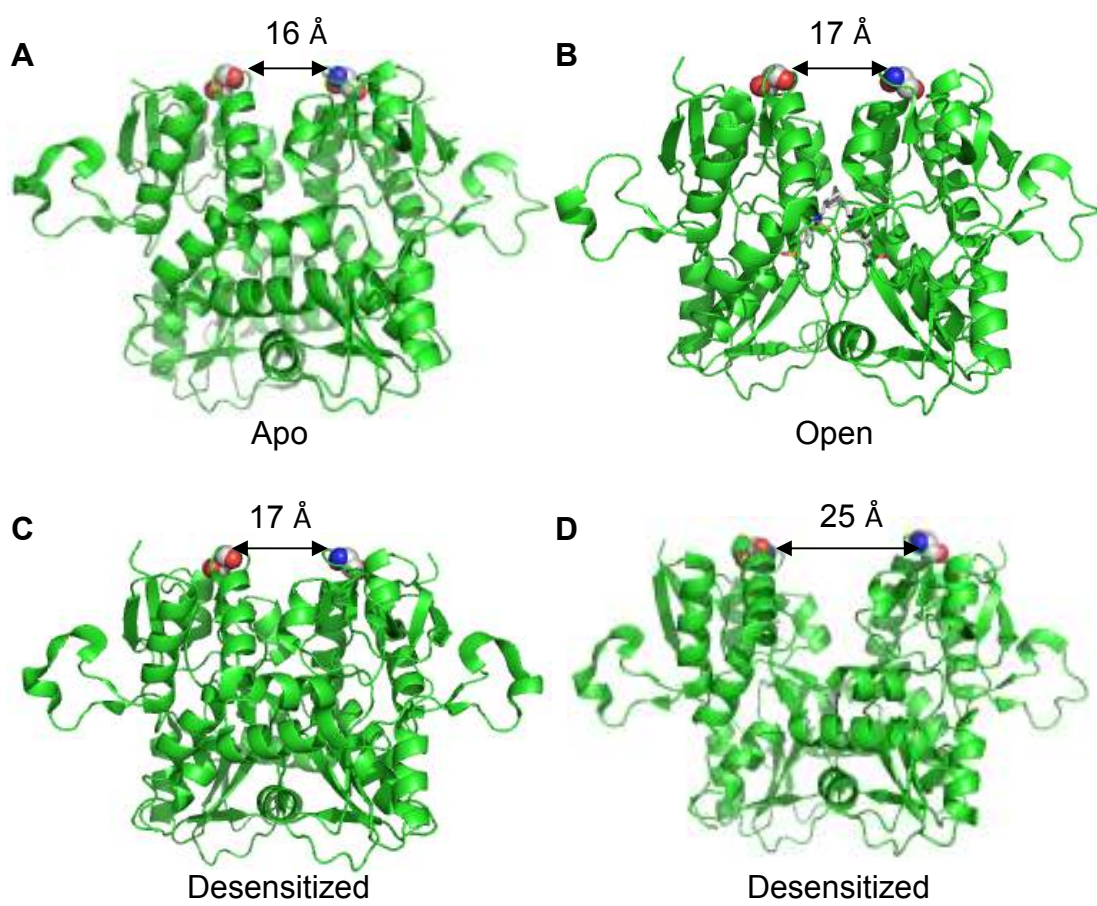
**Figure 10** Shown are isolated LBD crystal structures or diagrams with mutations or allosteric modulators that can block desensitization. (A) Two molecules of cyclothiazide bind to the isolated LBD to stabilize the dimer interface. (B) L483Y makes favorable interactions across the dimer to keep the dimer interface intact. (C) Aniracetam binds and stabilizes the closed cleft conformation. (D) R629E is a mutation outside the LBD and blocks desensitization by an unknown mechanism [72-74, 76].



desensitization. Does the mutation allosterically strengthen the dimer interface, or is the dimer interface decoupled as observed in the wild-type protein but the decoupling is not communicated to the channel segments due to the mutation? Structural investigations in a functional receptor are needed in order to answer these questions. Moreover, desensitization can be increased by introducing mutations in the LBD that reduce steric hindrance of an agonist in the LBD thus enhancing cleft closure and consequently destabilizing the dimer interface [11, 64, 77].

Furthermore, the isolated LBD crystallizes as a dimer in all states as shown in Figure 11 A-C, and until recently there has been no structural information for the desensitized state [21]. However, an in depth study by Armstrong et al. has indirectly shown structural aspects of desensitization in a full receptor via electrophysiology experiments as well as in artificially decoupled crystal structures of the isolated LBD. Armstrong and coworkers began by introducing cysteines at the dimer interface of a full receptor and measuring the rate at which modification by MTSES ((2-sulfonatoethyl) methane thiosulfonate) occurs in various states of the receptor. One mutant, E486C, proved to be more accessible in the desensitized state compared to the resting (antagonist-bound) state and open state. Structural information for the apo state was not obtained because this state has no functional consequence. The next step was to introduce various sized bi-functional crosslinkers in order to confine the dimer interface at different lengths and measure the functional response to report the state of the receptor. It was shown that short crosslinkers restrict dimer interface rearrangement and confine the receptor to a

**Figure 11** Intersubunit distances of the different states of the receptor in the isolated LBD. (A) In the apo state isolated LBD, there is an intersubunit distance of 16 Å between sites S741C suggesting that the interface is coupled. (B) In the open state, when glutamate and cyclothiazide is bound, the interface is coupled at a distance of 17 Å. (C) When glutamate is bound in the desensitized state, the isolated LBD shows a coupled interface at a distance of 17 Å. (D) In the S729C mutant, the artificially decoupled desensitized-like state shows a decoupled interface at a distance of 25 Å [56, 58, 74].



non-desensitizing state, and longer crosslinkers allow the dimer interface to decouple. Overall, Armstrong reported an intersubunit distance change of around 13 to 16 Å from the open to the desensitized state. Interestingly, the S729C mutation, introduced deep in the dimer interface of the isolated LBD to artificially force the dimer apart, has been showed to be locked in a desensitized state as determined by electrophysiology. As seen in Figure 11 D, a recent structure of this mutant shows that the dimer interface is decoupled, consistent with the current hypothesis for desensitization [58]. However, all of the current structural inferences for the mechanism of desensitization are based on the structures of the isolated LBD in the context of the functional studies on the full receptor. Additionally, because the desensitized state structure has been acquired by artificially decoupling the dimer interface, this could lead to a more decoupled state than what is observed in a physiologically relevant state. What is needed to complete the picture is a study of the conformational changes in the presence of the transmembrane segments, particularly since desensitization involves more than a single subunit of the receptor and is stabilized due to the fact that the transmembrane domain exerts the stress leading to decoupling of the dimer interface.

#### f. Significance

Currently, crystal structures provide the foundation for the hypothesized conformational changes in the ligand binding domain; however, these structures are limited by crystallographic constraints [21, 56-61, 63, 68, 78]. In order to understand how agonist binding is coupled to channel activation and



desensitization, it is essential to study changes in the ligand binding domain in a dynamic state. Overall, the objective of these investigations is to determine the structural changes in the receptor that drive the transition between the resting, activated, and desensitized state by measuring the conformational changes in the ligand binding domain of a functional AMPA receptor. Studies to investigate the structure-function relationship of a functional AMPA receptor will be performed by using biophysical techniques such as LRET (luminescence resonance energy transfer) and electrophysiology, in addition to using a series of agonists and mutations. In this dissertation, I show the conformational changes induced by the agonist that consequently lead to ion flow in a functional AMPA receptor and compare the data with the current hypotheses for activation and desensitization.

## **Chapter 2—Electrophysiology of the AMPA receptors**

## **I. The *Xenopus laevis* oocyte expression system**

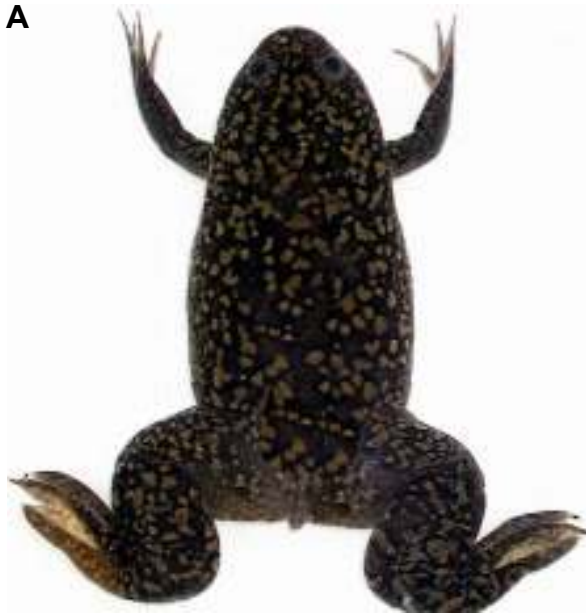
The *Xenopus laevis* oocyte is an unfertilized egg cell from the African clawed frog, shown in Figure 12. The frog itself is easily maintained and can produce oocytes throughout the year; thousands of oocytes can be extracted from a single frog. The *Xenopus* oocyte was first shown to express functional ion channels and receptors by Miledi et al. in 1982 [79], and since then have become a well-established expression system in the area of biophysics for the study of ion channels.

*Xenopus* oocytes are large cells, around 1 mm in diameter with a nucleus around 300  $\mu\text{m}$  across. These cells are arrested during the first meiotic prophase and can survive for around one week in an isotonic saline solution in the presence of antibiotics. Their size makes them convenient for manipulations such as injection of RNA or DNA and electrophysiology experiments. By injection of RNA/DNA encoding for the protein of interest, the *Xenopus* oocytes are able to translate the exogenous RNA/DNA messages [80] and traffic the protein to the plasma membrane. The *Xenopus* oocytes have a high capacity for protein synthesis, around 200 to 400 ng per day per oocyte. Remarkably, the oocyte allows for many post-translational modifications needed for protein function. Additionally, the *Xenopus* oocyte correctly assembles and orients multiple subunits into a functioning protein.

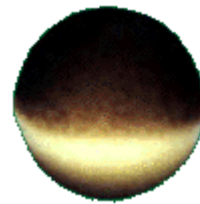
However, there are some limitations of the *Xenopus laevis* oocyte expression system. First, it is a transient expression system, and there is variation in expression across batches of oocytes, which could affect expression studies when

**Figure 12** The *Xenopus laevis* expression system. (A) Female African clawed frog, about 10-12 cm long. (B) An oocyte, about 1 mm in diameter. The oocyte has two poles, the animal pole (brown) and the vegetal pole (white).

**A**



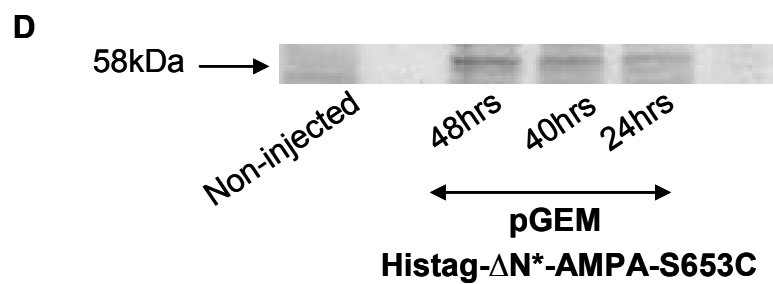
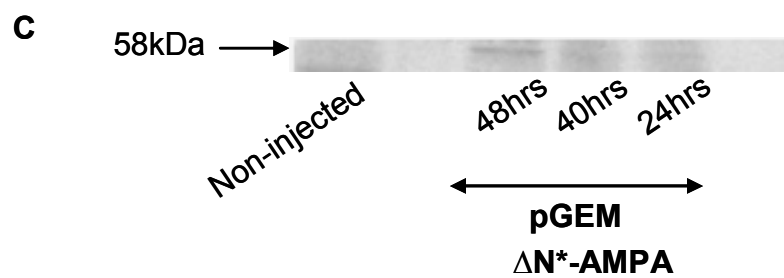
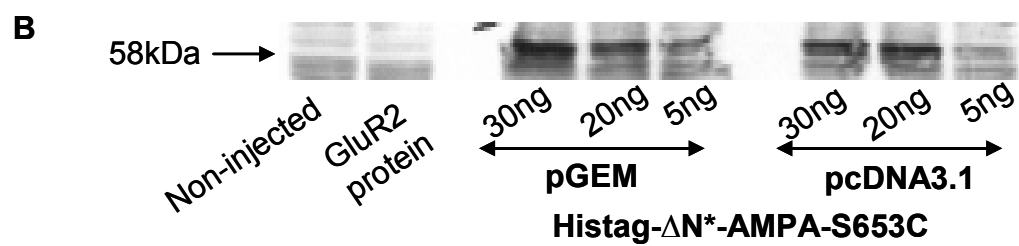
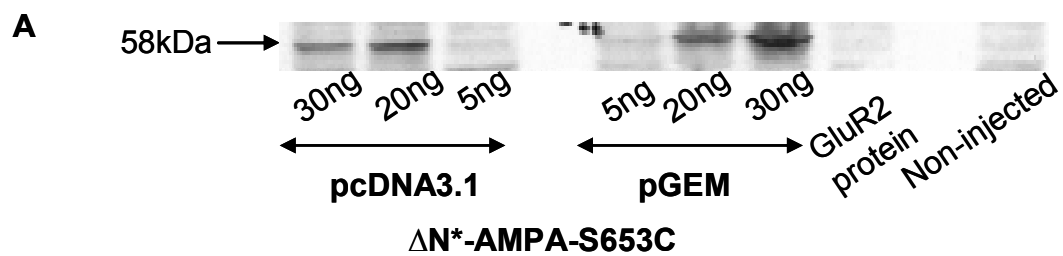
**B**



optimizing the system. Most importantly, endogenous proteins could be expressed that could interfere with the protein of interest [81, 82].

These limitations would prove to be critical when optimizing the expression system for future biophysical studies. First, the amount of RNA to inject into each oocyte and the expression pattern of the oocyte had to be determined. Optimizing was performed by testing different expression vectors (pcDNA3.1 and pGEM-HE) and by injecting various concentrations of RNA for two of the proteins of interests; cell lysates were collected and a Western blot was performed, as shown in Figure 13 A-B. After that, time points for expression for two of the proteins that would be used for future LRET studies were determined by Western blot, as shown in Figure 13 C-D. The final crucial step was to establish how to control the expression of the protein of interest without also increasing the background expression of the inherent proteins of the oocyte that could potentially interfere with the LRET studies, as discussed in the next chapter. For the LRET studies, the protein of interest would contain cysteine modifications for the attachments of fluorophores, so any inherent cysteines from the oocyte would contribute to non-specific LRET signals. Not only were the oocytes a robust expression system for the AMPA receptors, but the oocytes could be manipulated further for the LRET experiments. A pre-blocking procedure had successfully been used on oocytes expressing potassium channels to block inherent cysteines [83]. Using a similar pre-blocking procedure for oocytes expressing AMPA receptors, further optimization was performed and the background, non-specific signal was successfully decreased (see Appendix III for pre-blocking and expression protocol).

**Figure 13** Western blots for optimizing the *Xenopus laevis* oocyte expression system. Cell lysates from 5 oocytes were loaded per well and Anti-GluR4 pAb (Chemicon) was used as a probe for the protein of interest. For the expression studies, (A)  $\Delta N^*$ -AMPA-S653C and (B) Histag- $\Delta N^*$ -AMPA-S653C protein was collected after 24 hours of expression. RNA (30 ng) encoding for (A)  $\Delta N^*$ -AMPA and (B) Histag  $\Delta N^*$ -AMPA-S653C was injected and collected for time point studies.





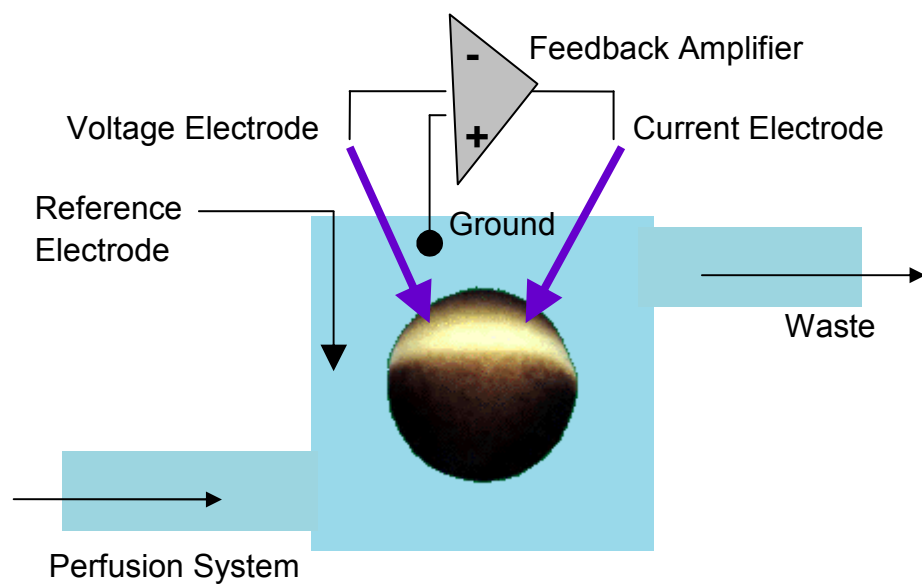
## **II. The two-electrode voltage clamp**

Much of what is known about the properties of ion channels in cell membranes has come from experiments using a voltage clamp, which allows the control of membrane potential in order to measure ion flow as electrical currents. This method was first developed by Cole et al. (1949) and Hodgkin et al. (1952) for use with the squid giant axon [84-86]. Since then, many variations of the technique have been developed, namely the two-electrode voltage clamp—the focus of the rest of this chapter. Now that the oocyte expression system had been established for the AMPA receptor, the protein function could be characterized by this technique.

Oocytes are biological circuits, and as mentioned previously, the voltage clamp controls the membrane potential of the oocyte. The membrane potential is measured in volts, and voltage ( $V$ ) is attained by the charge separation across the membrane. Current ( $I$ ), on the other hand, is generated by the movement of ions across the membrane. The basic configuration of the two-electrode voltage clamp is shown in Figure 14 [87]. First, two electrodes are impaled into the oocyte. One electrode is the voltage electrode, where the membrane potential is measured relative to the ground. The second electrode is the current electrode, which is capable of injecting current into the oocyte. A holding voltage, or command potential is set ( $-60$  mV) and the voltage clamp uses negative feedback to maintain the oocyte at this voltage. Whenever the oocyte deviates from the holding voltage (as in a ligand is added, the channel opens, and ions flow through), the feedback amplifier detects the difference between the command potential and the membrane

potential of the oocyte. It then subtracts the membrane potential from the command potential, and sends out an output signal to the current electrode in order to maintain the holding potential. The signal equal and opposite to the ionic current is produced and this can be measured, giving an accurate reproduction of the currents flowing across the membrane [81, 87]. These type of experiments are performed for each AMPA receptor expressed in oocytes that has been modified for the LRET experiments in order to establish that the mutations such as cysteine modifications or the additions of histidine tags do not perturb the function of the receptor.

**Figure 14** The two-electrode voltage clamp. The system allows control of the membrane potential in order to measure ion flow as electrical currents. The oocyte sits in a small-volume chamber where ligands can be perfused quickly and removed to the waste [87].



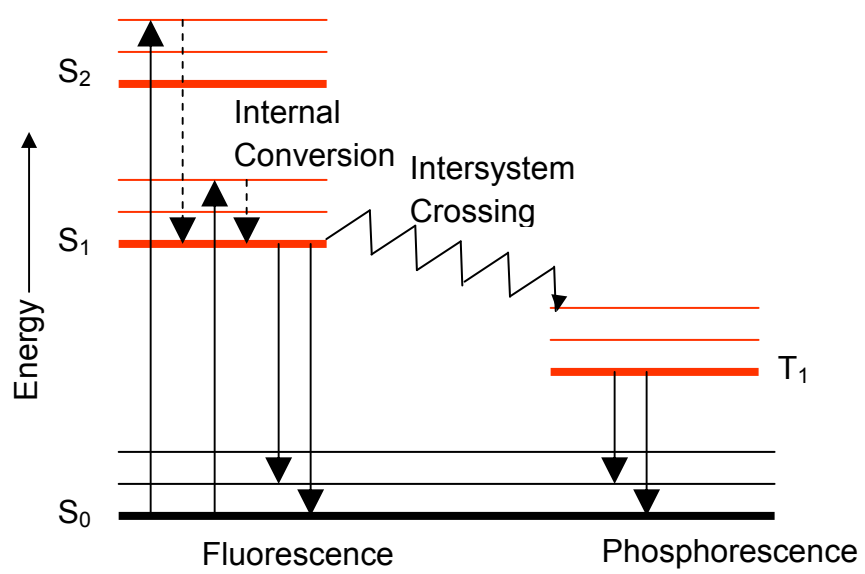
## **Chapter 3— Fluorescence Spectroscopy Methods**

## I. Introduction to Fluorescence

Luminescence is defined as the emission of light by a molecule due to either chemical, mechanical, or physical processes. Photoluminescence, or luminescence due to ultraviolet and visible (UV-Vis) light used to excite a molecule, can be subdivided further into fluorescence and phosphorescence [88]. An introduction to fluorescence is provided here in order to describe the foundation of the fluorescence spectroscopy technique used in this dissertation. Fluorescence spectroscopy is an important tool in biological studies with uses ranging from the detection of a protein to investigations of the structure of a protein.

In order to describe fluorescence and phosphorescence, the two processes are depicted by the Jablonski diagram as seen in Figure 15 to show the various energy levels involved [89]. When a molecule at ground state ( $S_0$ ) absorbs a photon of energy, it is excited to one of many vibrational states of a higher energy electronic state ( $S_1$  or  $S_2$ ). Excitation occurs on the femtosecond timescale. Next, the excited state electrons relax to the lowest energy level by internal conversion/vibrational relaxation on the picosecond timescale. On the nanosecond timescale, decay to the ground state ( $S_1$  to  $S_0$ ) and release of a photon describes fluorescence. The excitation energy is greater than the emission energy due to the loss of energy during this process, thus the excitation wavelength is shorter than the emission wavelength; this principle is referred to as Stoke's shift. The timescale for a molecule to absorb a photon at a particular wavelength and emit a photon at a longer wavelength is the fluorescence lifetime. During phosphorescence, however, the excited electron can go through intersystem crossing from the  $S_1$  to the triplet

**Figure 15** The Jablonski Diagram [89]. Upon the transition from  $S_1$  state to  $S_0$  state, fluorescence occurs. After intersystem crossing, upon the transition from the forbidden  $T_1$  state to  $S_0$  state, phosphorescence occurs [88].





state  $T_1$ , and then transition from the  $T_1$  state to the  $S_0$  state, a forbidden transition. Thus, phosphorescence occurs on the millisecond timescale, much slower than fluorescence.

Molecules that are capable of fluorescence are also known as fluorophores. Fluorophores can be classified by their excitation and emission properties, which stem from their molecular structure [88]. The organic dyes that are used in this work include ATTO465-maleimide and  $(\text{Ni-NTA})_2\text{Cy3}$ , which contain a rigid ring structure capable of fluorescence and do not phosphoresce. The maleimide-derived fluorophores is commercially available, and the Ni-NTA derivative of Cy3 is synthesized (as described in Kapanidis et al. [90]); the fluorophores are easily attached to the protein of interest by chemical modification. The organic dyes will serve as acceptor molecules tagged to the protein of interest for future structural studies, in which their fluorescent properties will be exploited. The lifetime of these fluorophores when excited are on the nanosecond timescale; these short-lived lifetimes is an advantage for the temporal resolution of lifetimes discussed later in this chapter. Another advantage of using these organic dyes include high quantum yields, or the ratio of photons emitted to the photons absorbed, which makes these molecules very bright. These molecules also have high extinction coefficients as well as broad emission spectra [88].

## **II. Fluorescence Resonance Energy Transfer**

Fluorescence Resonance Energy Transfer (FRET) is a technique that is commonly used to measure distances between two points separated by approximately 15 to 100 Å, and has been widely used to study large scale

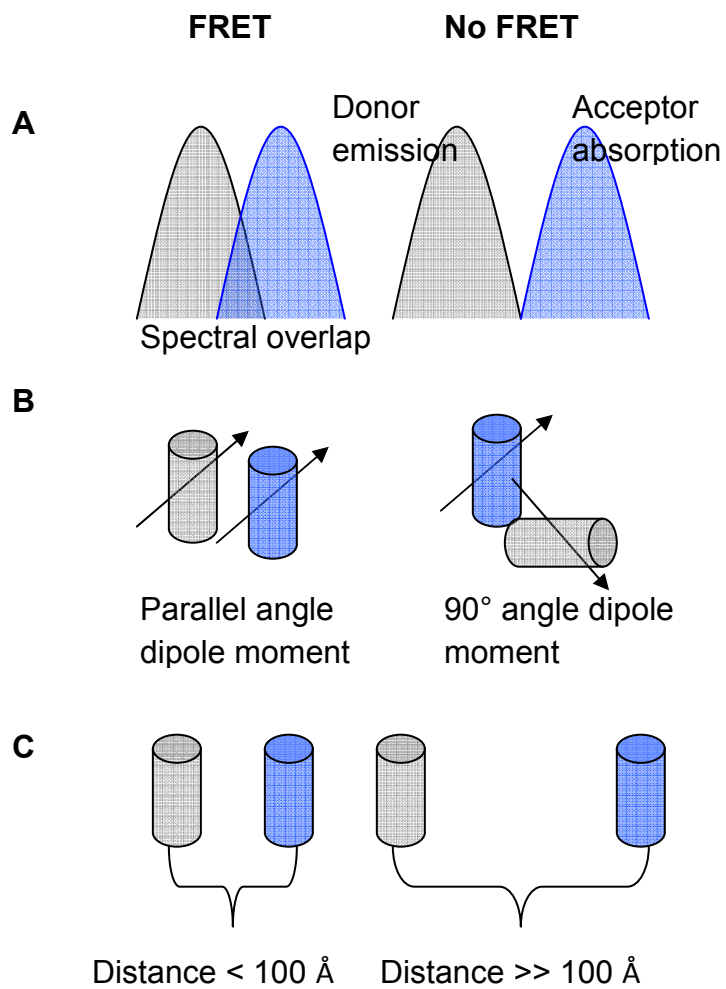
conformational changes in proteins, the focus of this dissertation [91-93]. In order to study protein conformational changes, a donor fluorophore and an acceptor fluorophore are tagged to the protein such that a conformational change will be reflected. In order for FRET to occur, the donor fluorescence must overlap with the absorption of the acceptor, as seen in Figure 16 A. Additionally, the transition dipole moments of the fluorophore pair should be approximately parallel (Figure 16 B). Next, the distance between the donor and acceptor fluorophore must be less than 100 Å (Figure 16 C). Once these conditions are met by the fluorophore pair, FRET experiments can be performed on the protein labeled with the fluorophores [94]. The donor fluorophore is excited and the excitation energy can either return to ground state thus emitting a photon or FRET can occur and the energy is transferred to an acceptor. The transfer occurs by the interaction of the transition dipole moments between the donor and acceptor. The efficiency of this transfer can be calculated into distances that reflect conformational changes. The theory began with Forster's calculations for FRET [95], which have further been modified by Selvin [92] and discussed below.

The efficiency of energy transfer ( $E$ ) can be calculated by the equation 1:

$$E = \frac{I}{1 + (R/R_0)^6} \quad . \quad \text{eq. 1}$$

$R$  is the distance between the fluorophores and  $R_0$  is the distance where energy transfer is 50%. This equation reveals how sensitive this technique is for measuring distances, as seen by the distance,  $R$ , to the sixth power.

**Figure 16** Conditions for FRET. (A) FRET occurs when there is a spectral overlap between the donor excitation and the acceptor absorption. (B) The dipole moments of the fluorophores must be approximately parallel for FRET to occur. (C) FRET is distance dependent, so the fluorophores should be less than 100 Å apart [94].



By slightly increasing the distance between the fluorophores,  $R$ , the efficiency,  $E$ , dramatically drops, as shown in Figure 17. Thus, by keeping  $R$  close to  $R_0$ , the technique can sensitively detect changes in distance.  $R_0$  is then calculated by equation 2:

$$R_0^6 = \frac{8.785 * 10^{-5} * \kappa^2 * \phi_D * J}{n^4}. \quad \text{eq. 2}$$

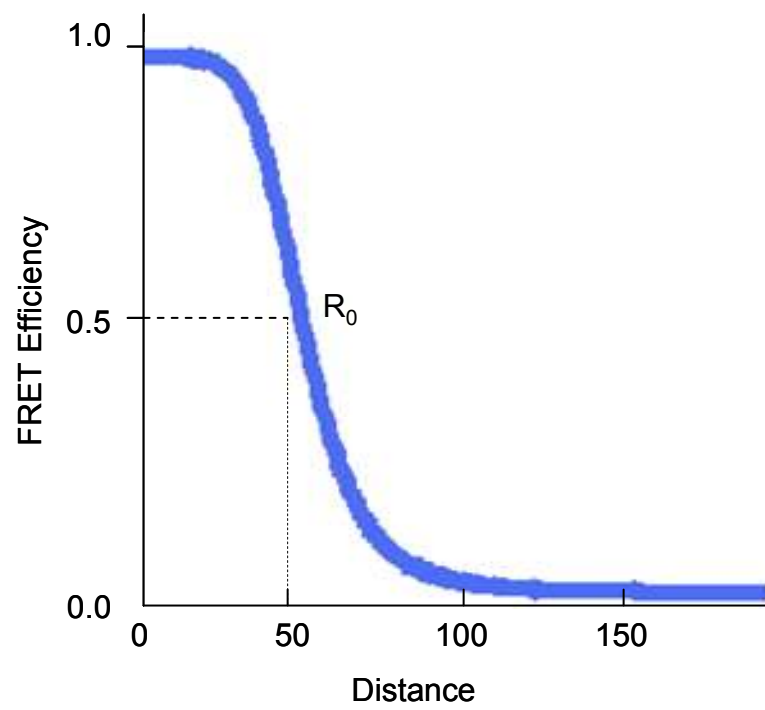
In equation 2,  $\kappa^2$  is the orientation factor that accounts for the direction of the dipoles of the donor and the acceptor fluorophores. In most cases, the factor is assumed to be 2/3, when the fluorophores are not polarized and free to occupy all angles. This factor is a major source of error in this calculation. However, this issue is addressed in LRET and will be discussed in the next sections. Next, the  $\phi_D$  is the quantum yield of the donor fluorophore. The  $n$  is the refractive index, and in this case the refractive index for water is 1.3. The  $J$  is the spectral overlap integral between the donor fluorescence and the acceptor absorption and is calculated by equation 3:

$$J = \frac{\sum_i F_D(\lambda_i) * \epsilon_A(\lambda_i) * \lambda_i^4}{\sum_i F_D(\lambda_i)}. \quad \text{eq. 3}$$

The  $F_D(\lambda)$  is the fluorescence spectrum and  $\epsilon_A(\lambda)$  is the molar extinction coefficient of the acceptor. Additionally,  $\lambda$  is the wavelength.

A modified FRET technique called Luminescence Resonance Energy Transfer (LRET) is utilized in this dissertation to study conformational changes in the ligand binding domain of a functional AMPA receptor and has been successfully used to study conformational changes in both soluble and membrane bound

**Figure 17** FRET Efficiency versus Distance. Sensitive distance changes are obtained when the distance between the fluorophores,  $R$ , is near the  $R_0$ , where the efficiency of energy transfer is 50% [94].



proteins [70, 96]. There are several advantages of using LRET instead of FRET; however, the basic principles of FRET are still utilized. These details are discussed in the next section.

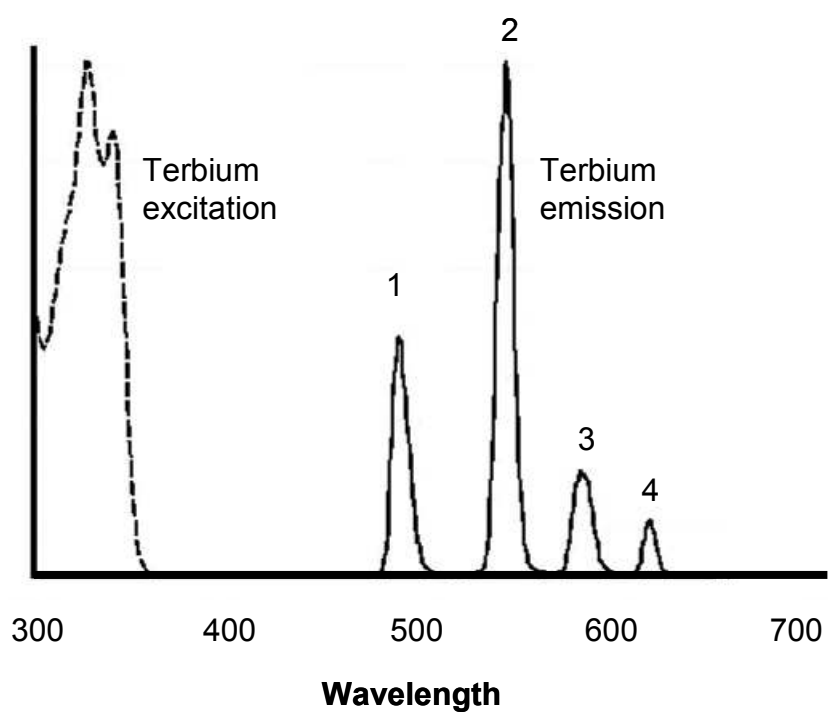
### **III. Luminescence Resonance Energy Transfer**

The recently improved FRET technique is referred to as LRET (Luminescence Resonance Energy Transfer) because the donor is luminescent [92, 97]. In the LRET technique, a luminescent lanthanide donor such as terbium chelate is excited and transfers energy to a fluorescent acceptor dye, such as the organic dyes discussed previously, ATTO465-maleimide, and (Ni-NTA)<sub>2</sub>Cy3. LRET has a number of improvements including greater distance range; temporal resolution of signals; a decrease in error due to the orientation factor; and multiple distances can be determined for a single system [92].

The advantages of using LRET are due to the inherent properties of terbium chelate, the donor. First, terbium chelate has a high quantum yield. Additionally, terbium chelate is isotropic, which greatly reduces the error associated with the FRET calculations discussed above [92, 97]. Terbium chelate has four sharp emission peaks that allow spectral separation of donor and acceptor fluorescence, shown in Figure 18 [98]. This also allows a wide range of acceptors to be paired with terbium chelate to give a variety of  $R_0$  values to choose from. This feature also reduces the background by choosing an acceptor that fluoresces where terbium is dark. Most importantly, terbium chelate has a long lifetime in the microsecond to millisecond timescale compared to the organic dyes used as acceptors, which have



**Figure 18** Terbium chelate excitation and emission spectrum. Terbium is excited at 337 and the 4 sharp peaks of the fluorescence spectrum at 490, 546, 585, and 620 nm are shown [98].



a nanosecond lifetime. The long lifetime allows temporal separation of the acceptor only, donor only, and LRET signal. The donor only sample does not contribute to the LRET signal since LRET is measured at the wavelength of the acceptor, referred to as sensitized emission. Thus, the sensitized emission is due to the acceptor gaining fluorescence from the donor. The acceptor only sample has a nanosecond lifetime, while the LRET lifetime is long lived in the microsecond to millisecond timescale. The equation for distance calculations based on lifetimes is shown below:

$$R = R_0 \left( \frac{\tau_{DA}}{\tau_D - \tau_{DA}} \right)^{1/6} . \quad \text{eq. 4}$$

In equation 4, the time constants for donor fluorescence decay in the absence of the acceptor,  $\tau_D$ , and the sensitized emission of the acceptor due to the energy transfer from the donor,  $\tau_{DA}$ , are measured in order to determine the distance between the fluorophores based on lifetimes [92].

This allows for an investigation where the donor and acceptor can be introduced into a system with multiple tagging sites that leads to a complex mixture. For example, in a cysteine light protein, multiple cysteines can be introduced and can be labeled by maleimide derivatives of both a donor and acceptor. Thus by manipulating the concentrations of donor to acceptor ratios, distances between two cysteines can be determined. Cha et al. has successfully performed these types of LRET investigations to study intersubunit distances in the potassium channel [83]. Additionally, another LRET labeling strategy (a histag to serve as the acceptor tagging site for (Ni-NTA)<sub>2</sub>Cy3 and a cysteine site for the maleimide derivative of

terbium chelate) has been used to study cleft closure conformational changes in the isolated ligand binding domain of the AMPA receptor [70].

#### **IV. Instrumentation**

Two types of fluorescence instruments were utilized in measuring the fluorescence lifetimes for the determination of large scale conformational changes in AMPA receptors. Basic fluorescence spectrometers have three fundamental components: a light source, a sample compartment, and a detector. Monochromators are also used to adjust excitation and/or emission wavelengths [88].

The first fluorescence lifetime spectrometer used is the *TimeMaster* Model TM-3/2003 from Photon Technology International (P.T.I., NJ). The light source is a pulsed 337 nm nitrogen dye laser in which a fiber optic cable connects the light source to the sample compartment. In this system, the sample is placed in a cuvette. The *TimeMaster* contains an emission monochromator with variable slit widths in addition to a stroboscopic detector. The Felix 32 software provided with the *TimeMaster* was used to collect data and then studied using Origin, a mathematical graphing software (OriginLab Corp., MA) [96]. This system was accurate and used for the cleft closure distance measurements; however, it would not be ideal for the type of experiments using a 4:1 labeling ratio of donor:acceptor used to measure intersubunit distance measurements. This ratio drastically reduces the signal (sensitized emission of the acceptor), and this instrument has limitations in sensitivity. Because the signal from the labeled functional receptor

expressed in oocytes was small with a suboptimal signal-to-noise ratio, a more sensitive instrument was used.

The next spectrometer used for fluorescence lifetime measurements is the *QuantaMaster* Model QM3-SS also from Photon Technology International. The sample holder was also a cuvette; a Peltier TE temperature sample controller holds the sample at 15 °C. A high powered, pulsed xenon lamp serves as the light source. An excitation and emission monochromator control the desired wavelengths and are also equipped with variable slit widths to further control the transmitted light. Ultimately, the fluorescence signal reaches the detector, or the PMT (photomultiplier tube). Fluorescan software from PTI is used to collect the data and is analyzed using Origin.

Donor-only lifetimes were measured at the wavelength of donor emission and sensitized emission lifetimes of the acceptor were collected in dark regions of donor emission. Three individual data sets were collected for statistical analysis and the averages were fit to collect the lifetimes. It should be noted that individual sets are also fit in order to show that each set exhibit similar lifetimes. These lifetimes were then used to calculate the distances as mentioned in the previous section.

## **V. Anisotropy of the Fluorophores**

In order to evaluate the error associated with the distances obtained by LRET, the orientation factor,  $\kappa^2$ , must be analyzed in detail. A fluorophore becomes polarized when exposed to polarized light. Anisotropy is defined as extent of the

polarized component of the emission of the fluorophore [88]. The equation for anisotropy,  $r$ , is shown below:

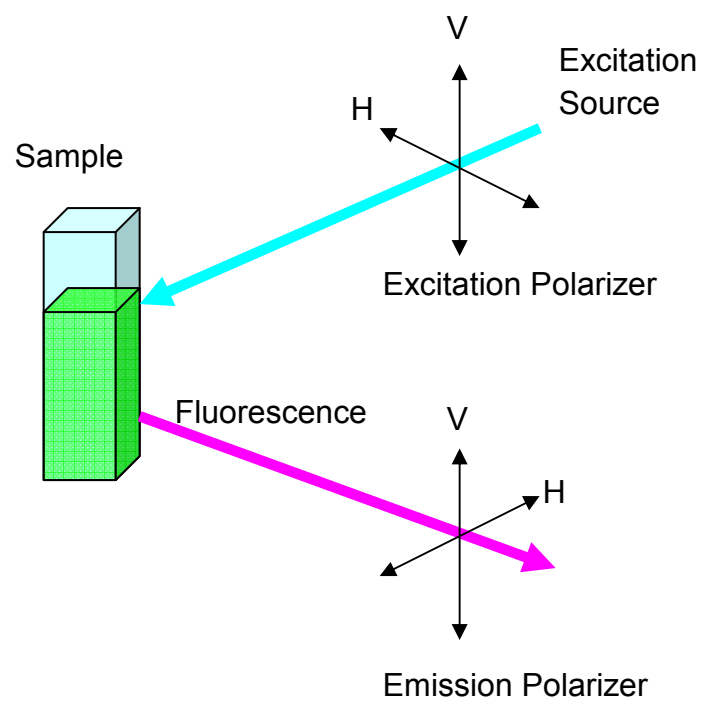
$$r = \frac{I_{VV} - G * I_{VH}}{I_{VV} + 2 * G * I_{VH}} \quad . \quad \text{eq. 5}$$

In equation 5,  $I_{VV}$  is the intensity measured when both the excitation and emission polarizers are positioned vertically.  $I_{VH}$  is the intensity measured when the excitation polarizer is positioned vertically and the emission polarizer is horizontal. The  $G$  factor is the ratio of  $I_{HV}$  to  $I_{HH}$ .  $I_{HH}$  is the intensity measured when both the excitation and emission polarizers are positioned horizontally.  $I_{HV}$  is the intensity measured when the excitation polarizer is positioned horizontally and the emission polarizer is vertical. The polarizer positions are demonstrated in Figure 19 [88]. For fluorophores, the polarized emission becomes less polarized due to rotational diffusion; thus, the anisotropy is low. However, as mentioned previously, the anisotropy for the lanthanide donor, terbium, is zero [92, 97]. This is the case because the lifetime for terbium is in the microsecond to millisecond timescale, much greater than an organic dye, which is in the nanosecond timescale. Thus, the source of error for the LRET experiments is the orientation factor from the acceptor fluorophore, which is greatly affected by the attachment of the fluorophore to the protein. Thus, the errors in absolute distances reported in this dissertation are from equation 2 for the  $R_0$  value which includes the orientation factor. These errors are calculated from the anisotropy experiments on the fluorophores using equations summarized in Haas et al [99]. Additionally, the anisotropy measurements reveal that in different ligated states, the anisotropy remains the

same for a donor-acceptor tagged protein, thus the relative errors between each ligated state is expected to be less.

**Figure 19** A schematic representation of the anisotropy experiments. Polarized light excites the fluorophore in the sample holder and then the polarized fluorescence emission is detected. The position of the polarizers, vertical (V) and horizontal (H), are shown [88].





## **Chapter 4—LRET Part I: Cleft Closure Conformational Changes in the Ligand Binding Domain of a Functional AMPA Receptor**

## **I. Testing the activation hypothesis**

As discussed in the first chapter of this dissertation, the changes seen in the isolated ligand binding domain along with functional data from the full receptor suggest that the extent of cleft closure correlates with the extent of activation [56, 59, 60, 67]. The hypothesis for activation describes how the conformational state of the ligand binding domain is coupled to the functional response of the receptor. This chapter aims to test this hypothesis by measuring the cleft closure distance change in response to various agonists in a functional AMPA receptor and correlate these changes seen with functional data. Why is this investigation important if an extensive amount of data is readily available from the isolated LBD of the receptor and the full receptor structure was recently solved? Although the isolated LBD has provided initial insight into the functional transitions of the receptor once it is activated, the isolated LBD is in the absence of the functional portion of the receptor, the transmembrane segments. These isolated LBD structures in general were shown to be limited by the lack of desensitized state structure; only when the isolated LBD was artificially decoupled, was a desensitized-like structure obtained [58]. While the crystal structure of the full receptor has been recently solved, the crystal structures are not in a dynamic state; the receptor is confined to crystallographic constraint [62]. Thus, cleft closure conformational changes must be investigated in a functional receptor in a dynamic, near physiological state.

Previously, the Jayaraman lab has investigated conformational changes in the ligand binding domain of a functional AMPA receptor expressed in HEK-293 cells. The LRET strategy used included the use of GFP, green fluorescent protein,

fused to the N-terminus of an AMPA receptor to serve as an acceptor fluorophore [100]. However, GFP is a bulky protein that is similar in size to the ligand binding domain of the receptor [101]. Thus, the conformational changes seen were possibly restricted in the AMPA receptor fusion protein. In this chapter, the LRET technique was cleverly modified in order to study conformational changes in a functional AMPA receptor in a physiologically relevant state.

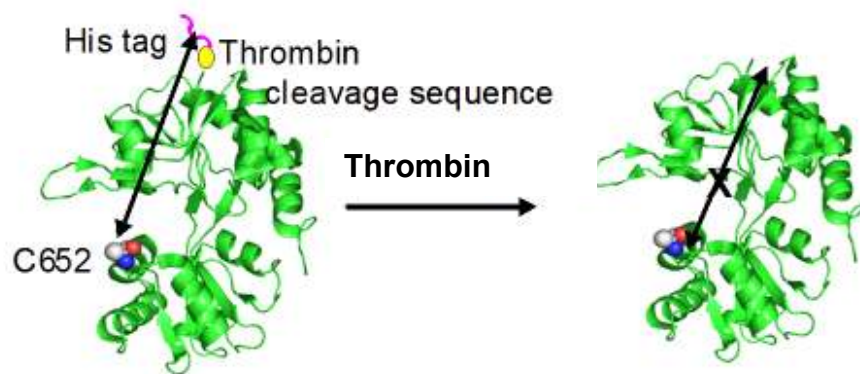
## **II. Establishing LRET studies in a non-purified system**

LRET is an excellent tool to study conformational changes in protein in their dynamic state [92]. A significant impediment for the generalized use of LRET based methods for determining conformational changes in proteins lies in designing unique sites that can be tagged with donor and acceptor fluorophores. The current strategies used have several limitations such as the large size of the fluorophores as is the case with GFP-like proteins [102] or difficulty in incorporating the site such as with unnatural amino acids [103]. The use of histidine tags as possible recognition site by a nickel-nitrilotriacetate (Ni-NTA) based fluorophore shows significant promise due to their small size and simple introduction. However their use has been somewhat restricted because of the non-specific background signal that arises from the non-specific binding due to the weak non-covalent interactions between the nickel-nitrilotriacetate and the histidine tag [90]. Reduction of the background fluorescence or quantification subtraction of the background FRET would greatly diversify and expand the applicability of this method for protein conformation determination. This modified method allows the determination of the LRET between the Ni-NTA fluorophore bound to the histidine tag and a second

target site by quantitatively determining the non-specific background LRET. For these investigations, a protease recognition or stop site between the histidine tag and the protein of interest is introduced. This allows the histidine tag to be cleaved off, thus removing the acceptor site for LRET experiments. The initial total LRET signal is obtained from the sample first. The LRET signal measured after the cleavage of the histidine tag is the background non-specific signal. The non-specific signal is then subtracted from the total signal in order to obtain the specific LRET signal produced only from the protein of interest. The usefulness of the technique lies in the fact that the protein does not have to be purified, which allows for studying proteins in a near physiological state.

The applicability of this strategy was first shown by examining the conformational changes in the isolated ligand binding domain of the GluR2 subunit of the AMPA receptors expressed in *E. coli*. The cleft closure conformational distance changes have been intensely investigated by crystallography as well as by LRET by the Jayaraman lab [56, 59, 60, 67, 70, 104], thus the data from modified LRET investigations can be compared to previous data published to show the feasibility of the modified LRET technique. This cleft closure conformational change is reflected as a 6 Å distance change between the N-terminus and residue 652 in the isolated GluR2-LBD crystal structure, thus making these good sites to be tagged with donor and acceptor fluorophores [56]. For the LRET investigations, a histidine tag was introduced at the N-terminus followed by a thrombin digestion sequence prior to the isolated GluR2-LBD sequence, and a cysteine was introduced

**Figure 20** A schematic representation of the experiments performed with the isolated ligand binding domain. A histag and a thrombin cleavage sequence were introduced at the N-terminus and a cysteine was introduced at site S652 to serve as acceptor and donor sites, respectively, to provide a direct readout of cleft closure. LRET was measured between the donor and acceptor fluorophores before and after the addition of thrombin.



at site 652, as shown in Figure 20. This labeling strategy serves as a direct readout of cleft closure.

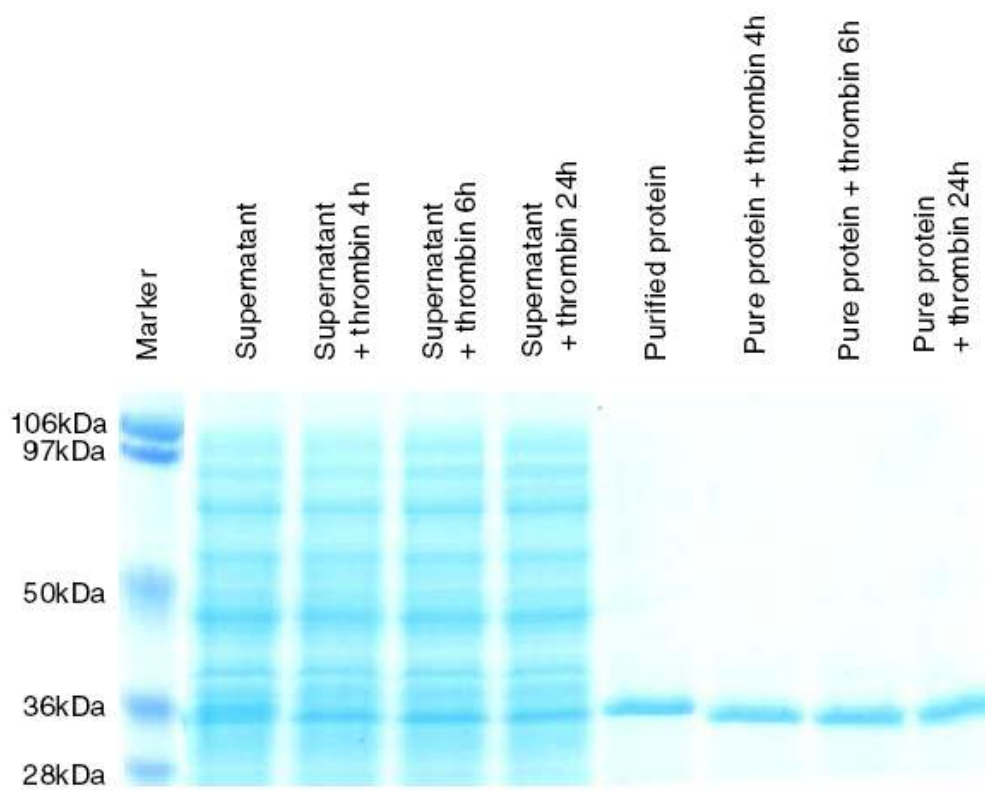
In order to compare a purified and non-purified system, the protein was expressed in Origami B cells (Novagen) and the non-purified supernatant of the cell lysate was collected for LRET experiments; additionally, the cell lysate was then further purified on a Ni-NTA HiTrap affinity column and collected for LRET experiments. Further details on protein production and purification are explained in detail in Appendix VIII. As shown in Figure 21, before performing LRET experiments, a SDS-PAGE experiment was performed on the supernatant of the cell lysate, the purified isolated LBD, and protein samples subjected to thrombin digestion (2.5 U per mg of protein) collected at different time points. This experiment was performed in order to determine the time it takes for complete thrombin digestion to occur so that the histag/acceptor site is removed from the protein.

For LRET experiments, the non-purified supernatant and the purified protein were labeled with the donor terbium chelate (Invitrogen) and the acceptor (Ni-NTA)<sub>2</sub>Cy3 fluorophores [90]. First, the lifetime of the sensitized emission of the acceptor in the presence of the donor was measured to determine the total signal. To the same samples, thrombin was added and the sample was digested for 24 hours at 4 °C. The lifetime of the sensitized emission of the acceptor in the presence of the donor was measured post-thrombin digestion after the removal of the acceptor site to account for the non-specific background LRET signal. The before and after LRET signals were then subtracted in order to obtain the specific



**Figure 21** SDS-PAGE of GluR2 isolated LBD. Non-purified protein (supernatant) and purified protein samples were subjected to 4, 6, and 24 hour thrombin digestion at 4 °C. After the histag is removed by thrombin digestion, a decrease in the size of the protein is detected [96].

Reproduced in part with permission from Gonzalez, J., Rambhadran, A., Du, M., Jayaraman, V. 2008. LRET investigations of conformational changes in the ligand binding domain of a functional AMPA receptor. *Biochemistry* 47:10027-10032. Copyright 2008 American Chemical Society.



LRET signal between the donor and acceptor fluorophores tagged to the protein of interest.

For the apo state non-purified supernatant and the purified protein, the before and after thrombin digestion LRET signal for the sensitized emission of the acceptor is shown in Figure 22 A and B, respectively. It is clearly shown that there is a smaller non-specific background signal (post-thrombin digestion) coming from the purified isolated GluR2-LBD compared to the non-purified GluR2-LBD. The total signal and non-specific were then subtracted in order to obtain the specific lifetimes coming from the protein of interest. The donor-only lifetime and the lifetime obtained after the subtraction to represent the specific signal coming from the protein of interest could be well represented by a single exponential decay corresponding to a single distance measured (Figure 22, Table 1). The distance measured is between the fluorophores and not the protein itself, thus the trends in lifetimes corresponding to distances are studied. For the non-purified supernatant, the apo, unligated state had a lifetime of  $240 \pm 20$   $\mu$ s and the glutamate-bound state had a lifetime of  $145 \pm 10$   $\mu$ s (Figure 22, Table 1). For the purified isolated GluR2-LBD, the lifetimes for the subtracted LRET was  $210 \pm 10$   $\mu$ s for the apo state and  $130 \pm 10$   $\mu$ s for the glutamate-bound state as shown in Figure 21 and Table 1. The specific LRET lifetimes obtained for the non-purified supernatant and the purified protein was similar, thus suggesting that the subtracted lifetimes obtained using the modified LRET technique are unique to the isolated GluR2-LBD. Furthermore, the distance change as measured from the LRET investigations shown in Table 1 between the apo ( $51 \pm 2$  Å) and glutamate-bound state ( $46 \pm 2$  Å) was 5 Å in

**Figure 22** LRET lifetimes for the isolated LBD. The before and after thrombin digestion signal (sensitized emission of the acceptor measured at 575 nm) is shown for the apo state of (A) the supernatant from *E. coli* cell lysate and (B) purified GluR2-LBD. The before and after digestion with thrombin signal was subtracted for both the apo and glutamate-bound states for (C) the supernatant from *E. coli* cell lysate and the (D) purified GluR2-LBD [96].

Reproduced in part with permission from Gonzalez, J., Rambhadran, A., Du, M., Jayaraman, V. 2008. LRET investigations of conformational changes in the ligand binding domain of a functional AMPA receptor. *Biochemistry* 47:10027-10032. Copyright 2008 American Chemical Society.

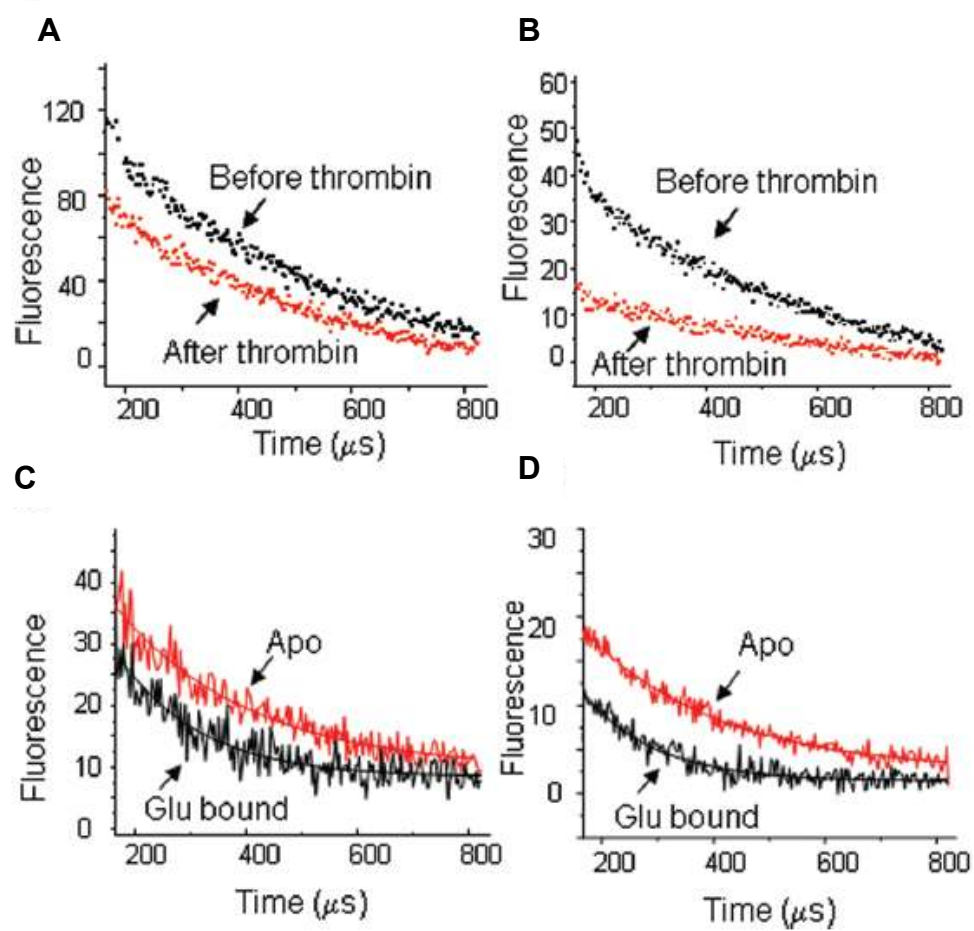


**Table 1** Fluorescent Lifetimes and Distances for GluR2-LBD and Histag- $\Delta N^*$ -AMPA-S653C Receptors. Lifetimes of the donor-only labeled protein and the subtracted lifetimes for the sensitized emission of the acceptor in the presence of the donor with the corresponding distances for the conformational states of the AMPA receptor for the apo, glutamate, and kainate (Histag- $\Delta N^*$ -AMPA-S653C Receptors) bound states [96].

Reproduced in part with permission from Gonzalez, J., Rambhadran, A., Du, M., Jayaraman, V. 2008. LRET investigations of conformational changes in the ligand binding domain of a functional AMPA receptor. *Biochemistry* 47:10027-10032. Copyright 2008 American Chemical Society.

Protein	Ligand	Donor lifetime ( $\mu$ s)	Sensitized emission lifetime ( $\mu$ s)	Distance ( $\text{\AA}$ )
GluR2-LBD supernatant	Apo	1590 $\pm$ 45	240 $\pm$ 20	51 $\pm$ 2
GluR2-LBD supernatant	Glutamate	1575 $\pm$ 60	145 $\pm$ 10	46 $\pm$ 2
GluR2-LBD purified protein	Apo	1490 $\pm$ 40	210 $\pm$ 10	51 $\pm$ 2
GluR2-LBD purified protein	Glutamate	1455 $\pm$ 65	130 $\pm$ 10	46 $\pm$ 2
histag- $\Delta$ N*-AMPA-S653C receptor	Apo	1575 $\pm$ 60	260 $\pm$ 25	51 $\pm$ 2
histag- $\Delta$ N*-AMPA-S653C receptor	Glutamate	1580 $\pm$ 45	165 $\pm$ 15	47 $\pm$ 2
histag- $\Delta$ N*-AMPA-S653C receptor	Kainate	1585 $\pm$ 45	190 $\pm$ 10	49 $\pm$ 2

experiments performed with the supernatant as well as with the purified protein and in good agreement with the crystal structure based distances, showing that this technique can be used to study relatively small distance changes associated with conformational changes in the protein.

### **III. LRET Results and Discussion**

Since the modified LRET experiments were successful in probing cleft closure conformational changes in the isolated ligand binding domain of GluR2 in a non-purified system, the technique was extended to investigate conformational changes in the ligand binding domain of a functional AMPA receptor in response to various ligands.

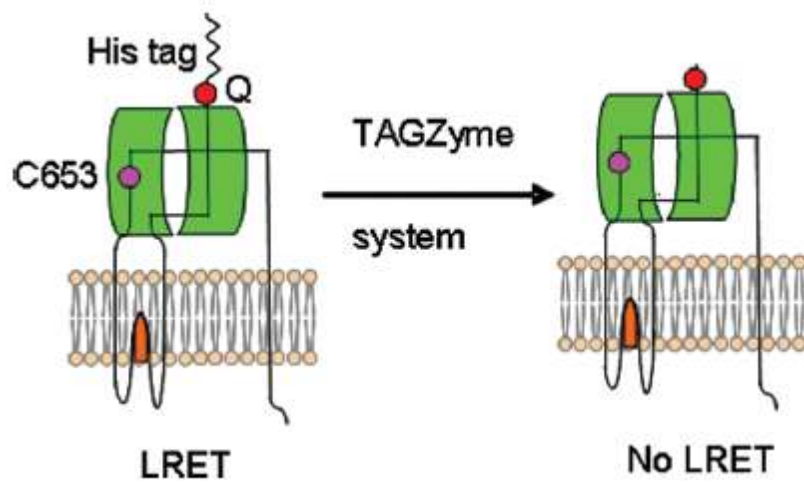
#### **a. Modified AMPA receptors**

A similar LRET labeling strategy from the isolated GluR2-LBD was also used in the functional AMPA receptors LRET investigations to probe cleft closure distance measurements. In order to introduce cysteines at specific sites, the GluR4 subtype of the receptor has been modified such that there are no accessible cysteines by removing the N-terminal domain (which has previously been shown to not affect the receptor activation) and by mutating two of the accessible, extracellular cysteines (C426 and C529) to serines (this construct will be referred to as  $\Delta N^*$ -AMPA receptors). A hexa-histidine tag was introduced at the N-terminus of the  $\Delta N^*$ -AMPA receptor and a glutamine residue is introduced between the histag and the  $\Delta N^*$ -AMPA receptor sequence, as shown in Figure 23. For cloning details, see Appendix I. The introduction of the glutamine allows for the cleavage of the



**Figure 23** Diagram of the modified LRET experiments performed on modified AMPA receptors expressed in oocytes. The GluR4 subunit was modified by introducing a cysteine at site 653 and a hexa- histidine tag at the N-terminus with a glutamine residue between the histidine tag and the AMPA receptor sequence (histag-ΔN\*-AMPA-S653C). LRET is measured before and after the addition of TAGZyme, an enzyme that removes the histag and stops at the glutamine [96].

Reproduced in part with permission from Gonzalez, J., Rambhadran, A., Du, M., Jayaraman, V. 2008. LRET investigations of conformational changes in the ligand binding domain of a functional AMPA receptor. *Biochemistry* 47:10027-10032. Copyright 2008 American Chemical Society.



histag with TAGZyme (Qiagen), a dipeptidase enzyme that digests the histidine tag, and the cleavage stops when the enzyme encounters a glutamine. This allows for measurements of the LRET signal after cleavage of histag, the background non-specific LRET signal.

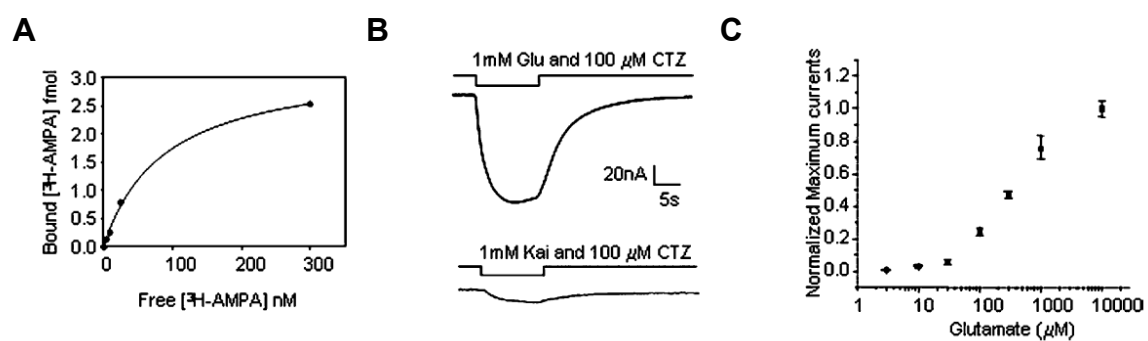
#### b. Receptor characterization by electrophysiology

The modified histag- $\Delta N^*$ -AMPA-S653C protein was expressed in oocytes by injecting the oocytes with RNA encoding the modified protein [105]. After injection the oocytes were incubated at 12 °C to prevent surface expression of the receptor. After for 2-3 days, the oocytes are pre-blocked with  $\beta$ -maleimidopropionic acid for one hour. This procedure was first established in potassium channels where blocking inherent cysteines of the oocyte increases the specificity of the tagging of the receptor [83]. The blocked oocytes were placed at 18 °C for 24 to 36 hours allowing for the expression of the receptors. At the end of 24-36 hours, the oocytes were labeled with 2  $\mu$ M of maliemide derivative of terbium chelate for one hour. The excess fluorophore was then washed with buffer. These oocytes were used for electrophysiological measurements, while the oocyte membrane preps obtained by lysis of these oocytes were used for radioactive binding and LRET measurements (see Appendix III Membrane Preparation for protocol). The acceptor fluorophore, (Ni-NTA)<sub>2</sub>Cy3, is added to the membrane preparations for LRET investigations.

In order to establish the functionality of the modified AMPA receptor, histag- $\Delta N^*$ -AMPA-S653C, expressed in oocytes, radioactive binding and two-electrode voltage clamp were performed (Figure 24). Membrane preparations of several

**Figure 24** Functional studies of histag- $\Delta N^*$ -AMPA-S653C. (A) Radioactive [ $^3\text{H}$ ] AMPA binding studies with membrane preparations of oocytes expressing histag- $\Delta N^*$ -AMPA-S653C. (B) Current traces from oocytes expressing histag- $\Delta N^*$ -AMPA-S653C receptors in the presence of 1 mM glutamate and 1 mM kainate with 100  $\mu\text{M}$  cyclothiazide to block desensitization. (C) Maximum currents recorded at various glutamate concentrations in the presence of cyclothiazide for the histag- $\Delta N^*$ -AMPA-S653C receptors formed a dose response curve [96].

Reproduced in part with permission from Gonzalez, J., Rambhadran, A., Du, M., Jayaraman, V. 2008. LRET investigations of conformational changes in the ligand binding domain of a functional AMPA receptor. *Biochemistry* 47:10027-10032. Copyright 2008 American Chemical Society.



oocytes expressing the modified receptor were obtained for the radioactive binding experiments. The  $K_d$  for the wild type receptor was established as  $40 \pm 15$  nM [11], and the  $K_d$  for histag- $\Delta N^*$ -AMPA-S653C receptor was measured as  $88 \pm 10$  nM, establishing that the binding properties of the modified receptor are similar to the wild type receptor (Figure 24 A). The histag- $\Delta N^*$ -AMPA-S653C modified receptor expressed in oocytes was further characterized by performing two-electrode voltage clamp in order to study the currents elicited. Currents were recorded in the presence of agonist, 1 mM glutamate or 1 mM kainate, with the addition of 100  $\mu$ M cyclothiazide added to block desensitization (Figure 24 B). Peak currents were analyzed at various concentrations of glutamate in the presence of cyclothiazide, and normalized to currents collected at 10 mM glutamate. A dose response curve was obtained for the histag- $\Delta N^*$ -AMPA-S653C modified receptor. In Figure 24C, the  $EC_{50}$  for the modified receptor is 310  $\mu$ M, and the  $EC_{50}$  for the wild type receptor (data not shown) is 250  $\mu$ M. These results reiterate the similarity between the histag- $\Delta N^*$ -AMPA-S653C and the wild type receptor indicating that the mutations and fluorophores introduced for the LRET investigation do not perturb the function.

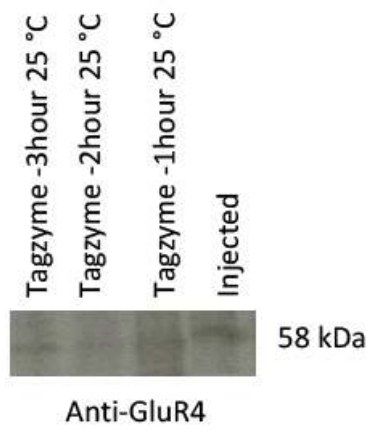
### c. LRET Studies

The modified AMPA receptor expressed in oocytes was tagged with the maliemide derivative of the terbium chelate and the Ni-NTA derivative of Cy3 is added to the membrane preparations of around 300 oocytes. The total LRET signal is recorded before the addition of thrombin and the non-specific LRET signal is measured after the digestion with TAGZyme to remove the histag. In Figure 25, the effectiveness of the TAGZyme enzyme removing the histag was tested by

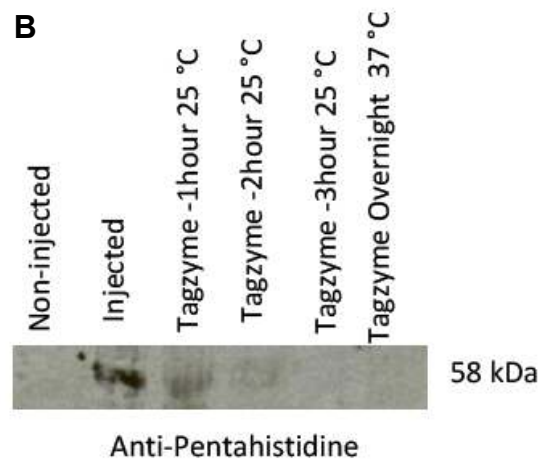
**Figure 25** Membrane preparations of histag- $\Delta N^*$ -AMPA-S653C expressed in oocytes were collected before and after TAGZyme digestion. Samples were run on SDS-PAGE in denaturing conditions. Western blots were either probed with (A) Anti-GluR4 and (B) Anti-Pentahistidine antibodies [96].

Reproduced in part with permission from Gonzalez, J., Rambhadran, A., Du, M., Jayaraman, V. 2008. LRET investigations of conformational changes in the ligand binding domain of a functional AMPA receptor. *Biochemistry* 47:10027-10032. Copyright 2008 American Chemical Society.

**A**



**B**



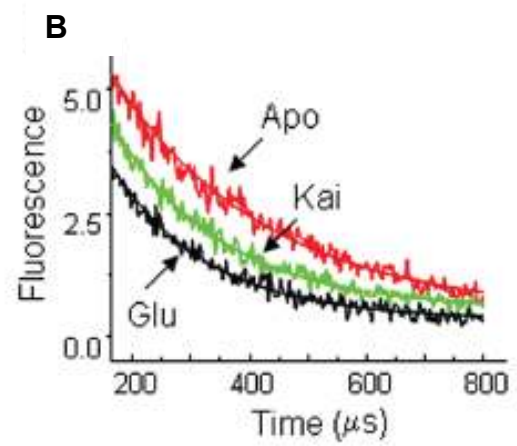
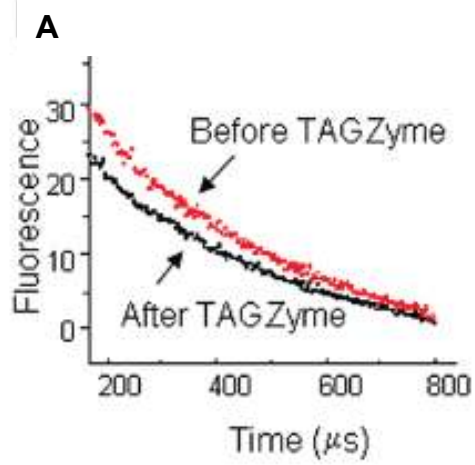


performing Western blots on membrane preparations from oocytes expressing histag- $\Delta N^*$ -AMPA-S653C receptor. Samples were incubated at 25 °C with TAGZyme at various time points. The blots were probed with either anti-GluR4 or anti-Pentahistadine antibodies. The results indicate that the receptor is successfully probed after incubation; however, the histag is no longer detected after 3 hours of incubation with TAGZyme.

Figure 26 A shows the lifetimes for the sensitized emission of the acceptor in the presence of the donor measured before and after the addition of TAGZyme in the apo state of the receptor. Additionally, in Figure 26 B, the difference in the LRET lifetime before and after addition of the TAGZyme is shown for the apo, kainate-bound, and glutamate-bound states. The subtracted LRET signal can be fit to a single exponential decay, thus suggesting a single lifetime of  $260 \pm 25 \mu s$  (apo),  $165 \pm 15 \mu s$  (kainate-bound state), and  $190 \pm 10 \mu s$  (glutamate-bound state). Parallel experiments were also performed on donor-only labeled samples and no significant changes were observed in the lifetimes between the receptor states, suggesting that the changes observed in the LRET signal are not due to changes in the environment of the fluorophore but due to changes in the donor:acceptor distance. Hence, the histag- $\Delta N^*$ -AMPA-S653C receptor serves as a probe to detect distance changes in cleft closure. Using the lifetimes and the  $R_0$  values, the absolute distances calculated are shown in Table 1 for each state of the receptor. The absolute distances for the apo, kainate-bound state, and the glutamate-bound state are  $51 \pm 2 \text{ \AA}$ ,  $49 \pm 2 \text{ \AA}$ , and  $47 \pm 2 \text{ \AA}$ , respectively. Furthermore, the distance

**Figure 26** LRET lifetimes for the histag- $\Delta N^*$ -AMPA-S653C receptor. (A) The before and after TAGZyme treatment signal (sensitized emission of the acceptor measured at 575 nm) is shown for the apo state. (B) The before and after TAGZyme treatment signal was subtracted for the apo, kainate-bound state, and the glutamate-bound state [96].

Reproduced in part with permission from Gonzalez, J., Rambhadran, A., Du, M., Jayaraman, V. 2008. LRET investigations of conformational changes in the ligand binding domain of a functional AMPA receptor. *Biochemistry* 47:10027-10032. Copyright 2008 American Chemical Society.



change as measured from the LRET investigations between the apo and glutamate-bound state is 4 Å, and the distance change between apo and kainate-bound state is 2 Å. Although the absolute distance change from apo to kainate-bound state is within the error of the measurements, the trends should be noted. As previously discussed, the distances reported in this dissertation are absolute distances and relative changes between the states are expected to be less because the source of error, the orientation factor, is not likely to change among states.

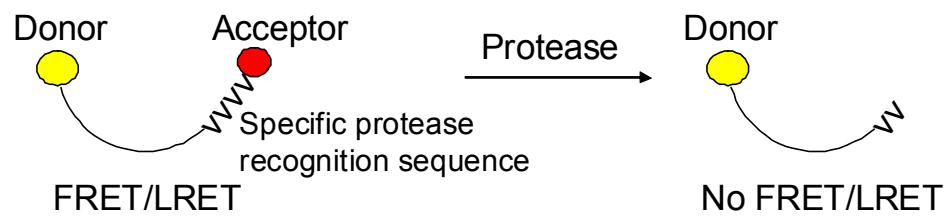
The distance changes for the histag-ΔN\*-AMPA-S653C receptor reflecting cleft closure (4 Å) upon the addition of glutamate are similar to those seen in the isolated LBD of 5 Å, clearly indicating that the modified AMPA receptor in the presence of transmembrane segments experiences cleft closure conformational changes like those seen in the isolated LBD. The absolute distances obtained from the LRET investigations of the functional receptor cannot not be directly compared to that of the isolated LBD LRET distances since the soluble protein used in the LRET investigations was in the GluR2 background with a thrombin digestion site and not the TAGZyme site as in the functional receptor, thus trends are identified. The crystal structure of the isolated GluR2-LBD reveals a cleft closure conformational change of 6 Å upon glutamate binding, where the distance measured is between site S652 and the N-terminus [56]. This distance is similar to the LRET distances obtained from the soluble protein, although the distance measured includes the hexahistidine tag. Moreover, the kainate-bound state cleft closure distance obtained from the histag-ΔN\*-AMPA-S653C receptor follows the trend of intermediary distances between apo and glutamate bound receptor as

observed in the isolated GluR2-LBD crystal structure. These results indicate that this LRET based probe can clearly differentiate between the extents of cleft closure and provide another clue that the isolated LBD is a good model for the full receptor to study activation. Additionally, the hypothesis for activation holds true, where structural information from a functional receptor coupled with functional data from the full receptor suggest that the extent of cleft closure correlates with the extent of activation [96].

Moreover, the results with the AMPA receptors as well as the soluble ligand binding domain of the receptor establish the modified LRET method of using a polyhistidine tag with the Ni-NTA based fluorophore for LRET investigations of small distance changes without the requirement for purification. This methodology can be extended to any protein in which a polyhistidine tag can be introduced with no effect on the function. Furthermore, the method of inserting a protease recognition site between the donor and acceptor fluorophore to accurately determine the specific FRET/LRET is not limited to the histidine tag-cysteine pair but can be universally applied to any FRET/LRET investigations with any donor-acceptor sites (Figure 27) [96].

**Figure 27** Modified FRET/LRET as a molecular ruler. The modified method allows the determination of the FRET/LRET signal between a donor and acceptor fluorophore by quantitatively determining the non-specific background FRET/LRET. A protease recognition or stop site between the acceptor site and the protein of interest is introduced. This allows the fluorophore to be cleaved off, thus removing the acceptor site for FRET/LRET experiments [96].

Reproduced in part with permission from Gonzalez, J., Rambhadran, A., Du, M., Jayaraman, V. 2008. LRET investigations of conformational changes in the ligand binding domain of a functional AMPA receptor. *Biochemistry* 47:10027-10032. Copyright 2008 American Chemical Society.



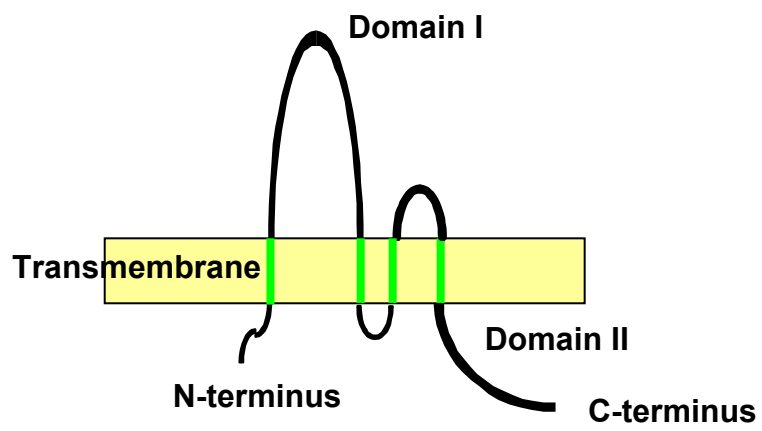
#### **IV. Future experiments**

Does this hypothesis for activation hold true in an even more physiological state, in the presence of regulatory proteins that co-assemble with the AMPA receptors? The transmembrane AMPA receptor regulatory protein (TARP) family consists of several proteins that alter AMPA receptor function. Stargazin, a member of the TARP family, was first studied in the stargazer mouse, which displays an unsteady gait and has absence epilepsy. These mice were later found to be deficient in functional AMPA receptor expression in the cerebellar granule cells [106, 107]. Stargazin is a 38 kD membrane protein containing four transmembrane segments, an extracellular domain, and an intracellular domain (Figure 28). It has previously been shown that the intracellular C-terminal domain is required for AMPA receptor trafficking and the first large loop in the extracellular domain alters AMPA receptor biophysical properties [106, 108-116]. Enhanced trafficking of the AMPA receptor increases the total currents elicited, and whole-cell current measurements show that stargazin slows glutamate-mediated AMPA receptor deactivation and desensitization [106, 110]. At the single channel level, stargazin increases the channel opening to the large conductance states and increases the bursting activity of single channels, similar to that of inherent AMPA receptor activity found in neurons [110]. Interestingly, the presence of stargazin increases the efficacy of the partial agonist kainate [116]. In regards to the current hypothesis for activation, does an increase in kainate efficacy suggest that stargazin's interactions with the LBD enhance kainate-induced cleft closure? This question can be answered with the modified LRET technique used to measure AMPA receptor cleft closure



conformational changes in the presence of stargazin, and test the hypothesis for activation in a functional receptor in a physiologically relevant state.

**Figure 28** Detailed schematic of stargazin topology. Stargazin contains an intracellular N-terminus, four transmembrane segments, an extracellular domain, and an intracellular C-terminal domain.



## **Chapter 5—LRET Part II: Dimer Interface Rearrangement in a Functional AMPA Receptor**

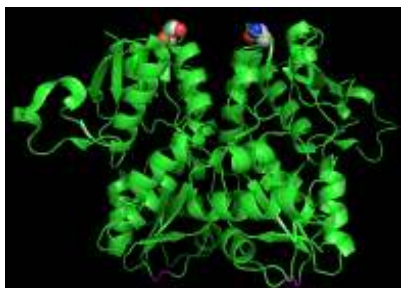
## **I. Testing the desensitization hypothesis**

Currently, no direct structural information exists for a functional AMPA receptor in the desensitized state. As previously mentioned, it is hypothesized that glutamate binding to the bi-lobed ligand binding domain causes cleft closure, which pulls apart the transmembrane segments causing the channel to open. At prolonged times, the receptor desensitizes; the stress on the transmembrane segments causes the decoupling of the dimer interface resulting in the channel closure [61].

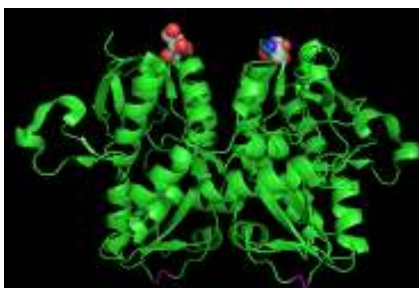
The hypothesis for desensitization is based on indirect structural information from isolated LBD crystal structures that showed cyclothiazide, an allosteric modulator, and mutations in the dimer interface, such as L483Y, that stabilize the dimer interface block the entrance to the desensitized state. Based on the crystal structures, it is expected that desensitization will increase the intersubunit distance between domain 1 due to the decoupling of the dimer interface [61, 72-74]. This conformational change is well reflected at residue S741 where the crystallographic intersubunit distance reveals a coupled dimer interface in the resting and open state of the receptor as shown in Figure 29 A and C, respectively. Two possible desensitized state structures of the isolated LBD are available including glutamate-bound structure with a coupled dimer interface (Figure 29 B) and glutamate-bound GluR2-S729C with an artificially decoupled dimer interface (Figure 29 D). It has not been shown directly which structure is an accurate representation of the desensitized state.

**Figure 29** AMPA receptor isolated LBD (GluR2-S1S2) crystal structure highlighting dimer interface conformational changes. The structures are shown in the (A) resting state, (B) glutamate-bound state, (C) glutamate-bound state in with cyclothiazide bound (open state), and (D) artificially decoupled desensitized state with the S729C mutation present [56, 58, 74]. The residue at position 740 (741 in GluR4) reflects dimer interface conformational changes and is represented as spheres. The linker region that represents changes at the channel is in magenta.

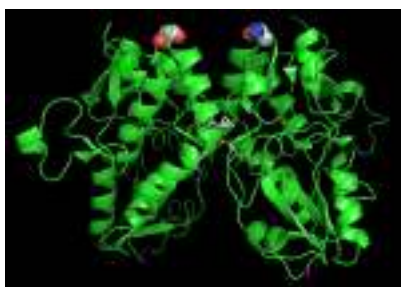
**A**



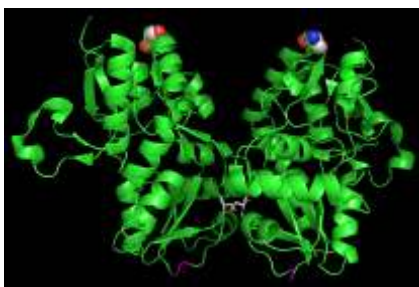
**B**



**C**



**D**



Functional studies of the desensitized state by electrophysiology have been performed on the full receptor to elucidate structural changes at the dimer interface; however, the resting state does not exhibit currents and thus cannot be studied by this method [58]. The crystal structure of the full receptor was obtained in the presence of the competitive antagonist, ZK 200775 [62]. The antagonist-bound form shows a cleft that is more open than the resting, apo state and shows a coupled dimer interface. It is currently not known whether the antagonist-bound form of the full receptor is an accurate representation of the apo, resting state.

## **II. Establishing LRET to study intersubunit distances**

### **a. LRET labeling strategy**

Chapter 5 aims to examine the current desensitization hypothesis by using a modified LRET technique to directly measure the intersubunit distance change. Additionally, the resting state of the receptor has also been studied and compared to the activated state, the desensitized state, and in the presence of ZK 200775. These investigations are performed using functional AMPA receptors expressed in *Xenopus* oocytes and Human Embryonic Kidney-293 (HEK-293) cells.  $\Delta N^*$ -AMPA receptors, as discussed in the previous chapter serve as the background, control construct for the LRET studies, where the N-terminal domain and 2 extracellular cysteines have been removed. Cysteines were introduced at sites G740C, S741C, or S742 to produce three probes that reflect dimer interface conformational changes. Each modified receptor was tagged with maleimide derivatives of donor and acceptor fluorophores, as depicted in Figure 30. A 1:4 ratio of the ATTO465 (acceptor) to terbium chelate (donor) were used to tag the receptor; this type of



labeling strategy has been successfully performed in the study of intersubunit distances in potassium channels [83]. These fluorophores label the cysteines introduced in each of the subunits of the tetramer, and the labeling ratio makes certain that a large number of receptors contain at least one acceptor. The donor only or acceptor only labeled receptor will not contribute to sensitized emission measured at 510 nm, as there are no donor:acceptor pairs in these receptors (Figure 31 A). The acceptor fluorophore was further characterized by assessing ATTO465-maleimide absorption in the presence of glutamate and cyclothiazide (Figure 31 B). No significant changes were identified, thus the addition of agonist and modulator does not perturb the fluorophore's environment. Although the 1:4 ratio labeling strategy limits accurate measure of absolute distances, it does not significantly impact the changes in distances measured using the same protein sample, as will be performed in this investigation. The intersubunit distance will be measured by studying the LRET lifetimes, and changes in the distance in the resting (apo) state, glutamate-bound (desensitized), glutamate-bound in the presence of cyclothiazide or the L483Y mutation (open), and in the presence of competitive antagonist, ZK 200775, will reveal the conformational changes at the dimer interface.

**Figure 30** The modified GluR4 subunit of the AMPA receptor for LRET investigations. In this protein the N-terminal domain (22-402 amino acids) has been deleted, two cysteines at site 426 and 529 replaced with serines, and a cysteine introduced at site G740, S741, or S742. The modified receptor is tagged with maleimide derivatives of ATTO465 and a terbium chelate through a thiol linkage at the cysteine sites.

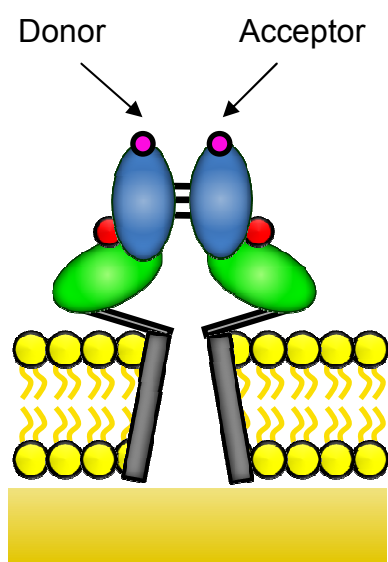
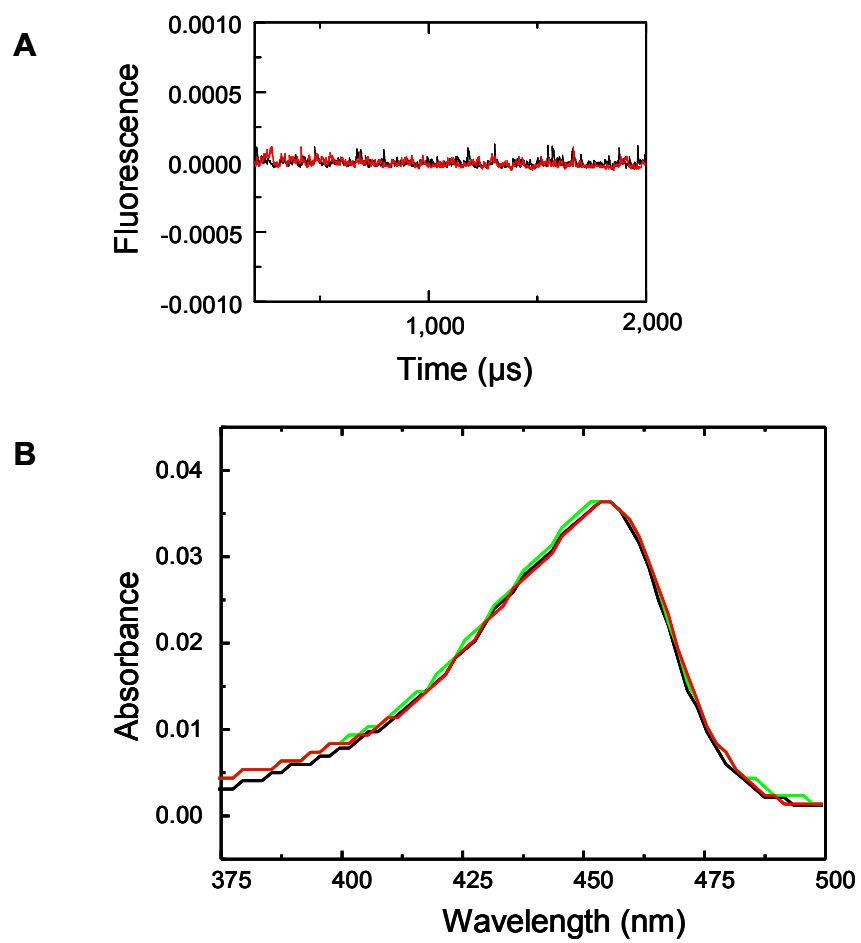


**Figure 31** Fluorophore control experiments. (A) To assess background LRET signal, donor only fluorophore (black) and acceptor only fluorophore (red) samples were studied at 510 nm, the wavelength of sensitized emission. (B) Absorption of ATTO465-maleimide (acceptor) was measured (black). The addition of 10 mM glutamate (green) and 100  $\mu$ M cyclothiazide (red) did not perturb the absorption spectrum.



## b. Receptor characterization by electrophysiology

Each of the mutant proteins were expressed in either oocytes or HEK-293 cells and characterized by electrophysiological investigations to ensure that the labeled, modified receptors exhibit similar functional properties as the wild-type receptor (Figure 32). The two well-established membrane protein expression systems were utilized to show that the LRET data obtained was not system specific. Dose response curves were obtained by studying the normalized maximum current measured by two-electrode voltage clamp (oocytes) or whole-cell recordings (HEK-293 cells) at various concentrations of glutamate. Mutants receptors,  $\Delta N^*$ -GluR4-G740C,  $\Delta N^*$ -GluR4-S741C, and  $\Delta N^*$ -GluR4-S742C, expressed in oocytes displayed similar dose response curves to the control,  $\Delta N^*$ -GluR4 receptors. Mutant receptors ( $\Delta N^*$ -GluR4-Th-S741C-Th) expressed in HEK-293 cells also had a similar dose response curve to the wild type GluR4-flip receptors.

For AMPA receptor expression in oocytes, in order to reduce non-specific labeling, the cysteine blocking procedure with  $\beta$ -maleimidopropionic acid was implemented [83, 96]. For the 1:4 labeling ratio, 0.5  $\mu$ M ATTO465 (acceptor) and 2  $\mu$ M terbium chelate (donor) was added to oocytes in storage solution and incubated for one hour at 18 °C. The excess fluorophore was removed from the oocytes with gentle rinsing with storage solution. Membranes from 300 oocytes expressing mutant receptors were prepared for LRET studies and other electrophysiological investigations. In Figure 33, single channel recordings were performed on membranes reconstituted into bilayers in order to establish if the manipulations during tagging the receptor and membrane preparations alter the function of the

**Figure 32** Dose response curves for mutant and wild-type AMPA receptors. (A) Normalized glutamate-evoked currents from  $\Delta$ N-GluR4 receptors (red),  $\Delta$ N\*-GluR4-G740C (blue),  $\Delta$ N\*-GluR4-S741C (green),  $\Delta$ N\*-GluR4-S742C (black) receptors expressed in oocytes were plotted as a function of glutamate concentration. (B) Mutant  $\Delta$ N\*-GluR4-Th-S741C-Th receptors (black) and Wild type GluR4-flip receptors (red) expressed in HEK-293 cells were studied. Currents elicited by various concentrations of glutamate were normalized to currents evoked by 10 mM glutamate in the presence of saturating concentrations of cyclothiazide to block desensitization.

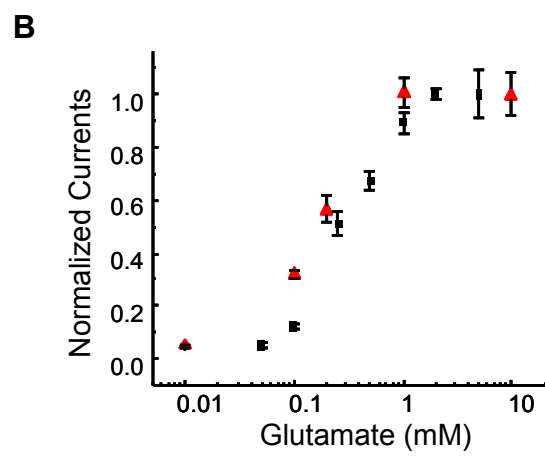
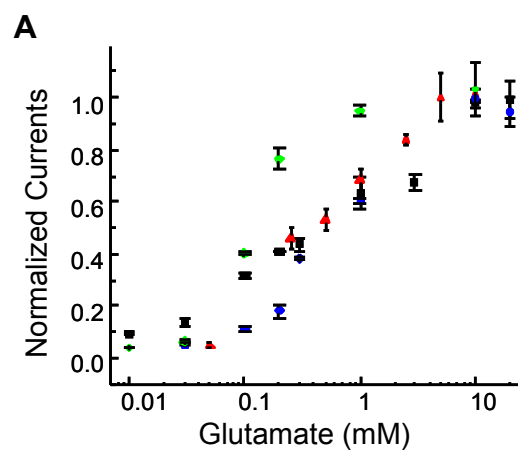
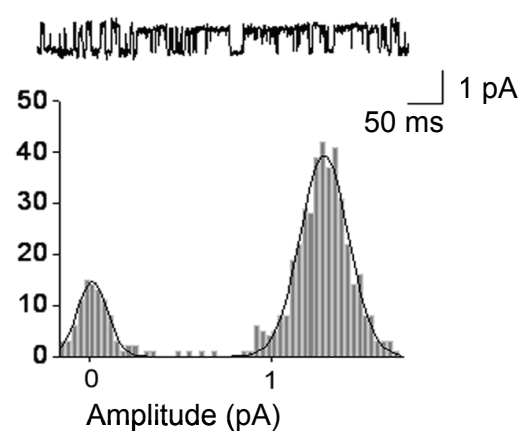


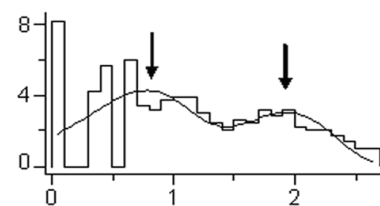


**Figure 33** Single channel recordings performed on membrane preparations of labeled, mutant receptors reconstituted in lipid bilayers (A) Single channel traces were analyzed to produce amplitude histograms for fluorophore tagged  $\Delta N^*$ -GluR4-S741C receptors. The voltage was held at 120 mV and recordings were measured at 1 mM Glutamate in the presence of 100  $\mu$ M cyclothiazide. The major conductance state is found to be at 9-12 pS. Time distributions for two separate (B) open times and (C) close times for tagged  $\Delta N^*$ -GluR4-S741C.

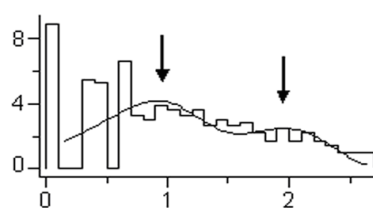
**A**  $\Delta N^*$ -GluR4 S741C



**B** Log open time (ms)



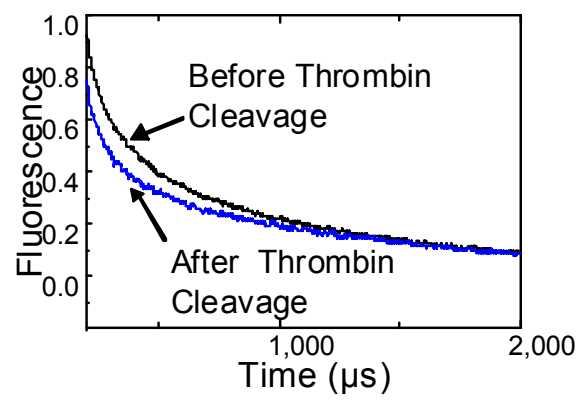
**C** Log close time (ms)



receptor. The recordings were performed by our collaborator at Auburn University in Alabama and determined that mutated receptors (tagged with fluorophores) exhibit similar single channel open probability and conductance to the wild-type receptor suggesting that the manipulations for the LRET do not have a significant effect on the receptor function. Additionally, for the LRET control experiments, non-AMPA receptor expressing oocytes (non-injected) were prepared and studied in parallel in order to subtract remaining background LRET.

For AMPA expression in HEK-293 cells, the  $\Delta N^*$ -GluR4-S741C construct used for oocyte expression has been further modified. For HEK-293 cells, pre-blocking inherent cysteines with  $\beta$ -maleimidopropionic acid is not effective. In order to address non-specific background LRET in this expression system, a thrombin cleavage site (LVPRGS) was introduced on each side of the S741C mutation to create the  $\Delta N^*$ -GluR4-Th-S741C-Th receptor. A 1:4 labeling ratio of donor to acceptor in phosphate buffered saline (PBS) is added to cells expressing the receptor and incubated for one hour at room temperature. Excess fluorophores are removed by washing with PBS, and intact cells resuspended in PBS are used for LRET investigations. The LRET signal measured after the addition of thrombin and cleavage of the S741C provides a quantitative measure of the background non-specific LRET, which can be removed from the initial signal obtained prior to the addition of the protease to obtain the LRET signal of interest (Figure 34). For thrombin cleavage of the cysteine at position S741, 3 U of thrombin are added to the sample of HEK-293 cells used previously for initial LRET studies; the cells are

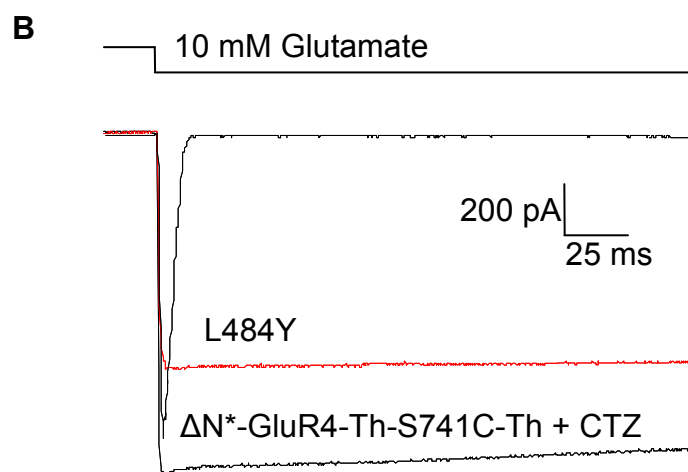
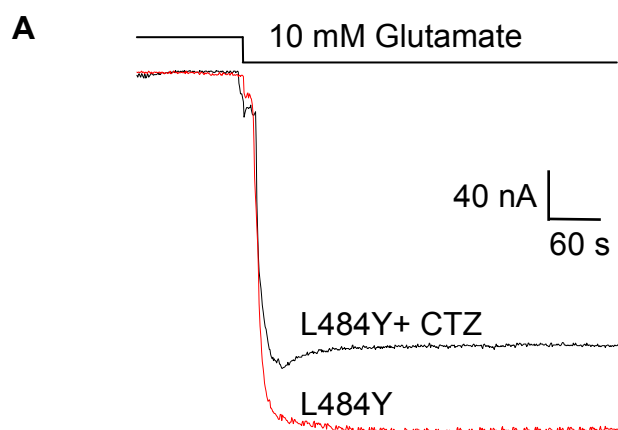
**Figure 34** Representative non-specific, background LRET for  $\Delta N^*$ -GluR4-Th-S741-Th receptors expressed in HEK-293 cells. For the resting state, the initial LRET signal (before thrombin cleavage) and the non-specific, background LRET signal (after thrombin cleavage) were obtained at 510 nm for tagged receptors.



incubated for three hours at room temperature.

Furthermore, the modified receptors were further tested by electrophysiology to ensure that each state of the receptor is entered upon the addition of agonist, modulator, or the introduction of mutations, simulating LRET experiments. In Figure 35, representative macroscopic currents obtained by two-electrode voltage clamp (oocytes) and whole-cell recordings (HEK-293 cells) are shown. In Figure 35 A, currents from  $\Delta N^*$ -GluR4-L484Y-S741C receptors were measured in the presence of saturating concentrations of glutamate and cyclothiazide to reproduce conditions for the open state. In the presence of glutamate alone and in the presence of glutamate plus cyclothiazide, the desensitized state is not entered. Additionally, in the unligated, apo state, the presence of the L484Y mutation in the absence of glutamate does not evoke currents. In Figure 35 B, for  $\Delta N^*$ -GluR4-Th-S741C-Th expressed in HEK-293 cells, no currents were obtained in the absence of ligand to obtain the apo, resting state. Saturating concentrations of glutamate (10mM) were added to show that the receptor enters the desensitized state. The open state is obtained in the presence of glutamate and 100  $\mu$ M cyclothiazide. Additionally, in the presence of the L484Y mutation, desensitization is blocked. Hence, it is clear that the modified receptors are capable of entering various states of the receptor under the conditions for LRET investigations. For the LRET investigations, the lifetimes are used to calculate the average distance between with donor and acceptor fluorophore in conditions for the receptor to enter the resting, open, and desensitized state.

**Figure 35** Current traces from modified receptor subjected to LRET conditions to obtain various states of the receptor. (A) Currents elicited by saturating concentrations of glutamate (10 mM) and in the presence and absence of cyclothiazide (100  $\mu$ M) were recorded by two-electrode voltage clamp from  $\Delta$ N\*-GluR4-L484Y-S742C receptors expressed in oocytes. (B) Currents elicited by saturating concentrations of glutamate (10 mM), in the presence glutamate plus cyclothiazide (100  $\mu$ M), and for the L484Y mutant were recorded by whole-cell recordings from  $\Delta$ N\*-GluR4-Th-S741C-Th receptors expressed in HEK-293 cells.





### III. LRET Results and Discussion

#### a. Intersubunit distance measurements for the states of the receptor

By studying the LRET lifetimes in the unligated, glutamate-bound, and glutamate-bound in the presence of cyclothiazide or the L483Y mutation will reveal the conformational changes at the dimer interface in the apo, desensitized, and open states, respectively. The LRET signal measured for fluorophore tagged non-injected, control oocytes or after thrombin cleavage of receptors expressed in HEK-293 cells provides a direct quantification of the background non-specific LRET, which can be removed from the initial signal to provide the specific LRET signal as shown in Figure 36-37. Figure 38 reveals that LRET lifetimes recorded from donor-only tagged  $\Delta N^*$ -AMPA-S741C receptors at 488 nm does not significantly change among the various states of the receptor, suggesting that changes in sensitized emission lifetimes are significant.

The sensitized emission lifetimes obtained could be well-represented by a two exponential decay for donor:acceptor labeled  $\Delta N^*$ -GluR4-G740C,  $\Delta N^*$ -GluR4-S741C, and  $\Delta N^*$ -GluR4-S742C expressed in oocytes and  $\Delta N^*$ -GluR4-Th-S741C-Th expressed in HEK-293 cells. The faster lifetime and hence shorter distance makes up the majority of the LRET signal obtained (90%), and these shorter distances are similar to those observed in the crystal structures (Table 2). For example, the shorter distance obtained in the open state (represented by the presence of the L484Y mutation with saturating concentrations of glutamate and cyclothiazide) are  $20 \pm 0.5$  Å at position 740,  $19 \pm 0.6$  Å ( $22 \pm 0.2$  Å in HEK-293 cells) at position 741, and  $21 \pm 0.3$  Å at position 742, which are similar to nitrogen backbone crystallographic

**Figure 36** Sensitized emission measured at 510 nm for donor:acceptor tagged receptors expressed in oocytes. LRET lifetimes for (A)  $\Delta N^*$ -GluR4-G740C, (B)  $\Delta N^*$ -GluR4- S741C, (C)  $\Delta N^*$ -GluR4- S742C, (D)  $\Delta N^*$ -GluR4-L484Y-G740C, (E)  $\Delta N^*$ -GluR4-L484Y-S741C, and (F)  $\Delta N^*$ -GluR4-L484Y-S742C receptors in the unligated state (black), with 10 mM glutamate (green), and with 10 mM glutamate plus 100  $\mu$ M cyclothiazide (red).

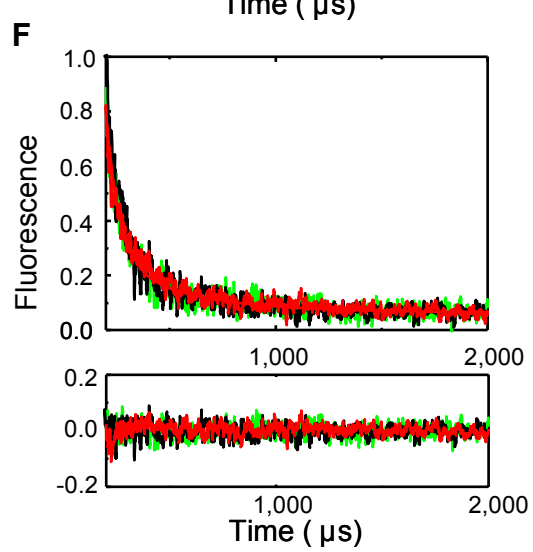
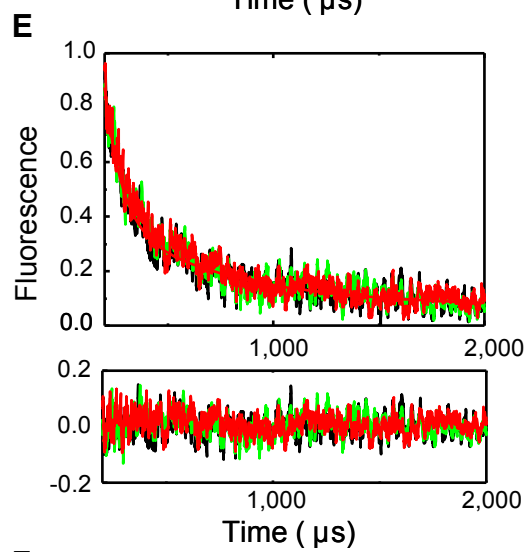
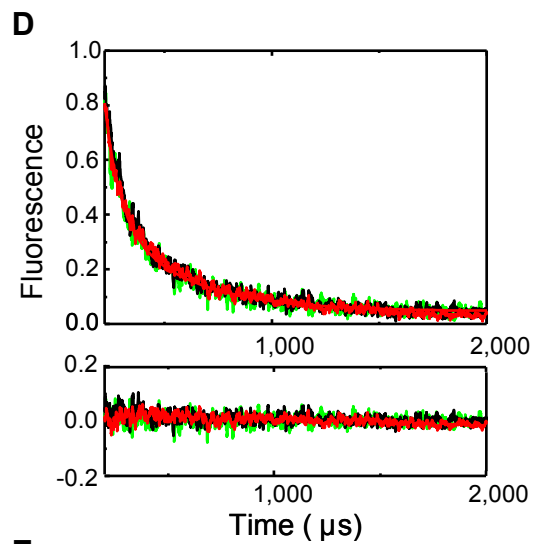
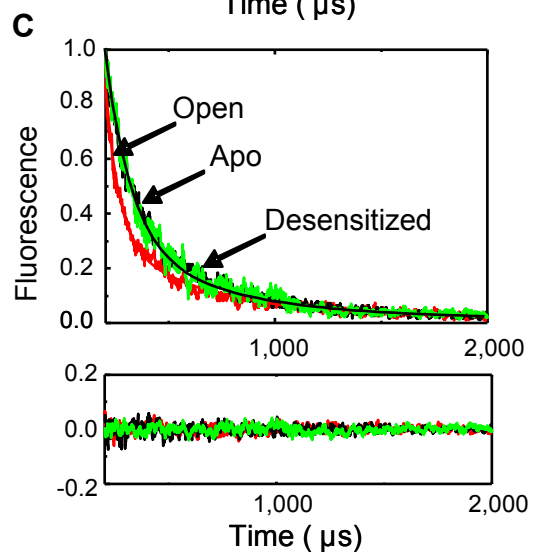
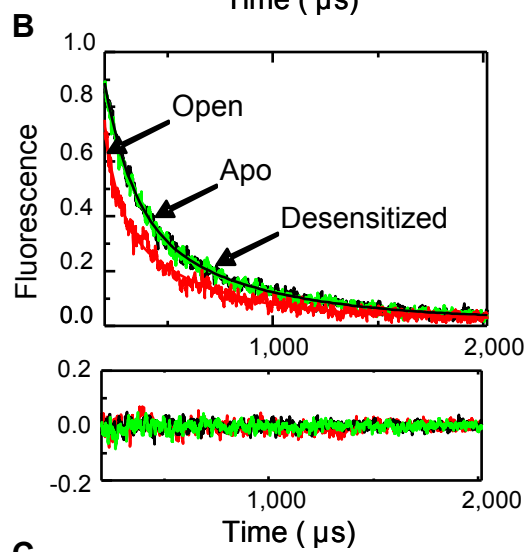
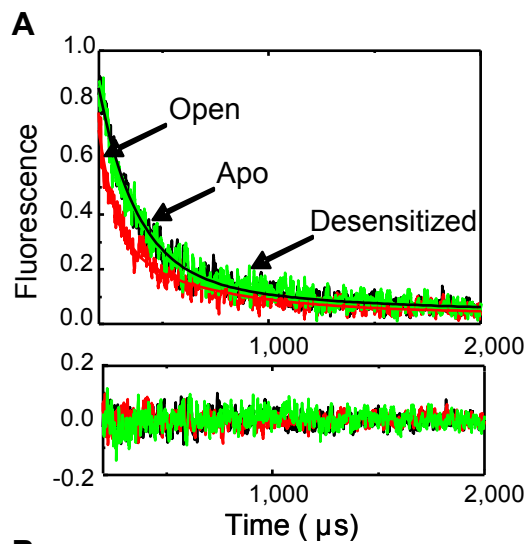


**Figure 37** Specific LRET signal obtained after background subtraction for donor:acceptor tagged receptors expressed in HEK-293 cells. LRET signal obtained in the unligated state (black), with 10 mM glutamate (green), with 10 mM glutamate plus 100  $\mu$ M cyclothiazide (red), and in the presence of 200 nM antagonist ZK 200775 (blue) for (A)  $\Delta$ N<sup>\*</sup>-GluR4-Th-S741-Th and (B)  $\Delta$ N<sup>\*</sup>-GluR4-L484Y-Th-S741-Th receptors.

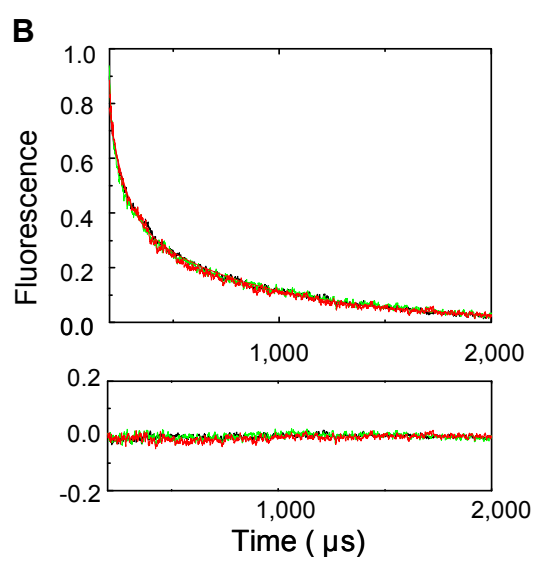
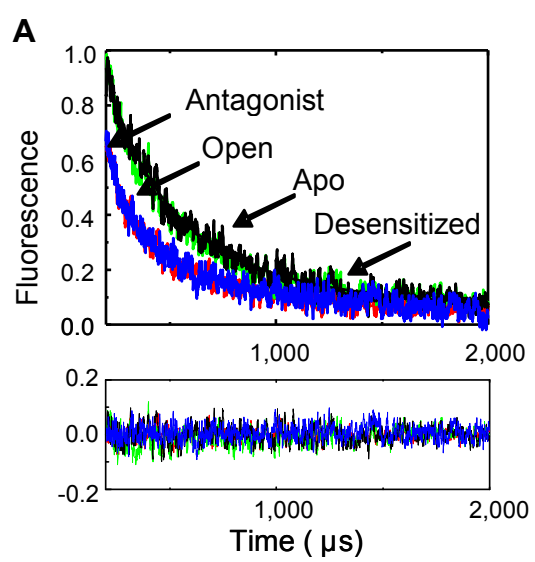


**Figure 38** Sensitized emission measured at 488 nm for donor-only labeled  $\Delta N^*$ -GluR4-S741 receptors expressed in oocytes. LRET lifetimes were obtained in the apo (black), open (10 mM glutamate plus 100  $\mu$ M cyclothiazide-red), and desensitized (10 mM glutamate-green) states.

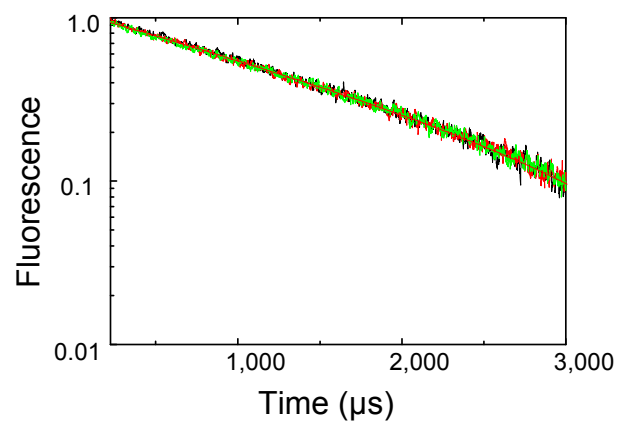


**Table 2** LRET lifetimes and calculated intersubunit distances. Lifetimes of the donor-only labeled protein and the subtracted lifetimes for the sensitized emission of the acceptor in the presence of the donor with the corresponding distances for the apo/resting state, the open channel state, and the desensitized state.



Protein	Ligand/State	Donor lifetime ( $\mu$ s)	Sensitized emission lifetime ( $\mu$ s)	Distance ( $\text{\AA}$ )
$\Delta$ N*-GluR4-G740C	Apo/resting	1526 $\pm$ 50	188 $\pm$ 12 535 $\pm$ 15	25 $\pm$ 0.3 32 $\pm$ 0.3
$\Delta$ N*-GluR4-G740C	Glu/desensitized	1510 $\pm$ 45	173 $\pm$ 10 534 $\pm$ 18	25 $\pm$ 0.3 32 $\pm$ 0.3
$\Delta$ N*-GluR4-G740C	Glu+CTZ/open	1534 $\pm$ 45	73 $\pm$ 10 439 $\pm$ 15	21 $\pm$ 0.5 30 $\pm$ 0.3
$\Delta$ N*-GluR4-G740C-L484Y	Apo	1841 $\pm$ 50	63 $\pm$ 5 336 $\pm$ 18	20 $\pm$ 0.3 27 $\pm$ 0.3
$\Delta$ N*-GluR4-G740C-L484Y	Glu	1845 $\pm$ 60	67 $\pm$ 3 357 $\pm$ 20	20 $\pm$ 0.2 28 $\pm$ 0.3
$\Delta$ N*-GluR4-G740C-L484Y	Glu+CTZ/open	1845 $\pm$ 60	61 $\pm$ 8 444 $\pm$ 21	20 $\pm$ 0.5 29 $\pm$ 0.3
$\Delta$ N*-GluR4-S741C	Apo/resting	1682 $\pm$ 50	132 $\pm$ 9 595 $\pm$ 23	23 $\pm$ 0.3 32 $\pm$ 0.3
$\Delta$ N*-GluR4-S741C	Glu/desensitized	1686 $\pm$ 60	126 $\pm$ 10 522 $\pm$ 20	23 $\pm$ 0.3 31 $\pm$ 0.3
$\Delta$ N*-GluR4-S741C	Glu+CTZ/open	1612 $\pm$ 60	60 $\pm$ 7 367 $\pm$ 15	20 $\pm$ 0.4 29 $\pm$ 0.3
$\Delta$ N*-GluR4-S741C-L484Y	Apo	1877 $\pm$ 45	53 $\pm$ 9 542 $\pm$ 19	19 $\pm$ 0.6 30 $\pm$ 0.3
$\Delta$ N*-GluR4-S741C-L484Y	Glu	1820 $\pm$ 45	55 $\pm$ 10 565 $\pm$ 17	20 $\pm$ 0.6 31 $\pm$ 0.3
$\Delta$ N*-GluR4-S741C-L484Y	Glu+CTZ/open	1818 $\pm$ 50	51 $\pm$ 10 584 $\pm$ 15	19 $\pm$ 0.6 31 $\pm$ 0.3

$\Delta N^*$ -GluR4-Th-S741C-Th	Apo/resting	1578 $\pm$ 45	188 $\pm$ 13 535 $\pm$ 16	25 $\pm$ 0.3 31 $\pm$ 0.3
$\Delta N^*$ -GluR4-Th-S741C-Th	Glu/desensitized	1505 $\pm$ 45	174 $\pm$ 4 534 $\pm$ 20	25 $\pm$ 0.2 32 $\pm$ 0.3
$\Delta N^*$ -GluR4-Th-S741C-Th	Glu+CTZ/open	1579 $\pm$ 55	73 $\pm$ 3 439 $\pm$ 15	21 $\pm$ 0.2 30 $\pm$ 0.3
$\Delta N^*$ -GluR4-Th-S741C-Th	ZK200775	1679 $\pm$ 45	77 $\pm$ 5 489 $\pm$ 15	21 $\pm$ 0.2 30 $\pm$ 0.3
$\Delta N^*$ -GluR4-Th-S741C-Th-L484Y	Apo	1609 $\pm$ 60	92 $\pm$ 3 502 $\pm$ 15	22 $\pm$ 0.2 31 $\pm$ 0.3
$\Delta N^*$ -GluR4-Th-S741C-Th-L484Y	Glu	1565 $\pm$ 55	70 $\pm$ 3 504 $\pm$ 15	21 $\pm$ 0.2 31 $\pm$ 0.3
$\Delta N^*$ -GluR4-Th-S741C-Th-L484Y	Glu+CTZ/open	1579 $\pm$ 50	92 $\pm$ 3 572 $\pm$ 20	22 $\pm$ 0.2 32 $\pm$ 0.3
$\Delta N^*$ -GluR4-S742C	Apo/resting	1704 $\pm$ 60	124 $\pm$ 7 596 $\pm$ 22	23 $\pm$ 0.3 32 $\pm$ 0.4
$\Delta N^*$ -GluR4-S742C	Glu/desensitized	1730 $\pm$ 60	118 $\pm$ 6 517 $\pm$ 15	23 $\pm$ 0.2 30 $\pm$ 0.3
$\Delta N^*$ -GluR4-S742C	Glu+CTZ/open	1682 $\pm$ 55	62 $\pm$ 5 444 $\pm$ 15	20 $\pm$ 0.3 29 $\pm$ 0.3
$\Delta N^*$ -GluR4-S742C-L484Y	Apo	1557 $\pm$ 45	66 $\pm$ 5 464 $\pm$ 15	21 $\pm$ 0.3 30 $\pm$ 0.3
$\Delta N^*$ -GluR4-S742C-L484Y	Glu	1517 $\pm$ 45	67 $\pm$ 5 477 $\pm$ 15	21 $\pm$ 0.3 31 $\pm$ 0.3
$\Delta N^*$ -GluR4-S742C-L484Y	Glu+CTZ/open	1509 $\pm$ 45	64 $\pm$ 5 446 $\pm$ 15	21 $\pm$ 0.3 30 $\pm$ 0.3

distances measured at these sites, 17 Å, 20 Å, and 22 Å, respectively. The full receptor crystal structure suggests that distances between these sites across the dimer vary from 55 to 70 Å, well outside the preferred efficiency range for the fluorophore pair chosen ( $R_0=35$  Å) [62]. The 10% of the lifetime observed are in the range of 30 to 32 Å, and hence can be attributed to the distances across the dimer. The longer distances may be due to a small fraction of the receptors in a different state or residual, non-specific signal.

The shorter distances that correspond to distances within the dimer show that the open channel state undergoes an increase distance change of around 3 to 5 Å upon desensitization of the receptor (glutamate-bound). This conformational change coincides with the current hypothesis for desensitization where the dimer interface is coupled in the open state and upon entrance into the desensitized state, the interface rearranges and decouples [61]. Additionally, the GluR2-S729C isolated LBD crystal structure shows a greater distance change (8 Å) from the open to desensitized state at site 740 (741 in GluR4) [58]; because this structure has been acquired by artificially decoupling the dimer interface, this could lead to a more decoupled state than what is observed in a physiologically relevant state. It should be noted that the LRET distances observed are representative of the on average distances that the dynamic receptor enters during a given state.

#### b. Mechanism for the resting, activated, and desensitized states

LRET lifetimes were also obtained for the apo, resting state of the receptor (in the absence of the L484Y mutation), for which no direct structural data exists.

Moreover, the intersubunit distances obtained in the apo state for each of the probes is not consistent with the current hypothesis; the expected crystallographic distance for the apo state shows that the interface is coupled at 16 Å much like that of the open state. The LRET intersubunit distances, however, reveal that the apo state is 3 to 5 Å longer than the distances measured for the open state (Table 2). In fact, the apo state resembles that of the desensitized state where the dimer interface is decoupled, and hence the dimer interface is not pre-formed as suggested by the isolated LBD crystal structure. This also suggests that in the absence of transmembrane segments, the isolated LBD has a propensity to crystallize as a dimer that is coupled no matter what state the receptor is in. Additionally, detailed GluR2-S729C crosslinking experiments revealed that the dimer interface is dynamic by showing that the disulfide bond is not formed within the interface when the L484Y mutation is present; however, it is formed in both the resting and desensitized state and the presence of antagonist reduced disulfide formation [117]. Thus, stabilization of the dimer interface by L484Y blocked the formation of the disulfide, and the formation of the disulfide in the unligated, resting state suggest that dimer interface contacts were broken.

The crosslinking studies as well as the crystal structure of the isolated LBD L483Y (L484Y in GluR4) mutant suggest that the dimer interface is stabilized [61, 117]. LRET distances obtained from the L484Y mutants are similar in the apo state, in the presence of glutamate, and in the presence of glutamate plus cyclothiazide suggesting that the dimer interface is coupled. The LRET distances for each of the L484Y probes resemble the LRET distances in the open state

(glutamate in the presence of cyclothiazide). This data supports the notion that the dimer interface is pre-formed and hence stabilized in the L484Y mutant. As shown in the electrophysiological characterization of the L484Y modified receptors, glutamate is required to activate the channel; no currents in this mutant were elicited in the absence of agonist (Figure 35). A pre-form dimer would, on the other hand, aid in the energetics of the conformational changes associated with the activation of the receptor, as shown by a decreased  $EC_{50}$  compared to wild-type receptors.

The LRET distances thus far have been compared to crystallographic distances measured in the well-characterized isolated LBD dimer; however, these structures are limited by the lack of the transmembrane segments, the functional portion of the receptor. With the recently solved structure of the full receptor, LRET distances can now be compared to a more relevant structure. GluA<sub>cryst</sub> was solved with ZK 200775 bound resulting in an elongated cleft distance; the structure showed a coupled dimer interface measuring around 20 Å [62]. Thus, LRET distances were obtained for  $\Delta N^*$ -GluR4-Th-S741C-Th receptors in the presence of the competitive antagonist (Figure 37). The measured LRET distance of  $21 \pm 0.2$  Å would suggest that the dimer interface is coupled like the open state as detected by LRET and is similar to the antagonist-bound full receptor structure. Together, these results support that the dimer interface is dynamic, and the resting state of the receptor primarily exhibits a decoupled dimer interface.

With the insight from the LRET intersubunit measurements of the dimer interface, a mechanism is proposed that differs from the mechanism based on

crystallographic measurements (Figure 39). The LRET investigations suggest that in the apo/resting state, the channel is closed, the cleft is open, and dimer interface is decoupled. Upon ligand binding to the ligand binding domain, the cleft closes by domain 2 moving up towards domain 1. Contacts form between the dimer interface at domain 1 to transiently stabilize the open channel. Cleft closure pulls apart the transmembrane segments causing the channel to open (activation) and stress on the transmembrane segments causes the decoupling of the dimer interface resulting in the channel closure (desensitization).

#### **IV. Future directions**

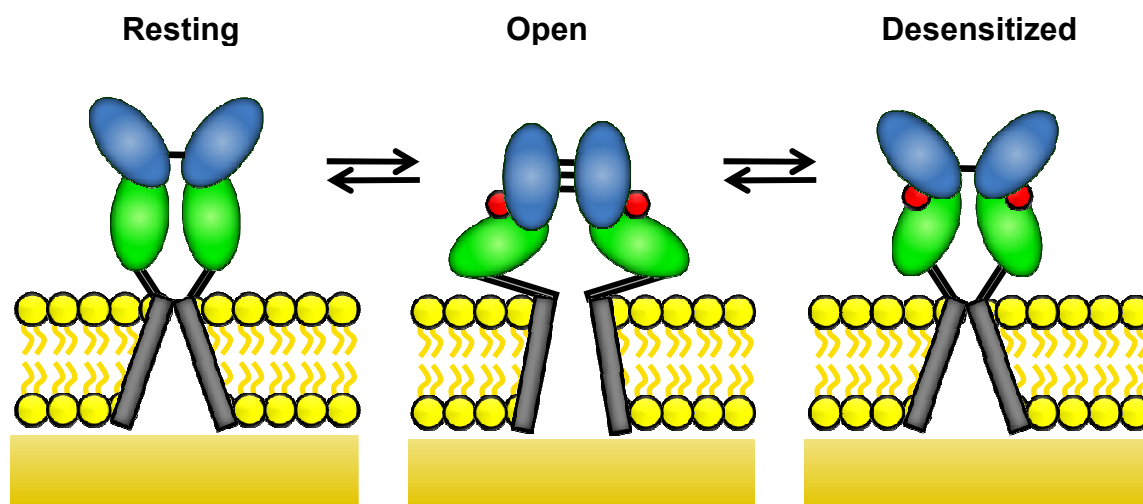
Dimer interface rearrangement has proven to play an important role in all states of the AMPA receptor. As posed earlier during the activation studies, how would the conformational changes seen in the functional receptor behave in an even more physiologically relevant environment? Stargazin, known to alter AMPA receptor biophysical properties [109-111, 113-116], could act similarly to the L484Y mutation by stabilizing the dimer interface thereby enhancing receptor activation.

Additionally, the dimer interface is also being investigated in other glutamate receptor subtypes; however, no in depth structural information exists. Receptor modulators including  $\text{Zn}^{2+}$  and protons have been shown to bind to the N-terminal domain and consequently alter activation and desensitization at the dimer interface [118-120]. Similar LRET studies could be performed in order to test the state of the interface in the presence of modulators.

Furthermore, studies show that the R629E, a mutation outside the ligand binding domain, blocks desensitization [76]. Hence, there is currently no structural evidence for this mutant. For the proposed experiments the intersubunit distance will be determined by FRET using the G740C, S741C, and S742C. The same protocol as mentioned above will be used in the FRET measurements where a 1:4 ratio of acceptor and donor will be used to label the mutant protein. The only difference is that the current experiments will be performed in the context of the R629E mutation. This mutation will provide insight into desensitization by determining the intersubunit distances in different states of the receptor. From our studies, if there is no change in the intersubunit distance between the apo and glutamate bound forms in the R629E mutation, it would suggest that the mutation allosterically stabilizes the domain 1 interface. However, if the intersubunit distance increases upon going from the apo to the glutamate bound form, then it would suggest that dimer decoupling occurs but is not communicated to the channel segments due to the R629E mutation, and that the R629E mutation stabilizes the open channel form by stabilizing near the channel. These studies might reveal another level by which desensitization is controlled and call for further investigation.

**Figure 39** Proposed mechanism for the resting, open, and desensitized state based on LRET investigations. In the resting state, no ligand is bound and the cleft is open. Upon ligand binding, the cleft closes and pulls apart the transmembrane segments thereby opening the channel. Contacts form between the dimer interface to transiently stabilize the open channel. Stress on the linker to the transmembrane segments causes the decoupling of the dimer interface resulting in a closed channel, the desensitized state.





## **Chapter 6—LRET Part III: $\text{Ca}^{2+}$ subdomain orientation of $\text{Na}^+/\text{Ca}^{2+}$ exchangers**

## I. $\text{Na}^+/\text{Ca}^{2+}$ exchanger Structure and Function

In previous chapters, I have established LRET as a powerful tool capable of measuring conformations within a protein in a dynamic state. This chapter of the dissertation discusses a collaborative project with Dr. Lei Zheng and his post-doctoral fellow Mousheng Wu (UT-Houston Medical School), where LRET measurements are performed on the  $\text{Ca}^{2+}$  regulatory domain of the  $\text{Na}^+/\text{Ca}^{2+}$  exchanger in order to support its crystal structure solved by his lab.  $\text{Na}^+/\text{Ca}^{2+}$  exchangers (NCX) play a critical role in  $\text{Ca}^{2+}$  homeostasis throughout the mammalian system, a process vital for cardiac contractibility in addition to excitation/relaxation coupling in the brain [121, 122]. These highly regulated antiporter proteins enable the exchange of  $\text{Na}^+$  and  $\text{Ca}^{2+}$  ( $3 \text{ Na}^+ : 1 \text{ Ca}^{2+}$ ) ions across the plasma membrane depending on the membrane potential and chemical gradient of the ions [123]. In order to understand the function of the  $\text{Na}^+/\text{Ca}^{2+}$  exchanger, detailed investigations of the structure of the protein are required.

$\text{Na}^+/\text{Ca}^{2+}$  exchangers are a family of proteins that contain nine transmembrane segments including a  $\text{Ca}^{2+}$  regulation domain, a large intracellular loop (~500 amino acid residues) flanked by the fifth and sixth transmembrane segments. The domain consists of two subdomains, CBD1 and CBD2, which serve as  $\text{Ca}^{2+}$  sensors [124]. Although CBD1 is conserved throughout the family, alternative splicing of CBD2 enables further fine tuning of  $\text{Ca}^{2+}$  regulation (Wu). The structures of individual  $\text{Ca}^{2+}$  sensors, CBD1 and CBD2 from canine exchanger NCX1 and *Drosophila* exchanger CALX, were solved by NMR and x-ray crystallography [125-129]. It has been shown that upon  $\text{Ca}^{2+}$  interaction,

conformational changes are induced within the CBD domains and each is capable of  $\text{Ca}^{2+}$  interaction, however,  $\text{Ca}^{2+}$  binding to an individual domain does not induce large scale conformational changes [128, 130, 131]. No structural information for the complete CBD domain is available; however, it has been shown by mutagenesis that interaction between the domains is required for function [132, 133]. It is currently hypothesized that  $\text{Ca}^{2+}$  binding induces a conformational change within the CBD domain and this is translated to the adjacent transmembrane segments such that the ion exchange pore opens/closes. Nevertheless, the mechanism for  $\text{Ca}^{2+}$  conductivity by  $\text{Ca}^{2+}$  binding is not completely clear without the full structure of the CBD domain. Additionally, it is not understood how the varied residues in CBD2 introduced by alternative splicing alters NCX  $\text{Ca}^{2+}$  regulation, as shown in isoforms, CALX1.1 and CALX1.2. Each isoform clearly demonstrates drastically different  $\text{Ca}^{2+}$  regulation properties [134]. In order to elucidate the mechanism for  $\text{Ca}^{2+}$  regulation, Wu determined crystal structures of complete NCX  $\text{Ca}^{2+}$  regulatory domain of two splice variants, CALX1.1 and CALX1.2, in the apo form.

## **II. LRET Results and Discussion**

The crystal structures of the CBD domain revealed an open V-shape of CBD1 and CBD2. Additionally,  $\text{Ca}^{2+}$  binding sites of CBD1 were determined to be located at the hinge region. As shown in Figure 40 A, three cysteine mutations were introduced at various positions (S581, T560, T567) on the CBD2 of the CALX1.1 isoform which contained an N-terminus histidine tag. These probes allow the measurements of the conformation of the CALX1.1 isoform in its open state in order to support the structure solved by Wu. LRET measurements were performed

between the introduced cysteine mutant and the N-terminus his-tag labeled with terbium chelate and (Ni-NTA)<sub>2</sub>Cy3, respectively. LRET lifetimes were obtained (Figure 40 B-C) and distances were calculated (Table 3). These measurements demonstrate that the distance from the histag (N-terminus) to T567C, the cysteine farthest from the hinge region, is significantly longer ( $56 \pm 5$  Å) than to those closer to the hinge region. LRET distances for T560C and S581C are shorter at distances of  $41 \pm 2$  Å and  $42 \pm 2$  Å. These studies reveal that the open V-shape conformation observed in the crystal structures exists in solution without crystallographic constraints.

Wu solved the crystal structure of both isoforms, CALX1.1 and CALX1.2, and the conformational comparison between isoforms reveals that the orientation angle of the open V-shape is different. CALX1.1 exhibits a strong response to regulatory  $\text{Ca}^{2+}$ , dissimilar to the regulatory  $\text{Ca}^{2+}$  independence of CALX1.2 [134]. Hence, the difference in orientation angles observed in the crystal structures suggest that the orientation angle of the CBD subdomain is the primary means for  $\text{Ca}^{2+}$  mediated NCX regulation. Therefore, Wu proposed that CALX  $\text{Ca}^{2+}$  regulation occurs by  $\text{Ca}^{2+}$  binding at CBD1 thus stabilizing the subdomain interaction between CBD1 and CBD2. This interaction changes the orientation angle between CBD1 and CBD2, and consequently repositions the transmembrane segments close the ion translocation pathway. Despite various members of the family (NCX1 and CALX) displaying opposite  $\text{Ca}^{2+}$  regulation properties, they have conserved hinge regions. Wu suggests that the altered orientation angle established by the crystal structures

of the splice variants of CALX may represent a common structural feature of the NCX family exhibited for  $\text{Ca}^{2+}$  mediated NCX regulation.

**Figure 40** LRET measurements in the  $\text{Ca}^{2+}$  regulatory domain of CALX1.1. (A) Representation of the donor and receptor positions in LRET measurements. Acceptor Cy3 was coordinated with the histag at N-terminus of the  $\text{Ca}^{2+}$  regulatory domain of CALX1.1 spaced with a thrombin cleavage sequence. (B) Donor-only life collected at 545 nm. (C) The LRET lifetimes as measured by the sensitized emission of the acceptor at 575 nm for the mutant proteins containing an N-terminal histag and cysteines located at positions 581 (red), 560 (blue), and 567 (black) on CBD2.

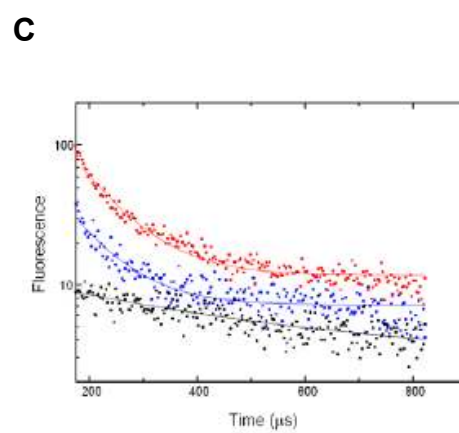
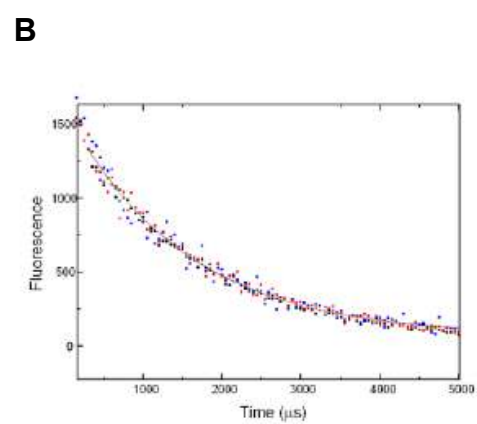
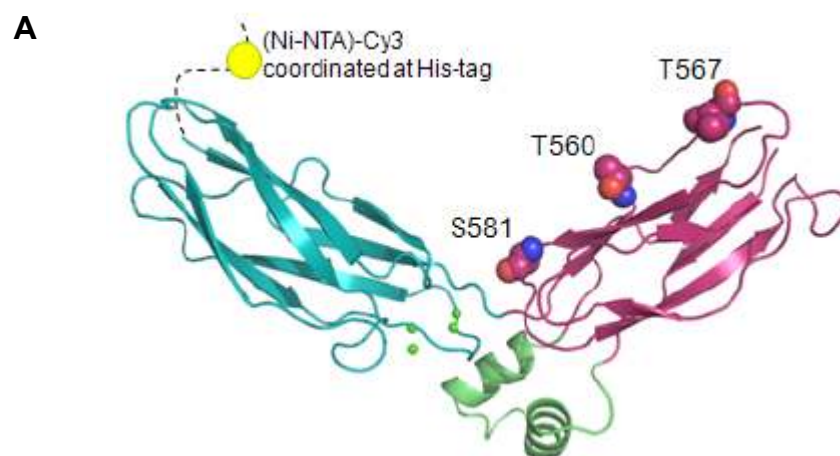




**Table 3** LRET lifetimes and distances between N-terminus His tag to different positions on CBD2. Crystallographic distances are measured between the C $\alpha$  atoms between the N-terminal I422 and respective donor residue.

Position	Donor lifetime ( $\mu\text{s}$ )	Sensitized emission lifetime ( $\mu\text{s}$ )	Distance to His-tag (LRET) ( $\text{\AA}$ )	Distance to N terminus 422 (in structure) ( $\text{\AA}$ )
581	1607 $\pm$ 55	81 $\pm$ 2	42 $\pm$ 2	44
560	1607 $\pm$ 69	77 $\pm$ 4	41 $\pm$ 2	53
567	1612 $\pm$ 38	380 $\pm$ 32	56 $\pm$ 5	70

## **Chapter 7-Overall Conclusions**

Neurons communicate with each other by chemical signals and transmit information by electrical signals. An abundant protein in the brain known as a glutamate receptor is a key player in this process by converting chemical signals into electrical signals. The glutamate receptor is a ligand-gate ion channel, and its unique three-dimensional structure resembling a cleft enables the protein to bind to glutamate (chemical signal), and in consequence this interaction allows the receptor to open its pore and act as a gateway to allow charged ions (electrical signal) to pass through, hence sending the message to the next neuron [17-21]. Thus, glutamate receptors, a model to study allostereism, couple ligand binding to receptor function. So the question arises, how does a small molecule like glutamate induce allosteric changes in glutamate receptors and in turn dictate function? Recently, the structure of the full receptor was solved [62]; however, these structures are not dynamic representations of the receptors in a physiologically relevant state. The approach in this dissertation includes biophysical techniques that can measure the conformational changes in the structure of a functional, ligand-bound receptor and directly correlate this structural data with the function of the receptor, as probed by the electrical signal produced by the receptor.

To reiterate the importance of the mechanism based on LRET distances, I return to the subject of the allosteric behavior of AMPA receptors and its implications for other subtypes of glutamate receptors. As discussed in Chapter 1, Jin et al. studies suggest that AMPA receptors are allosteric proteins that closely follow the multi-state induced fit, KNF model. Jin et al. provided an explanation for agonist efficacy using the 5-substituted willardiines. These partial agonists showed

a graded cleft closure, which is consistent with the KNF model. They showed how partial agonists, at saturating concentrations, could induce submaximal currents and cleft closure [59]. In addition, the extent of cleft closure as a result of the occluding size of the substituent was correlated to the efficacy for activation of the receptor, which also strongly supports the KNF model [18]. The degree of cleft closure determines an individual subunit's response to the ligand binding and ultimately ion channel opening. So, each subunit's opening can then contribute to the opening of higher subconductance states as it becomes more favored as the coupling efficiency increases between ligand binding and activation of the channel [59]. The structural studies, however, were performed in the isolated ligand binding domain, lacking the functional portion of the receptor. Additionally, because the isolated LBD is dimeric, the cooperative structural changes between the domains is lacking. To test the activation hypothesis in a functional receptor, I measured the extent of cleft closure in the  $\Delta N^*$ -AMPA using a series of agonists which exhibit a wide range of activations. In summary, the LRET experiments with the modified receptor reveal that the distance change between the apo state and glutamate-bound state, is in agreement with crystal structure distances, clearly indicating that the modified, functional AMPA receptor undergoes similar graded cleft closure conformational changes as seen in the crystal structures of the isolated LBD. The kainate-bound, partial agonist bound state showed an intermediate distance compared to the difference between the apo and glutamate bound, full agonist bound state as expected from the crystal structures. The extent of activation of the receptor shows a correlation to the extent of cleft closure induced

by the agonist binding to the receptor. These results show that the isolated LBD is a good model of the domain in the full receptor, thus the allosteric behavior established by the isolated LBD studies can be extended to the functional receptor [96]. It has been shown by LRET on isolated LBD of kainate receptors, that these receptors exhibit a graded cleft closure [135]. However, the structure of the NMDA receptor has not been extensively studied; these receptors are obligate heteromers of glycine-binding NR1 or NR3 subunits and glutamate-binding NR2 [136-141]. NR1 isolated ligand binding domain structures reveal no changes in cleft closure between full and partial agonists; and the NR2A isolated ligand binding domain has only been solved in the presence of glutamate [139-141]. Thus, LRET studies could be performed on NMDA receptors to determine if the NR2A subunit has graded cleft closure.

The current hypothesis for desensitization is that the stress on the transmembrane segments induced by cleft closure upon agonist binding results in the separation of the interface (domain 1) between two subunits in the glutamate receptor tetramer leading to desensitization [58]. This hypothesis is based on indirect structural investigations and functional investigations of the isolated LBD where the dimer interface is stabilized or destabilized. There is still no direct structural evidence for this hypothesis. In order to obtain a more direct readout of the conformational changes associated with these states, I have measured the intersubunit distance in the apo and full agonist glutamate bound state of the protein in the presence and absence of desensitization. Previous functional and structural investigations using cyclothiazide and the L484Y mutation in AMPA receptors,

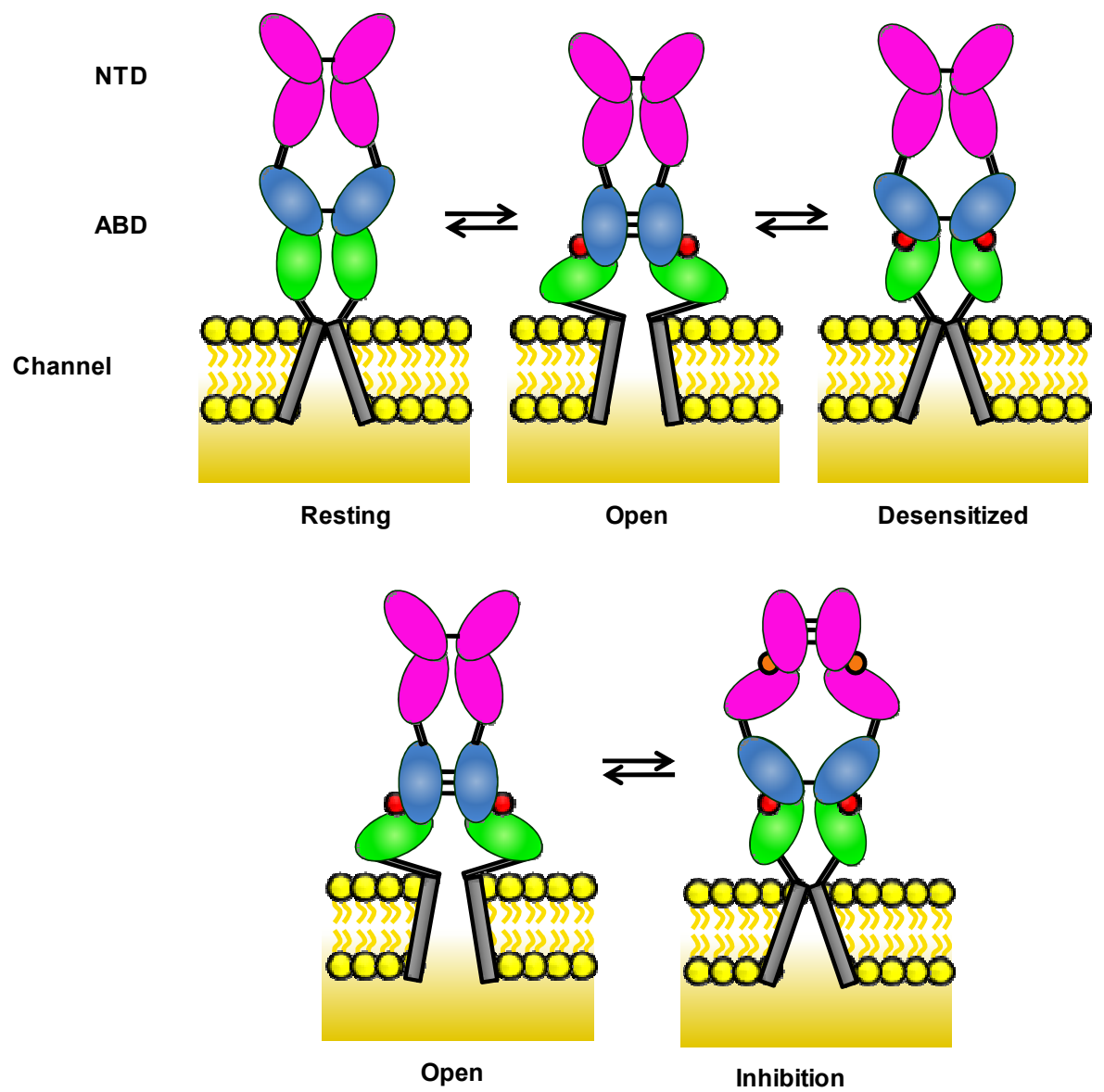
which stabilize the dimer interface thus decreasing desensitization, as well as the recent structure of isolated ligand binding domain of the S729C mutant, where the protein is stabilized in the desensitized state and dimer interface is found to be decoupled, have been used to describe the process of desensitization [56, 58, 74]. For studying intersubunit distances in the ligand binding domain of the AMPA receptor, I modified the  $\Delta N^*$ -AMPA subunit to serve as a probe to reflect intersubunit distance changes. These investigations suggest that the apo state of a modified a functional AMPA receptor in the presence of the transmembrane segments is decoupled, and during activation, the interface is coupled due to the driving force of cleft closure, thereby stabilizing the open channel, and then the interface decouples thus leading to desensitization.

The AMPA receptor studies were performed in functional receptors in the absence of the NTD. Why are the LBD structural implications provided by the LRET studies in the AMPA receptors important in NTD cleft closure studies in NMDA receptors? The LBD as previously mentioned are connected to the NTD by linker regions. Based on the functional investigations of NMDA receptors, it has been hypothesized that non-competitive inhibitors such as  $Zn^{2+}$  and ifenprodil mediate their effects by inducing a cleft closure of the NTD [118-120]. Additionally, the allosteric coupling between the NTD and dimer interface at the LBD has also been indirectly established by electrophysiological studies. It was found that when the dimer interface is destabilized, there is an increase in  $Zn^{2+}$  inhibition, and the reverse is true where stabilizing it decreases  $Zn^{2+}$  inhibition [118]. Thus, the LRET-based mechanism for AMPA receptors in addition to the fact that altering the dimer

interface modulates the non-competitive inhibitors ability to inhibit the channel, another molecular mechanism for NMDA and non-NMDA receptors is proposed (Figure 41). Cleft closure in the LBD due to ligand binding leads to separation of the linker regions to the transmembrane domain, opening the channel. Contacts at the dimer interface of the LBD form to transiently stabilize to open state. Loss of strain by the decoupling of the dimer interface results in channel closure. However, in the presence of inhibitor, the NTD can undergo cleft closure conformational change, and the linker region between the NTD and LBD separates. This results in decoupling of the dimer interface of the LBD that in turn inhibits the channel. This type of allosteric coupling can be tested using similar LRET investigations of the NMDA receptor.



**Figure 41** Proposed mechanism for activation, desensitization and inhibition by modulators. Agonist binding to the LBD induces cleft closure pulling apart the linker to the transmembrane domain thus opening the channel (activation). The open channel form is transiently stabilized by LBD dimer contacts. Stress on the linker domain results in decoupling of the LBD dimer interface interactions leading to channel closure (desensitization). Modulator binding to NTD causes cleft closure of the NTD, which would lead to a separation of the linker region between NTD and LBD, causing the decoupling of LBD dimer interface leading to channel closure (inhibition). This inhibition is stabilized by dimer interactions at the NTD.



The ultimate goal of this dissertation is to develop an understanding of how a small molecule such as glutamate can bind to its receptor and cause a cascade of events that alters the way neurons communicate with each other. This type of regulation underlies complex brain activity like learning and memory. Hence, in order to develop the next generation of drugs to treat neurological diseases associated with excitotoxicity, such as Alzheimer's and Lou Gehrig's disease [17-30], further insight into how these receptors work is paramount.

## Appendix

## **I. Molecular Biology**

### **a. $\Delta N^*$ -AMPA Receptor**

Dr. Keinanen (University of Helsinki, Helsinki, Finland) provided the plasmid for the GluR4-flip receptor with the N-terminal domain (residues 22-402) deleted. It has been further modified by eliminating accessible cysteines by mutating two of the accessible cysteines (C426, C529) on the extracellular side to serines, producing a modified AMPA receptor. Cysteine mutations were introduced using the Stratagene QuikChange site-directed mutagenesis kit (Stratagene, CA). The coding region was sequenced in order to verify the integrity of the plasmid.

### **b Primers for mutagenesis**

For cloning the cleft closure probe, histag- $\Delta N^*$ -AMPA-S653C, a cysteine was introduced at site S653. Additionally, a hexahistidine tag was introduced at the N-terminus with a glutamine residue (P382Q) mutated between the histag and the modified AMPA receptor sequence.

More specifically, the hexahistidine tag was inserted into the N-terminal domain deleted GluR4 receptor after the viral signal peptide to replace the N-terminal flag epitope [45]. For introducing the hisidine tag, the forward primer included a *NheI* restriction site, signal peptide, and a hexahistidine tag followed by P382Q mutation:

GGCTAGCTATAAATATGACTATTCTCTGCTGGCTTGCGCTGTTGTCAACACTTA  
CCGCCGTGAACGCACACCATCATCATCATCACCAGACTCTGGGCAATGAC.

The backward primer contained an *EcoRI* restriction site,  
CGGAATTCTTTTGTTGACCCAGAATCAAGT.

The PCR product was digested with *NheI* and *EcoRI* restriction enzymes, and then cloned into the corresponding sites of the modified receptor [96].

For cloning modified receptors for the intersubunit distance measurements, a cysteine was introduced at site G740, S741, or S742 to create modified AMPA receptors ( $\Delta N^*$ -GluR4-G740C,  $\Delta N^*$ - GluR4-S741C, and  $\Delta N^*$ - GluR4-S742C). A thrombin cleavage site (LVPRGS) was added on each side of the S741C mutant to create  $\Delta N^*$ -GluR4-Th-S741C-Th.

For introducing the two flanking thrombin cleavage site in addition to the cysteine at site 741, the following forward and backward primers were used.

The forward primer is:

GTAGCAACGCCCAAGGGTCTGGTGCCGCGCGGCAGCTGTCTGGTGCCGCGC  
GGCAGCTCATTAAGAACTCCTGTA.

The backward primer is:

TACAGGAGTTCTTAATGAGCTGCCGCGCGGCACCAGACAGCTGCCGCGCGGC  
ACCAGACCCTTGGGCGTTGCTAC.

### c. RNA synthesis

For the *in vitro* synthesis of capped RNA, the mMessage mMachine Kit (Ambion) was used. In brief, for a single reaction (20  $\mu$ L), 0.5 to 1  $\mu$ g of linearized template plasmid DNA (gel-extracted to remove impurities and eluted in nuclease-free water) is used. To complete the reaction, add 10  $\mu$ L of 2X NTP/CAP, 2  $\mu$ L of 10X reaction buffer, 2  $\mu$ L of enzyme mix, and complete desired volume with nuclease-free water. The reaction mix is incubated at 37 °C for 1 hour. Then, add 1  $\mu$ L of TURBO DNase to remove template DNA and incubate at 37 °C for 15

minutes. For the recovery of the RNA, precipitate with lithium chloride by adding 30  $\mu$ L and chill overnight at -20 °C. Centrifuge at max speed to isolate pellet, wash with 70% ethanol, and resuspend in nuclease-free water.

## **II. *Xenopus* oocyte extraction and preparation**

For the extraction of oocytes, African clawed frogs are put under anesthesia using 500-2000 mg/L of tricaine methane sulfonate (MS222) powder will be dissolved in deionized autoclaved water, buffered with 5mM Hepes (1.192 g/L) and titrated to a pH of 7.5 with sodium bicarbonate. A solution of MS222 will be prepared fresh and will be filter-sterilized and autoclaved prior to use. The solution will be applied by bath.

For non-survival frog surgery/oocyte harvest, at the start of the procedure, using aseptic techniques in a designated area, the frog is placed in a bucket with anesthesia (MS222) in water. Frog is placed on tray with ice covered with saran wrap to induce hypothermia and prolong analgesic effect. To keep the frog's skin moist, pre-wet paper towels with frog water will be placed on the saran wrap. Anesthetized frogs verified by disturbance. Surgical procedure begins by cutting a small incision (~0.5cm) in the lower left or right abdomen. Make an identical incision through the frog's abdominal muscle. The abdominal cavity is then opened and a strand of eggs containing approximately 100-200 oocytes is removed with forceps. As for euthanizing, the frog is decapitated and pithed under anesthetic or given an anesthetic overdose (>1500 mg/L).

For survival surgery on the frogs, all survival surgery will be performed using aseptic procedures, including surgical gloves, sterile instruments, and aseptic techniques. Surgical procedures on frogs will be performed only in areas intended for surgery, which will be maintained under aseptic conditions. Pre-surgery preparations include sterilizing surgical instruments with 70% ethanol and flaming.



The frog is anesthetized by immersion in MS222 solution for 15 to 30 minutes and is verified by frog's response to disturbance. Anesthesia will persist for a minimum of 20 minutes. Frog is placed on tray with ice covered with saran wrap to induce hypothermia and prolong analgesic effect. To keep the frog's skin moist, pre-wet paper towels with frog water to be placed on the saran wrap. The aseptic surgical procedure begins by cutting a small incision (~0.5cm) in the lower left or right abdomen. Make an identical incision through the frog's abdominal muscle. The abdominal cavity is then opened and a strand of eggs (ovaries) containing approximately 100-200 oocytes is removed with forceps. The incision is sutured closed (braided coated synthetic absorbable suture making sure not to trap air under the skin). The frog is placed head-above-water in a bucket without anesthetic. The frog is monitored until it is actively swimming. The frog is then placed in a separate tank to monitor its health. Due to a natural antibiotic in *Xenopus* skin, no additional antibiotic treatments are necessary. Each frog is used up to 2 survival surgeries, one on each side of the abdomen. If the frog is distressed, it will be brought to the attention of the veterinarians to determine the appropriate course of action. Typically, for frogs the problems are noted as a lack of vigorous swimming when disturbed, poor eating, or skin rash. If appropriate treatment is unavailable, it is euthanized. Also, if the frog is unable to produce quality oocytes, it is euthanized. If the frog shows abnormal bleeding during surgery it will be euthanized. Typically, there are few complications from this surgery, but if there is any problem of the frog from surgery, it is decapitated and pithed under anesthetic or given an anesthetic overdose.

Oocytes were defolliculated by incubation of extracted ovaries with 1.5-3 mg/ml collagenase dissolved in  $\text{Ca}^{2+}$ -free solution containing (in mM): 83 NaCl, 2 KCl, 1  $\text{MgCl}_2$ , 5 HEPES (pH 7.5) for 60 to 90 minutes. The defolliculated oocytes were rinsed with storage solution containing (in mM): 88 NaCl, 2.5  $\text{NaHCO}_3$ , 1.1 KCl, 0.4  $\text{CaCl}_2$ , 0.3  $\text{Ca}(\text{NO}_3)_2$ , 0.8  $\text{MgCl}_2$ , 2.5 mM sodium pyruvate, 10 HEPES (pH 7.3), and 5  $\mu\text{g/ml}$  gentamicin. The oocytes were stored overnight at 12 °C. Stage V–VI oocytes were injected with RNA of the modified AMPA receptor [96].

### **III. Pre-blocking and Expression**

After injection, the oocytes were incubated for 2-3 days at 12 °C and then pre-labeled to block the inherent cysteines with  $\beta$ -maleimidopropionic acid for 1 hour. This procedure has been modified from the protocol discussed in the LRET investigations of potassium channels [142, 143]. The blocked oocytes were placed at 18 °C for 24 to 36 hours, allowing for the expression of the receptors. At the end of 24-36 hours, the oocytes were labeled as described in the next section [96].

Human Embryonic Kidney 293 (HEK-293) cells were cultured as described in Du et al., 2005. [100]. Transfected cells were allowed to grow for 24-36 hours before use.

#### IV. Labeling oocytes (cells)

For the cleft closure experiments with Histag- $\Delta N^*$ -AMPA-S653C, 2  $\mu$ M terbium chelate is added for donor-only experiments. Membrane preparations are made as explained in the next section. Then, 5  $\mu$ M (Ni-NTA)<sub>2</sub>Cy3 is added directly to the sample for donor:acceptor experiments. Background LRET was measured 3 hours after the addition of TAGZyme (room temperature) and subtracted from the total LRET signal to serve as the specific signal from the modified receptors [96].

For intersubunit distance measurements for  $\Delta N^*$ -GluR4-S741C, 2 $\mu$ M terbium chelate plus 0.5  $\mu$ M ATTO465 in a 4:1 ratio are added simultaneously for 1 hour to label the oocytes (cells) in storage solution (extracellular buffer). The membrane preparations from oocytes obtained by lysis were used for single channel recordings and LRET experiments. To obtain the background LRET for  $\Delta N^*$ -GluR4-Th-S741C-Th, the cells used for the LRET measurements were incubated at room temperature with 3 U of thrombin obtained from Calbiochem, CA. Background LRET was measured 3 hours after the addition of the thrombin and subtracted from the total LRET signal in order to obtain the LRET signal from  $\Delta N^*$ -GluR4-Th-S741C-Th.

## **V. Membrane Preparation**

Around 300 labeled oocytes expressing AMPA receptors were lysed in 1.5 mL of lysis buffer, containing 20 mM Tris ( pH 7.6), 200 mM NaCl, 1% Triton X-100, and EDTA-free Complete Protease Inhibitor Cocktail (Roche). Clarify by centrifugation for 10 minutes (13,000 rpm) at 4°C. Collect the supernatant and repeat on membrane samples for two more centrifugation spins. Resuspend in storage solution to achieve desired volume [96].

## **VI. Electrophysiology**

Two-electrode voltage clamp experiments were performed using the NPI TEC amplifier (ALA Scientific, NY) with a small-volume recording chamber to reduce solution exchange time. The voltage and current electrodes were filled with 3 M KCl with a resistance of 1-4 MOhms. The extracellular solution includes (in mM): 100 NaCl, 1 KCl, 0.7 BaCl<sub>2</sub>, 0.8 MgCl<sub>2</sub>, and 5 HEPES, pH 7.5 (pH with NaOH). Currents were recorded using Cell Works software (ALA Scientific, NY) and analyzed using Origin 4.0 (OriginLab, MA) [96]. Whole-cell current recordings were performed as previously described [100].

## VII. Radioactive Ligand Binding

To test the binding affinity of AMPA for the receptors expressed in oocytes, a saturation binding analysis was performed. Membrane protein (12 µg) was incubated with varying concentrations of [<sup>3</sup>H]-AMPA, and non-specific binding of [<sup>3</sup>H]-AMPA was determined by including 10 mM glutamate in the assay. Using Whatman nitrocellulose filters for rapid filtration, bound and free [<sup>3</sup>H]-AMPA were separated, and radioactivity is counted with a liquid scintillation counter. The K<sub>d</sub> values were determined by fitting the binding data using equation 6:

$$y = \frac{x \times B_{\max}}{x + K_d} \quad \text{Eq. 6}$$

where y is the total binding of [<sup>3</sup>H]-AMPA, B<sub>max</sub> is the maximum amount of bound [<sup>3</sup>H]-AMPA, and x is the concentration of free ligand [96].

## VIII. Expression of the isolated LBD of GluR2

Proteins were expressed and purified as previously described by Armstrong et al. [11]. Briefly, the protein was expressed in *Escherichia coli* Origami-B(DE3) cells, then clarified and concentrated. Next, either the cell culture supernatant or purified protein (Ni-NTA HiTrap affinity column) was used for the LRET measurements. The supernatant or purified protein was labeled with maleimide derivatives of terbium chelate for donor only samples, and dialyzed against PBS to remove excess donor fluorophore. 5  $\mu$ M of (Ni-NTA)<sub>2</sub>Cy3 was added additionally for donor:acceptor samples. 2.5 U of thrombin per mg of protein were added to the labeled protein samples used for the LRET measurements, and the protein was maintained at 4 °C. LRET measurements were performed 24 hours later [96].



## Bibliography

1. Hille, B. (2001). Ion channels of excitable membranes, 3rd Edition (Sunderland, Mass.: Sinauer).
2. Gouaux, E., and Mackinnon, R. (2005). Principles of selective ion transport in channels and pumps. *Science* 310, 1461-1465.
3. Doyle, D.A., Cabral, J.M., Pfuetzner, R.A., Kuo, A., Gulbis, J.M., Cohen, S.L., Chait, B.T., and MacKinnon, R. (1998). The structure of the potassium channel: molecular basis of K<sup>+</sup> conduction and selectivity. *Science* 280, 69-77.
4. Monod, J., Wyman, J., and Changeux, J.-P. (1965). On the nature of allosteric transitions: a plausible model. *Journal of Molecular Biology* 12, 88-118.
5. Koshland, D.E., Jr., Nemethy, G., and Filmer, D. (1966). Comparison of experimental binding data and theoretical models in proteins containing subunits. *Biochemistry* 5, 365-385.
6. Ackers, G.K., Doyle, M.L., Myers, D., and Daugherty, M.A. (1992). Molecular code for cooperativity in hemoglobin. *Science* 255, 54-63.
7. Changeux, J.-P., and Edelstein, S.J. (1998). Allosteric receptors after 30 years. *Neuron* 21, 959-980.
8. Bucci, E., Razynska, A., Kwansa, H., Gryczynski, Z., Collins, J.H., Fronticelli, C., Unger, R., Braxenthaler, M., Moulton, J., Ji, X., and Gilliland, G. (1996). Positive and negative cooperativities at subsequent steps of oxygenation

- regulate the allosteric behavior of multistate sebacylhemoglobin. *Biochemistry* 35, 3418-3425.
9. Mathews, C.K., van Holde, K. E., and Ahern, K. G (1999). *Biochemistry. 3rd edition*, Addison Wesley Longman, CA.
  10. Perrella, M., and Russo, R. (2003). Allosteric proteins: lessons to be learned from the hemoglobin intermediates. *News Physiol Sci* 18, 232-236.
  11. Armstrong, N., Mayer, M., and Gouaux, E. (2003). Tuning activation of the AMPA-sensitive GluR2 ion channel by genetic adjustment of agonist-induced conformational changes. *Proc Natl Acad Sci U S A* 100, 5736-5741.
  12. Li, J., Zagotta, W.N., and Lester, H.A. (1997). Cyclic nucleotide-gated channels: structural basis of ligand efficacy and allosteric modulation. *Q Rev Biophys* 30, 177-193.
  13. Armstrong, N., De Lencastre, A., and Gouaux, E. (1999). A new protein folding screen: Application to the ligand binding domains of a glutamate and kainate receptor and to lysozyme and carbonic anhydrase. *Protein Science* 8, 1475-1483.
  14. Dingledine, R., Borges, K., Bowie, D., and Traynelis, S.F. (1999). The glutamate receptor ion channels. *Pharmacological Reviews* 51, 7-61.
  15. Madden, D.R. (2002). The structure and function of glutamate receptor ion channels. *Nat Rev Neurosci* 3, 91-101.
  16. Brauner-Osborne, H., Egebjerg, J., Nielsen, E.O., Madsen, U., and Krogsgaard-Larsen, P. (2000). Ligands for glutamate receptors: design and therapeutic prospects. *J Med Chem* 43, 2609-2645.

17. Mayer, M.L. (2006). Glutamate receptors at atomic resolution. *Nature* 440, 456-462.
18. Mayer, M.L., and Armstrong, N. (2004). Structure and function of glutamate receptor ion channels. *Annu Rev Physiol* 66, 161-181.
19. Mayer, M.L. (2005). Glutamate receptor ion channels. *Curr Opin Neurobiol* 15, 282-288.
20. Oswald, R.E. (2004). Ionotropic glutamate receptor recognition and activation. *Adv Protein Chem* 68, 313-349.
21. Gouaux, E. (2004). Structure and function of AMPA receptors. *J Physiol* 554, 249-253.
22. Malinow, R., and Malenka, R.C. (2002). AMPA receptor trafficking and synaptic plasticity. *Annu Rev Neurosci* 25, 103-126.
23. Riedel, G., Platt, B., and Micheau, J. (2003). Glutamate receptor function in learning and memory. *Behav Brain Res* 140, 1-47.
24. Parsons, C.G., Danysz, W., and Zieglgansberger, W. (2005). Excitatory amino acid neurotransmission. *Handb Exp Pharmacol*, 249-303.
25. Palmer, C.L., Cotton, L., and Henley, J.M. (2005). The molecular pharmacology and cell biology of alpha-amino-3-hydroxy-5-methyl-4-isoxazolepropionic acid receptors. *Pharmacol Rev* 57, 253-277.
26. Montgomery, J.M., and Madison, D.V. (2004). Discrete synaptic states define a major mechanism of synapse plasticity. *Trends Neurosci* 27, 744-750.

27. Van Den Bosch, L., Van Damme, P., Bogaert, E., and Robberecht, W. (2006). The role of excitotoxicity in the pathogenesis of amyotrophic lateral sclerosis. *Biochim Biophys Acta* 1762, 1068-1082.
28. Gardoni, F., and Di Luca, M. (2006). New targets for pharmacological intervention in the glutamatergic synapse. *Eur J Pharmacol* 545, 2-10.
29. Palmada, M., and Centelles, J.J. (1998). Excitatory amino acid neurotransmission. Pathways for metabolism, storage and reuptake of glutamate in brain. *Front Biosci* 3, d701-718.
30. Kwak, S., and Weiss, J.H. (2006). Calcium-permeable AMPA channels in neurodegenerative disease and ischemia. *Curr Opin Neurobiol* 16, 281-287.
31. Dingledine, R., and Conn, P.J. (2000). Peripheral glutamate receptors: molecular biology and role in taste sensation. *J Nutr* 130, 1039S-1042S.
32. Gill, S.S., and Pulido, O.M. (2001). Glutamate receptors in peripheral tissues: current knowledge, future research, and implications for toxicology. *Toxicol Pathol* 29, 208-223.
33. Hinoi, E., Takarada, T., Ueshima, T., Tsuchihashi, Y., and Yoneda, Y. (2004). Glutamate signaling in peripheral tissues. *Eur J Biochem* 271, 1-13.
34. Collingridge, G.L., and Bliss, T.V. (1995). Memories of NMDA receptors and LTP. *Trends Neurosci* 18, 54-56.
35. Geiger, J.R., Melcher, T., Koh, D.S., Sakmann, B., Seeburg, P.H., Jonas, P., and Monyer, H. (1995). Relative abundance of subunit mRNAs determines gating and Ca<sup>2+</sup> permeability of AMPA receptors in principal neurons and interneurons in rat CNS. *Neuron* 15, 193-204.

36. Lerma, J. (2003). Roles and rules of kainate receptors in synaptic transmission. *Nat Rev Neurosci* 4, 481-495.
37. Rosenmund, C., Stern-Bach, Y., and Stevens, C.F. (1998). The tetrameric structure of a glutamate receptor channel. *Science* 280, 1596-1599.
38. Tichelaar, W., Safferling, M., Keinänen, K., Stark, H., and Madden, D.R. (2004). The Three-dimensional Structure of an Ionotropic Glutamate Receptor Reveals a Dimer-of-dimers Assembly. *J Mol Biol* 344, 435-442.
39. Mankiewicz, K.A., and Jayaraman, V. (2007). Glutamate receptors as seen by light: spectroscopic studies of structure-function relationships. *Braz J Med Biol Res* 40, 1419-1427.
40. Chen, P.E., and Wyllie, D.J. (2006). Pharmacological insights obtained from structure-function studies of ionotropic glutamate receptors. *Br J Pharmacol* 147, 839-853.
41. O'Hara, P.J., Sheppard, P.O., Thøgersen, H., Benezia, D., Haldeman, B.A., McGrane, B., Houamed, K.M., Thomsen, C., Gilbert, T.L., and Mulvihill, E.R. (1993). The ligand-binding domain of metabotropic glutamate receptors is related to bacterial periplasmic binding proteins. *Neuron* 11, 41-52.
42. Kuusinen, A., Arvola, M., and Keinänen, K. (1995). Molecular dissection of the agonist binding site of an AMPA receptor. *EMBO Journal* 14, 6327-6332.
43. Krupp, J.J., Vissel, B., Heinemann, S.F., and Westbrook, G.L. (1998). N-terminal domains in the NR2 subunit control desensitization of NMDA receptors. *Neuron* 20, 317-327.

44. Villarroel, A., Regalado, M.P., and Lerma, J. (1998). Glycine-independent NMDA receptor desensitization -- localization of structural determinants. *Neuron* 20, 329-339.
45. Pasternack, A., Coleman, S.K., Jouppila, A., Mottershead, D.G., Lindfors, M., Pasternack, M., and Keinänen, K. (2002). Alpha-amino-3-hydroxy-5-methyl-4-isoxazolepropionic acid (AMPA) receptor channels lacking the N-terminal domain. *J Biol Chem* 277, 49662-49667.
46. Ayalon, G., Segev, E., Elgavish, S., and Stern-Bach, Y. (2005). Two regions in the N-terminal domain of ionotropic glutamate receptor 3 form the subunit oligomerization interfaces that control subtype-specific receptor assembly. *J Biol Chem* 280, 15053-15060.
47. Ayalon, G., and Stern-Bach, Y. (2001). Functional assembly of AMPA and kainate receptors is mediated by several discrete protein-protein interactions. *Neuron* 13, 103-113.
48. Masuko, T., Kashiwagi, K., Kuno, T., Nguyen, N., Pahk, A.J., Fukuchi, J., Igarashi, K., and Williams, K. (1999). A regulatory domain (R1-R2) in the amino terminus of the *N*-methyl-D-aspartate receptor: effects of spermine, protons, and ifenprodil, and structural similarity to bacterial leucine/isoleucine/valine binding protein. *Molecular Pharmacology* 55, 957-969.
49. Paoletti, P., Ascher, P., and Neyton, J. (1997). High-affinity zinc inhibition of NMDA NR1-NR2A receptors. *J Neurosci* 17, 5711-5725.

50. Perin-Dureau, F., Rachline, J., Neyton, J., and Paoletti, P. (2002). Mapping the binding site of the neuroprotectant ifenprodil on NMDA receptors. *J Neurosci* 22, 5955-5965.
51. Chen, G.-Q., Sun, Y., Jin, R., and Gouaux, E. (1998). Probing the ligand binding domain of the GluR2 receptor by proteolysis and deletion mutagenesis defines domain boundaries and yields a crystallizable construct. *Protein Science* 7, 2623-2630.
52. Panchenko, V.A., Glasser, C.R., and Mayer, M.L. (2001). Structural similarities between glutamate receptor channels and K<sup>+</sup> channels examined by scanning mutagenesis. *J. Gen. Physiol.* 117, 345-359.
53. Kuner, T., Seeburg, P.H., and Guy, H.R. (2003). A common architecture for K<sup>+</sup> channels and ionotropic glutamate receptors? *Trends Neurosci* 26, 27-32.
54. Soderling, T.R., and Derkach, V.A. (2000). Postsynaptic protein phosphorylation and LTP. *Trends Neurosci* 23, 75-80.
55. Tavalin, S.J., Colledge, M., Hell, J.W., Langeberg, L.K., Huganir, R.L., and Scott, J.D. (2002). Regulation of GluR1 by the A-kinase anchoring protein 79 (AKAP79) signaling complex shares properties with long-term depression. *J Neurosci* 22, 3044-3051.
56. Armstrong, N.A., and Gouaux, E. (2000). Mechanisms for activation and antagonism of an AMPA-sensitive glutamate receptor: crystal structures of the GluR2 ligand binding core. *Neuron* 28, 165-181.

57. Armstrong, N., Sun, Y., Chen, G.Q., and Gouaux, E. (1998). Structure of a glutamate-receptor ligand-binding core in complex with kainate. *Nature* 395, 913-917.
58. Armstrong, N., Jasti, J., Beich-Frandsen, M., and Gouaux, E. (2006). Measurement of conformational changes accompanying desensitization in an ionotropic glutamate receptor. *Cell* 127, 85-97.
59. Jin, R., Banke, T.G., Mayer, M.L., Traynelis, S.F., and Gouaux, E. (2003). Structural basis for partial agonist action at ionotropic glutamate receptors. *Nat Neurosci* 6, 803-810.
60. Hogner, A., Kastrup, J.S., Jin, R., Liljefors, T., Mayer, M.L., Egebjerg, J., Larsen, I.K., and Gouaux, E. (2002). Structural basis for AMPA receptor activation and ligand selectivity: crystal structures of five agonist complexes with the GluR2 ligand-binding core. *J Mol Biol* 322, 93-109.
61. Sun, Y., Olson, R., Horning, M., Armstrong, N., Mayer, M., and Gouaux, E. (2002). Mechanism of glutamate receptor desensitization. *Nature* 417, 245-253.
62. Sobolevsky, A.I., Rosconi, M.P., and Gouaux, E. (2009). X-ray structure, symmetry and mechanism of an AMPA-subtype glutamate receptor. *Nature* 462, 745-756.
63. McFeeters, R.L., and Oswald, R.E. (2002). Structural mobility of the extracellular ligand-binding core of an ionotropic glutamate receptor. Analysis of NMR relaxation dynamics. *Biochemistry* 41, 10472-10481.



64. Madden, D.R., Cheng, Q., Thiran, S., Rajan, S., Rigo, F., Keinänen, K., Reinelt, S., Zimmermann, H., and Jayaraman, V. (2004). Stereochemistry of glutamate receptor agonist efficacy: engineering a dual-specificity AMPA/kainate receptor. *Biochemistry* **43**, 15838-15844.
65. Jayaraman, V., Keeseey, R., and Madden, D.R. (2000). Ligand--protein interactions in the glutamate receptor. *Biochemistry* **39**, 8693-8697.
66. Mayer, M.L., Olson, R., and Gouaux, E. (2001). Mechanisms for ligand binding to GluR0 ion channels: crystal structures of the glutamate and serine complexes and a closed apo state. *J Mol Biol* **311**, 815-836.
67. Jin, R., and Gouaux, E. (2003). Probing the function, conformational plasticity, and dimer-dimer contacts of the GluR2 ligand-binding core: studies of 5-substituted willardiines and GluR2 S1S2 in the crystal. *Biochemistry* **42**, 5201-5213.
68. Jin, R., Horning, M., Mayer, M.L., and Gouaux, E. (2002). Mechanism of activation and selectivity in a ligand-gated ion channel: structural and functional studies of GluR2 and quisqualate. *Biochemistry* **41**, 15635-15643.
69. Mayer, M.L. (2005). Crystal structures of the GluR5 and GluR6 ligand binding cores: molecular mechanisms underlying kainate receptor selectivity. *Neuron* **45**, 539-552.
70. Ramanoudjame, G., Du, M., Mankiewicz, K.A., and Jayaraman, V. (2006). Allosteric mechanism in AMPA receptors: A FRET-based investigation of conformational changes. *Proc Natl Acad Sci U S A* **103**, 10473-10478.

71. Mankiewicz, K.A., Rambhadran, A., Du, M., Ramanoudjame, G., and Jayaraman, V. (2007). Role of the Chemical Interactions of the Agonist in Controlling  $\alpha$ -Amino-3-hydroxy-5-methyl-4-isoxazolepropionic Acid Receptor Activation. *Biochemistry* 46, 1343-1349.
72. Stern-Bach, Y., Russo, S., Neuman, M., and Rosenmund, C. (1998). A point mutation in the glutamate binding site blocks desensitization of AMPA receptors. *Neuron* 21, 907-918.
73. Patneau, D.K., Vyklicky, L., Jr., and Mayer, M.L. (1993). Hippocampal neurons exhibit cyclothiazide-sensitive rapidly desensitizing responses to kainate. *Journal of Neuroscience* 13, 3496-3509.
74. Jin, R., Clark, S., Weeks, A.M., Dudman, J.T., Gouaux, E., and Partin, K.M. (2005). Mechanism of positive allosteric modulators acting on AMPA receptors. *J Neurosci* 25, 9027-9036.
75. Partin, K.M., Fleck, M.W., and Mayer, M.L. (1996). AMPA receptor flip/flop mutants affecting deactivation, desensitization, and modulation by cyclothiazide, aniracetam, and thiocyanate. *Journal of Neuroscience* 16, 6634-6647.
76. Yelshansky, M.V., Sobolevsky, A.I., Jatzke, C., and Wollmuth, L.P. (2004). Block of AMPA receptor desensitization by a point mutation outside the ligand-binding domain. *J Neurosci* 24, 4728-4736.
77. Holm, M.M., Naur, P., Vestergaard, B., Geballe, M.T., Gajhede, M., Kastrup, J.S., Traynelis, S.F., and Egebjerg, J. (2005). A binding site tyrosine shapes

- desensitization kinetics and agonist potency at GluR2. A mutagenic, kinetic, and crystallographic study. *J Biol Chem* 280, 35469-35476.
78. Gill, A., Birdsey-Benson, A., Jones, B.L., Henderson, L.P., and Madden, D.R. (2008). Correlating AMPA receptor activation and cleft closure across subunits: crystal structures of the GluR4 ligand-binding domain in complex with full and partial agonists. *Biochemistry* 47, 13831-13841.
79. Miledi, R., Parker, I., and Sumikawa, K. (1982). Synthesis of chick brain GABA receptors by frog oocytes. *Proc R Soc Lond B Biol Sci* 216, 509-515.
80. Gurdon, J.B., Lane, C.D., Woodland, H.R., and Marbaix, G. (1971). Use of frog eggs and oocytes for the study of messenger RNA and its translation in living cells. *Nature* 233, 177-182.
81. (1998). Electrophysiology Recordings from *Xenopus* Oocytes. In *Methods in Enzymology*, Volume 293. (Academic Press), pp. 293-352.
82. (2006). *Methods in Molecular Biology* (New Jersey: Humana Press).
83. Cha, A., Snyder, G.E., Selvin, P.R., and Bezanilla, F. (1999). Atomic scale movement of the voltage-sensing region in a potassium channel measured via spectroscopy. *Nature* 402, 809-813.
84. Cole, K.S. (1979). Mostly membranes (Kenneth S. Cole). *Annu Rev Physiol* 41, 1-24.
85. Kandel, E.R., Schwartz, J.H., and Jessel, T.M. (1991). *Principles of neuronal sciences*, Third edition Edition (New York: Elsevier).
86. Huxley, A. (2002). From overshoot to voltage clamp. *Trends Neurosci* 25, 553-558.

87. (2008). The Axon Guide: A Guide to Electrophysiology and Biophysics Laboratory Techniques, MDS Analytical Technologies.
88. Lakowicz, J.R. (1983). Principles of Fluorescence Spectroscopy. Plenum Press, New York.
89. Jablonski, A. (1935). Über den mechanisms des photolumineszenz von farbstoffphosphoren. Zeitschrift für Physik 94, 38-46.
90. Kapanidis, A.N., Ebright, Y.W., and Ebright, R.H. (2001). Site-specific incorporation of fluorescent probes into protein: hexahistidine-tag-mediated fluorescent labeling with (Ni(2+):nitrilotriacetic Acid (n)-fluorochrome conjugates. J Am Chem Soc 123, 12123-12125.
91. Selvin, P.R. (2000). The renaissance of fluorescence resonance energy transfer. Nat Struct Biol 7, 730-734.
92. Selvin, P.R. (2002). Principles and biophysical applications of lanthanide-based probes. Annu Rev Biophys Biomol Struct 31, 275-302.
93. Heyduk, T. (2002). Measuring protein conformational changes by FRET/LRET. Curr Opin Biotechnol 13, 292-296.
94. Vogel, S.S., Thaler, C., and Koushik, S.V. (2006). Fanciful FRET. Sci STKE 2006, re2.
95. Forster, T. (1948). Zwischenmolekulare energiewanderung und fluoreszenz. Annalen der Physik 2, 55-75.
96. Gonzalez, J., Rambhadran, A., Du, M., and Jayaraman, V. (2008). LRET investigations of conformational changes in the ligand binding domain of a functional AMPA receptor. Biochemistry 47, 10027-10032.

97. Selvin, P.R., and Hearst, J.E. (1994). Luminescence energy transfer using a terbium chelate: improvements on fluorescence energy transfer. *Proc Natl Acad Sci U S A* 91, 10024-10028.
98. Invitrogen (2005). LanthaScreen TR-FRET Labeling Reagents Protocol.
99. Haas, E., Katchalski-Katzir, E., and Steinberg, I.Z. (1978). Effect of the orientation of donor and acceptor on the probability of energy transfer involving electronic transitions of mixed polarization. *Biochemistry* 17, 5064-5070.
100. Du, M., Reid, S.A., and Jayaraman, V. (2005). Conformational changes in the ligand-binding domain of a functional ionotropic glutamate receptor. *J Biol Chem* 280, 8633-8636.
101. Tsien, R.Y. (1998). The green fluorescent protein. *Annu Rev Biochem* 67, 509-544.
102. Tsien, R.Y. (1998). THE GREEN FLUORESCENT PROTEIN, vol. 67. pp. 509-544.
103. Kajihara, D., Abe, R., Iijima, I., Komiyama, C., Sisido, M., and Hohsaka, T. (2006). FRET analysis of protein conformational change through position-specific incorporation of fluorescent amino acids. *Nat Meth* 3, 923-929.
104. Mankiewicz, K.A., Rambhadran, A., Wathen, L., and Jayaraman, V. (2008). Chemical interplay in the mechanism of partial agonist activation in alpha-amino-3-hydroxy-5-methyl-4-isoxazolepropionic acid receptors. *Biochemistry* 47, 398-404.

105. Dascal, N. (1987). The use of *Xenopus* oocytes for the study of ion channels. *CRC Crit Rev Biochem* 22, 317-387.
106. Chen, L., Chetkovich, D.M., Petralia, R.S., Sweeney, N.T., Kawasaki, Y., Wenthold, R.J., Brecht, D.S., and Nicoll, R.A. (2000). Stargazin regulates synaptic targeting of AMPA receptors by two distinct mechanisms. *Nature* 408, 936-943.
107. Hashimoto, K., Fukaya, M., Qiao, X., Sakimura, K., Watanabe, M., and Kano, M. (1999). Impairment of AMPA receptor function in cerebellar granule cells of ataxic mutant mouse stargazer. *J Neurosci* 19, 6027-6036.
108. Bats, C., Groc, L., and Choquet, D. (2007). The interaction between Stargazin and PSD-95 regulates AMPA receptor surface trafficking. *Neuron* 53, 719-734.
109. Tomita, S., Shenoy, A., Fukata, Y., Nicoll, R.A., and Brecht, D.S. (2007). Stargazin interacts functionally with the AMPA receptor glutamate-binding module. *Neuropharmacology* 52, 87-91.
110. Tomita, S., Adesnik, H., Sekiguchi, M., Zhang, W., Wada, K., Howe, J.R., Nicoll, R.A., and Brecht, D.S. (2005). Stargazin modulates AMPA receptor gating and trafficking by distinct domains. *Nature* 435, 1052-1058.
111. Priel, A., Kollek, A., Ayalon, G., Gillor, M., Osten, P., and Stern-Bach, Y. (2005). Stargazin reduces desensitization and slows deactivation of the AMPA-type glutamate receptors. *J Neurosci* 25, 2682-2686.
112. Schnell, E., Sizemore, M., Karimzadegan, S., Chen, L., Brecht, D.S., and Nicoll, R.A. (2002). Direct interactions between PSD-95 and stargazin control

- synaptic AMPA receptor number. *Proc Natl Acad Sci U S A* 99, 13902-13907.
113. Turetsky, D., Garringer, E., and Patneau, D.K. (2005). Stargazin modulates native AMPA receptor functional properties by two distinct mechanisms. *J Neurosci* 25, 7438-7448.
  114. Tomita, S., Sekiguchi, M., Wada, K., Nicoll, R.A., and Brecht, D.S. (2006). Stargazin controls the pharmacology of AMPA receptor potentiators. *Proc Natl Acad Sci U S A* 103, 10064-10067.
  115. Bedoukian, M.A., Weeks, A.M., and Partin, K.M. (2006). Different domains of the AMPA receptor direct stargazin-mediated trafficking and stargazin-mediated modulation of kinetics. *J Biol Chem* 281, 23908-23921.
  116. Korber, C., Werner, M., Kott, S., Ma, Z.L., and Hollmann, M. (2007). The transmembrane AMPA receptor regulatory protein gamma 4 is a more effective modulator of AMPA receptor function than stargazin (gamma 2). *J Neurosci* 27, 8442-8447.
  117. Plested, A.J., and Mayer, M.L. (2009). AMPA receptor ligand binding domain mobility revealed by functional cross linking. *J Neurosci* 29, 11912-11923.
  118. Paoletti, P., Perin-Dureau, F., Fayyazuddin, A., Le Goff, A., Callebaut, I., and Neyton, J. (2000). Molecular organization of a zinc binding n-terminal modulatory domain in a NMDA receptor subunit. *Neuron* 28, 911-925.
  119. Karakas, E., Simorowski, N., and Furukawa, H. (2009). Structure of the zinc-bound amino-terminal domain of the NMDA receptor NR2B subunit. *Embo J* 28, 3910-3920.

120. Mony, L., Kew, J.N., Gunthorpe, M.J., and Paoletti, P. (2009). Allosteric modulators of NR2B-containing NMDA receptors: molecular mechanisms and therapeutic potential. *Br J Pharmacol* 157, 1301-1317.
121. Bers, D.M. (1991). Excitation-contraction coupling and cardiac contractile force, Kluwer Academic Publications: London.
122. Blaustein, M.P., Fontana, G., and Rogowski, R.S. (1996). The Na(+)-Ca<sup>2+</sup> exchanger in rat brain synaptosomes. Kinetics and regulation. *Ann N Y Acad Sci* 779, 300-317.
123. Hilgemann, D.W. (1990). Regulation and deregulation of cardiac Na(+)-Ca<sup>2+</sup> exchange in giant excised sarcolemmal membrane patches. *Nature* 344, 242-245.
124. Nicoll, D.A., Ottolia, M., and Philipson, K.D. (2002). Toward a topological model of the NCX1 exchanger. *Ann N Y Acad Sci* 976, 11-18.
125. Hilge, M., Aelen, J., and Vuister, G.W. (2006). Ca<sup>2+</sup> regulation in the Na<sup>+</sup>/Ca<sup>2+</sup> exchanger involves two markedly different Ca<sup>2+</sup> sensors. *Mol Cell* 22, 15-25.
126. Wu, M., Wang, M., Nix, J., Hryshko, L. V. and Zheng, L. (2009). Crystal structure of CBD2 from the *Drosophila* Na<sup>+</sup>/Ca<sup>2+</sup> exchanger: diversity of Ca<sup>2+</sup> regulation and its alternative splicing modification. *J. Mol. Biol* 387, 104-112.
127. Nicoll, D.A., Sawaya, M.R., Kwon, S., Cascio, D., Philipson, K.D., and Abramson, J. (2006). The crystal structure of the primary Ca<sup>2+</sup> sensor of the



- Na<sup>+</sup>/Ca<sup>2+</sup> exchanger reveals a novel Ca<sup>2+</sup> binding motif. *J Biol Chem* 281, 21577-21581.
128. Besserer, G.M., Ottolia, M., Nicoll, D.A., Chaptal, V., Cascio, D., Philipson, K.D., and Abramson, J. (2007). The second Ca<sup>2+</sup>-binding domain of the Na<sup>+</sup> Ca<sup>2+</sup> exchanger is essential for regulation: crystal structures and mutational analysis. *Proc Natl Acad Sci U S A* 104, 18467-18472.
  129. Hilge, M., Aelen, J., Foorce, A., Perrakis, A., and Vuister, G.W. (2009). Ca<sup>2+</sup> regulation in the Na<sup>+</sup>/Ca<sup>2+</sup> exchanger features a dual electrostatic switch mechanism. *Proc Natl Acad Sci U S A* 106, 14333-14338.
  130. Ottolia, M., John, S., Ren, X., and Philipson, K.D. (2007). Fluorescent Na<sup>+</sup>-Ca<sup>+</sup> exchangers: electrophysiological and optical characterization. *J Biol Chem* 282, 3695-3701.
  131. Johnson, E., Bruschweiler-Li, L., Showalter, S.A., Vuister, G.W., Zhang, F., and Bruschweiler, R. (2008). Structure and dynamics of Ca<sup>2+</sup>-binding domain 1 of the Na<sup>+</sup>/Ca<sup>2+</sup> exchanger in the presence and in the absence of Ca<sup>2+</sup>. *J Mol Biol* 377, 945-955.
  132. Matsuoka, S., Nicoll, D.A., Hryshko, L.V., Levitsky, D.O., Weiss, J.N., and Philipson, K.D. (1995). Regulation of the cardiac Na(+)-Ca<sup>2+</sup> exchanger by Ca<sup>2+</sup>. Mutational analysis of the Ca(2+)-binding domain. *J Gen Physiol* 105, 403-420.
  133. Dyck, C., Maxwell, K., Buchko, J., Trac, M., Omelchenko, A., Hnatowich, M., and Hryshko, L.V. (1998). Structure-function analysis of CALX1.1, a Na<sup>+</sup>-

- Ca<sup>2+</sup> exchanger from *Drosophila*. Mutagenesis of ionic regulatory sites. *J Biol Chem* 273, 12981-12987.
134. Omelchenko, A., Dyck, C., Hnatowich, M., Buchko, J., Nicoll, D.A., Philipson, K.D., and Hryshko, L.V. (1998). Functional differences in ionic regulation between alternatively spliced isoforms of the Na<sup>+</sup>-Ca<sup>2+</sup> exchanger from *Drosophila melanogaster*. *J Gen Physiol* 111, 691-702.
  135. Du, M., Rambhadran, A., and Jayaraman, V. (2008). Luminescence resonance energy transfer investigation of conformational changes in the ligand binding domain of a kainate receptor. *J Biol Chem* 283, 27074-27078.
  136. Johnson, J.W., and Ascher, P. (1987). Glycine potentiates the NMDA response in cultured mouse brain neurons. *Nature* 325, 529-531.
  137. Benveniste, M., and Mayer, M.L. (1991). Kinetic analysis of antagonist action at N-methyl-D-aspartic acid receptors. Two binding sites each for glutamate and glycine. *Biophys J* 59, 560-573.
  138. Clements, J.D., and Westbrook, G.L. (1991). Activation kinetics reveal the number of glutamate and glycine binding sites on the N-methyl-D-aspartate receptor. *Neuron* 7, 605-613.
  139. Furukawa, H., and Gouaux, E. (2003). Mechanisms of activation, inhibition and specificity: crystal structures of the NMDA receptor NR1 ligand-binding core. *Embo J* 22, 2873-2885.
  140. Furukawa, H., Singh, S.K., Mancusso, R., and Gouaux, E. (2005). Subunit arrangement and function in NMDA receptors. *Nature* 438, 185-192.

141. Inanobe, A., Furukawa, H., and Gouaux, E. (2005). Mechanism of partial agonist action at the NR1 subunit of NMDA receptors. *Neuron* 47, 71-84.
142. Mannuzzu, L.M., Moronne, M.M., and Isacoff, E.Y. (1996). Direct physical measure of conformational rearrangement underlying potassium channel gating. *Science* 271, 213-216.
143. Posson, D.J., Ge, P., Miller, C., Bezanilla, F., and Selvin, P.R. (2005). Small vertical movement of a K<sup>+</sup> channel voltage sensor measured with luminescence energy transfer. *Nature* 436, 848-851.

## Vitae

Jennifer Gonzalez-McGehee was born on September 4, 1982 in Dallas, Texas. She attended Saint Mary's University located in San Antonio, Texas beginning in 2001. Jennifer received a NIH MARC (Minority Access to Research Careers) undergraduate training grant, and participated in the University of Nebraska Medical Center-Omaha Summer Research Opportunity (SROP) program in 2004. Jennifer graduated with a B.S. in Chemistry in 2005 and continued her education in Biochemistry and Biophysics at the University of Texas Health Science Center at Houston Graduate School for Biomedical Sciences. In 2006, she joined Dr. Vasanthi Jayaraman's laboratory, and has gained the interdisciplinary experience in Biochemistry, Physical Chemistry, and Molecular Biology necessary to address important questions in protein structure-function. Jennifer has traveled to the National Institutes of Health in order to be trained in *Xenopus* techniques in the laboratory. In 2007, Jennifer received a MARC Pre-doctoral Fellowship, a National Research Service Award given to outstanding graduates of the MARC undergraduate program. Jennifer has presented her work at several prestigious conferences including the Biophysical Society Meeting in 2007 and 2008, in addition to the Gordon Research Conference-Ion Channels and the Neuropharmacology Conference-Ion Channels in 2008. Jennifer was awarded the 2009 City Federation of Women's Club Endowed Biomedical Scholarship in Structural Biology and the Dean's Research Award from UT-Houston Medical School Graduate Student Education Committee. She was granted a Ph.D. in Biochemistry and Biophysics in May of 2010. Her publications include:

**Gonzalez J**, Rambhadran A, Du M, and Jayaraman V. (2008) LRET Investigations of Conformational Changes in the Ligand Binding Domain of a Functional AMPA Receptor. *Biochemistry*. 47(38):10027-32.

Rambhadran A, **Gonzalez J**, and Jayaraman V. (2010) LRET Investigations of Subunit Arrangement in NMDA Receptors. *JBC. In Press*.

**Gonzalez J**, Du, M, Parameshwaran K, Suppiramanium V, and Jayaraman V. (2010) Role of dimer interface in activation and desensitization in AMPA receptors. *Proc. Natl. Acad. Sci. U.S.A. Manuscript under revision*.

Wu M, **Gonzalez J**, Jayaraman V, Spudich, JL, and Zheng L. Structural Basis of  $\text{Ca}^{2+}$  regulation and alternative splicing modification of  $\text{Na}^+/\text{Ca}^{2+}$  exchangers. *Manuscript in preparation*.